NRRA
National Road Research Alliance

Drainability of Base Aggregate and Sand

Authors: Hyunjun Oh, William Likos, Tuncer Edil

A pooled fund project administered by the Minnesota Department of Transportation

Report No. NRRA202107

DEPARTMENT OF TRANSPORTATION

To request this document in an alternative format, such as braille or large print, call 651-366-4718 or 1-800-657-3774 (Greater Minnesota) or email your request to ADArequest.dot@state.mn.us. Please request at least one week in advance.

Technical Report Documentation Page

1. Report No.	2.	3. Recipients Accession No.	
NRRA202107			
4. Title and Subtitle Drainability of Base Aggregate and Sand		5. Report Date August 2021 6.	
7. Author(s) Hyunjun Oh, William J. Likos, Tuncer B. Edil		8. Performing Organization Report No.	
9. Performing Organization Name and Address Department of Civil and Environmental Engineering University of Wisconsin-Madison Madison, WI 53706		10. Project/Task/Work Unit No. 11. Contract (C) or Grant (G) No. (c)1003328 (wo)02	
12. Sponsoring Organization Name and Address Minnesota Department of Transportation Office of Research & Innovation 395 John Ireland Boulevard, MS 330 St. Paul, Minnesota 55155-1899		13. Type of Report and Period Covered Final Report 14. Sponsoring Agency Code	
15. Supplementary Notes https://www.mndot.gov/research/reports/2021/NRRA202107.pdf			
16. Abstract (Limit: 250 words) Poor drainage of roadway base materials can lead to increased pore water pressure, reduction of strength and stiffness, and freeze-thaw damage. Drainability is dependent on soil/aggregate physical properties that affect water flow and retention in the porous matrix, notably including particle-size distribution, particle shape, fines content, and density or porosity. The objective of this project was to quantitatively assess permeability and water retention characteristics of soil and aggregates applicable to pavement applications and to evaluate and derive predictive equations for indirect estimation of these properties. Samples of 16 materials used in transportation geosystems were obtained and laboratory tests were conducted to determine grain size distribution, index properties, saturated hydraulic conductivity, and soil-water characteristic curves. Results were analyzed to examine applicability of estimation equations available in the literature and to develop dataset-specific equations for the specific suite of materials. Procedures were provided to qualitatively assess base course drainability as “excellent,” “marginal,” and “poor” from grain size properties, thereby offering rationale to reduce pavement life-cycle costs, improve safety, realize material cost savings, and reduce environmental impacts.			
17. Document Analysis/Descriptors Permeability coefficient, permeability, drainage, pavements, base course (pavements)		18. Availability Statement No restrictions. Document available from: National Technical Information Services, Alexandria, Virginia 22312	
19. Security Class (this report) Unclassified	20. Security Class (this page) Unclassified	21. No. of Pages 157	22. Price n/a

DRAINABILITY OF BASE AGGREGATE AND SAND

FINAL REPORT

Prepared by:

Hyunjun Oh
William J. Likos
Tuncer B. Edil

Department of Civil and Environmental Engineering
University of Wisconsin-Madison

August 2021

Published by:

Minnesota Department of Transportation
Office of Research & Innovation
395 John Ireland Boulevard, MS 330
St. Paul, Minnesota 55155-1899

ACKNOWLEDGMENTS

Financial support from the National Road Research Alliance (NRRA) is acknowledged and appreciated (Permeability of Base Aggregate and Sand; Contract number 1003328.). The Minnesota, Wisconsin, and Missouri departments of transportation collaborated in the selection and obtainment of the test samples. Jie Yin, faculty in Civil Engineering and Mechanics at Jiangsu University, China, and Tyler Klink, graduate research assistant at the Department of Civil and Environmental Engineering, University of Wisconsin-Madison, contributed to the literature review. These efforts are gratefully acknowledged.

TABLE OF CONTENTS

LIST OF FIGURES

LIST OF TABLES

EXECUTIVE SUMMARY

Drainability is a material property that describes fluid flow and retention in porous material and is a significant consideration in the design and long-term performance of pavement systems. Poor drainage in roadway base materials, for example, can lead to problems including increased pore water pressure, reduction of strength and stiffness, and freeze-thaw damage.

Base course drainability is dependent on soil/aggregate physical properties that affect water flow and retention in the porous matrix, notably including particle-size distribution, particle shape, fines content, and density or porosity. For unsaturated soil systems, both hydraulic conductivity and soil-water retention characteristics are necessary to predict drainage behavior. In lieu of direct measurements of these properties, empirical and theoretical relations are available and are often used to estimate them from more easily obtained surrogate properties such as gradation and porosity. The accuracy and applicability of such estimations, however, are uncertain and are often limited to the specific datasets from which they were obtained.

The objective of this project is to provide rationale to assess the drainability of coarse soil/aggregate materials applicable to pavement base course applications. Emphasis is placed on saturated hydraulic conductivity and water retention, including evaluation of existing predictive equations for indirect estimation of these properties from surrogate material properties (e.g., grain size distribution) and the development of new correlation equations for the materials examined here.

Samples of 16 representative materials were obtained from National Road Research Alliance (NRRA) stakeholders, including materials that are generally classified as gravels (7 samples) and sands (9 samples). Laboratory tests were conducted to determine grain size distribution, grain size index properties, saturated hydraulic conductivity (K_{sat}), and soil-water characteristic curves (SWCCs). Key findings from the experimental program included the following:

1) Measured K_{sat} of the 9 sandy materials is independent of hydraulic gradient (i) typical of field conditions for pavement base applications ($0.25 < i < 2.0$). Measured K_{sat} of the 7 gravels systematically decreases with increasing hydraulic gradient, potentially due to migration of fines and the effects of turbulent flow.
2) K_{sat} for all the materials generally increases as % gravels and particle diameters corresponding to 10%, 30%, 50%, and 60% finer (D_{10}, D_{30}, D_{50}, and D_{60}, respectively) increases. K_{sat} generally increases as % fines and dry unit weight (γ_d) of compacted samples decreases.
3) K_{sat} slightly increases with a decrease in uniformity coefficient (C_u), but the relationship is not significantly correlated. Air-entry pressure determined from the measured soil-water characteristic curves increases with an increase in C_u.
4) The van Genuchten (1980) SWCC parameters (α and n) increase with increases in D_{10}, D_{30}, D_{50}, D_{60}, and % retained gravels and with decreases in % fines, C_u, and γ_d. Comparisons among the experimentally measured K_{sat} values and the van Genuchten α and n parameters show a proportional relationship.
5) Effective (drainable) porosities for the 16 samples ranges from 0.09 to 0.36 with an average of 0.24. Corresponding minimum saturation (S_{min}), which is achieved by gravity, ranges from 0.01

to 0.69 with an average of 0.25. These results are comparable to typical values for similar materials in the literature.

Test results were analyzed to examine the accuracy and applicability of equations available in the literature for estimating K_{sat} and SWCC parameters and to develop dataset-specific equations for the suite of materials tested here. This analysis showed:

1) Estimated K_{sat} for materials that classified as poorly graded gravel (GP) are significantly higher than the experimentally measured K_{sat} values. Measured K_{sat} for a subset of samples that excludes the gravels is generally well estimated using the Harleman et al. (1963), Sauerbrei (1932), and Chapuis (2004) empirical equations.
2) New dataset-specific regression equations to estimate K_{sat} are derived using the experimentally obtained K_{sat} and grain size index properties (D_{10}, D_{30}, D_{50}, D_{60}). Measured K_{sat} values that are overestimated using the existing equations are reasonably estimated with the new equations, particularly using equations based on D_{10} and D_{30}.
3) The van Genuchten (1980) SWCC fitting parameters α and n are estimated using regression equations following procedures developed by Benson et al. (2014) for clean sands. Equations based on D_{30} and C_u show the best performance.

A qualitative rating system for assessing base course drainability is provided by setting criteria for saturated hydraulic conductivity (K_{sat}) and minimum saturation (S_{min}) at field capacity. The rating system may be used to qualitatively assess the drainability of candidate base course material as "excellent," "marginal," or "poor." Three approaches to obtain hydraulic conductivity and water retention characteristics are recommended:

1) Recommendation 1: Direct measurement of K_{sat} and S_{min} from laboratory tests.
2) Recommendation 2: Indirect estimation of K_{sat} and S_{min} from correlation to grain size parameters. Application of this approach requires a measurement of grain size distribution to obtain D_{30} and C_u using mechanical sieve analysis.
3) Recommendation 3: Indirect assessment of drainability from measured percent fines. Application of this approach requires a measurement percent passing the #200 sieve using mechanical sieve analysis.

While rigorous drainability analysis of in-situ pavement systems requires knowledge of material properties, pavement system design, and site environmental conditions, the approaches recommended in this research offer a rationale for material selection and quality assessment that will reduce pavement life-cycle costs, improve safety, realize material cost savings, and reduce environmental impacts.

CHAPTER 1: INTRODUCTION

1.1 PROBLEM STATEMENT

Geosystems such as roadway base course and retaining wall backfills are designed to quickly drain porewater to minimize elevated pore pressure, minimize freeze-thaw damage, and prevent loss of shear strength and stiffness. Requirements for drainability vary depending on the specific requirements of the structure. Simple and reliable tools capable of qualitatively estimating drainability for common aggregate types used in transportation infrastructure can be useful in material selection and design and to ensure longer-term performance.

Pavement base course layers are unsaturated under most field conditions, and thus both hydraulic conductivity (K) and soil-water retention characteristics are necessary to evaluate drainage behavior. Hydraulic conductivity and water retention characteristics, however, are not typically measured or used explicitly in design. In lieu of direct measurements of these properties, empirical and theoretical relations are available and often used to estimate saturated hydraulic conductivity (K_{sat}) and the soil-water characteristic curve (SWCC) from more easily obtained surrogate material properties, notably including grain size distribution and density, porosity, or void ratio. The accuracy and applicability of such estimations, however, are uncertain and often limited to the specific datasets from which they are obtained.

The objective of this study was to quantitatively determine hydraulic conductivity and water retention characteristics for representative coarse-grained soil/aggregate materials applicable to pavement base course applications and to evaluate and derive predictive equations for indirectly estimating K_{sat} and the SWCC. Samples of 16 materials were obtained from National Road Research Alliance (NRRA) stakeholders and tests were conducted to determine grain size distribution, grain size index properties (e.g., D_{10}, D_{30}, D_{50}, D_{60}, C_u), K_{sat} and SWCCs. Test results were analyzed to examine the accuracy and applicability of existing equations for estimating K_{sat} and SWCC parameters and to develop dataset-specific equations for the suite of test materials obtained here.

1.2 RESEARCH BENEFITS

Anticipated research benefits of the project include the following:

- Reduced Life-Cycle Costs
- Improved Safety
- Material Cost Savings
- Construction Savings
- Reduced Environmental Impacts

Drainability of pavement base and subbase is one of the main considerations in designing pavement systems and in the post-construction performance and safety of the pavement structure. Poor drainage of roadway base course and associated elevation of pore water pressure in the material will reduce stiffness and strength, which can lead to surface rutting and cracking, and can lead to damage from freeze/thaw processes. This can significantly reduce the pavement life cycle, increase maintenance costs, and lead to poor roadway performance and safety. Developing more robust methods to assess material drainability from surrogate material properties will thus reduce pavement life-cycle costs and improve safety. Improved empirical approaches to estimate drainability will also potentially realize material cost savings, construction savings, and reduce environmental impacts (e.g., material sourcing and transport) by providing rationale to allow a wider range of locally available materials to be considered for construction. Implementation of the results of this research will lead to improvement of safety and reduction of maintenance and engineering costs associated with repairing roadways.

1.3 METHODOLOGY

1.3.1 Literature Review

A literature review focused on select case studies related to performance evaluation of geosystems such as pavement base course, subbase, and retaining wall backfills. Case histories focused on evaluating subsurface drainage systems based on literature reviews, surveys, experiments, numerical modeling, and statistical analyses, with emphasis placed on research on pavement systems performed by the Minnesota Department of Transportation (MnDOT) and partner entities. Synthesis of the case studies provides a practical background for the project. Results from the case study literature review are provided in Appendix A.

A second literature review was conducted to synthesize information on permeability of coarse aggregates and sands, with emphasis on existing methods for estimating permeability from other index properties. Approaches were subdivided into those that correlate saturated hydraulic conductivity to i) grain size distribution, ii) void ratio, iii) compaction level, iv) fines content, and v) material type. Results from this portion of the literature review are provided in Appendix C.

1.3.2 Laboratory Testing

A suite of coarse-grained samples was obtained from NRRA stakeholders to represent a range of materials that have been used in (or have been considered for use in) transportation infrastructure systems. Materials included 17 discrete samples ranging from poorly graded sand (SP), silty sand (SM), well-graded sand (SW), poorly graded gravel (GP), silty gravel (GM), to well-graded gravel (GW). (16 of the samples were used in the project). Materials were selected in partnership with NRRA representatives from the Minnesota (MnDOT), Missouri (MoDOT), and Wisconsin (WisDOT) Departments of Transportation.

Particle-size distributions of the samples were determined by standard sieve analysis (ASTM D422) and hydrometer analysis (ASTM D7928). Materials were classified according to the ASTM D2487 unified soil classification system (USCS). Saturated hydraulic conductivity values (K_{sat}) were determined for samples compacted in a rigid-walled permeameter at dry density (γ_d) ranging from 15.6 kN/m^3 to 20.1 kN/m^3 using the constant head method (ASTM D2434). Hydraulic conductivity testing was repeated using five hydraulic gradients (i = 0.25, 0.5, 1.0, 1.5, and 2.0) selected to represent a range of field conditions typical for pavement base course applications and to quantify any effects of applied hydraulic gradient on measured conductivity (e.g., from particle migration or turbulent effects). Average K_{sat} values from tests spanning the range of gradients were calculated for subsequent modeling and analysis.

Soil water characteristic curves (SWCCs) were measured using the hanging column test apparatus (ASTM D6836). Samples for SWCC testing were compacted to dry density values within 1% of values used in the hydraulic conductivity tests. SWCCs were obtained along primary drying curves initiating at zero matric suction (ψ) and full saturation (S) to matric suction of approximately 100 kPa. The highest suction corresponded to degree of saturation ranging from near zero to 30%, depending on the material. Measured SWCCs were fit to the commonly adopted van Genuchten (1980) SWCC model using least-squared regression to calculate model parameters (α and n) used in subsequent analysis.

1.3.3 Analysis

Index properties obtained from the grain size distributions (D_{10}, D_{30}, D_{50}, D_{60}, % fines, % gravel) were used to evaluate relationships between these properties and measured K_{sat} values. Air-entry pressures determined from the SWCC measurements were related to index properties (e.g., grain size uniformity coefficient, C_u) and to the van Genuchten (1980) model parameters. The SWCC model parameters were then related to index properties including D_{10}, D_{50}, and % gravel, % fines, C_u, and dry unit weight, unsaturated K_{sat} functions, and K_{sat} values obtained from the hydraulic conductivity measurements. The SWCCs were also used to evaluate field capacity (θ_f) and minimum saturation (S_{min}).

Existing empirical and theoretical methods for estimating hydraulic conductivity identified in the literature review were assessed for their applicability to the suite of specific materials tested here. The experimentally obtained K_{sat} values and index properties were then considered to derive new equations for estimating K_{sat}. Finally, a new suite of equations was developed for estimating the van Genuchten SWCC parameters α and n from particle-size distribution data.

A qualitative rating system for assessing base course drainability is provided by setting criteria for saturated hydraulic conductivity (K_{sat}) and minimum saturation (S_{min}) at field capacity. The rating system may be used to qualitatively assess the drainability of candidate base course material as “excellent,” “marginal,” or “poor.” Three approaches to obtain hydraulic conductivity and water retention characteristics are recommended:

1) Recommendation 1: Direct measurement of K_{sat} and S_{min} from laboratory tests.
2) Recommendation 2: Indirect estimation of K_{sat} and S_{min} from correlation to grain size parameters. Application of this approach requires a measurement of grain size distribution to obtain D_{30} and C_u using mechanical sieve analysis.

3) Recommendation 3: Indirect assessment of drainability from measured percent fines. Application of this approach requires a measurement percent passing the #200 sieve using mechanical sieve analysis.

1.4 BACKGROUND

1.4.1 Drainability as an Unsaturated Soils Problem

Figure 1.1 is a conceptual illustration of a pavement base system illustrating the unsaturated state of the system under typical field conditions. The water table is located at the interface of the base and subgrade for illustration. Pore pressure in the base material at hydrostatic equilibrium varies from negative values (suction) above the water table to positive values below the water table. Corresponding degree of saturation of the base material is quantified by its soil-water characteristic curve. The existence of negative pressure in the base material contributes to strength and stiffness, thus enhancing its performance as a structural layer.

If a precipitation (or other wetting) event occurs that introduces water into the system, the pore pressure profile will shift to toward more positive values as the wetting front passes through the system until hydrostatic equilibrium is once again achieved, thus reducing effective stress in the material and reducing corresponding strength and stiffness. The duration of this transient process is controlled by both the hydraulic conductivity of the unsaturated soil system and the water retention characteristics, as governed by the soil-water characteristic curve. Materials that do not freely drain (i.e., having low hydraulic conductivity or high water retention capacity) will maintain elevated pore pressures for a longer period and, if not fully drained, can be subject to freeze-thaw processes. Full assessment of material drainability, and system performance, therefore, must take into consideration both the hydraulic conductivity and water retention characteristics of the material. These material characteristics depend on the properties of the soil/aggregate grains themselves (e.g., size, size distribution, shape), their compaction characteristics (e.g., density, void ratio, porosity), and of the permeant fluid (viscosity, density), and is referred to herein as “drainability.”

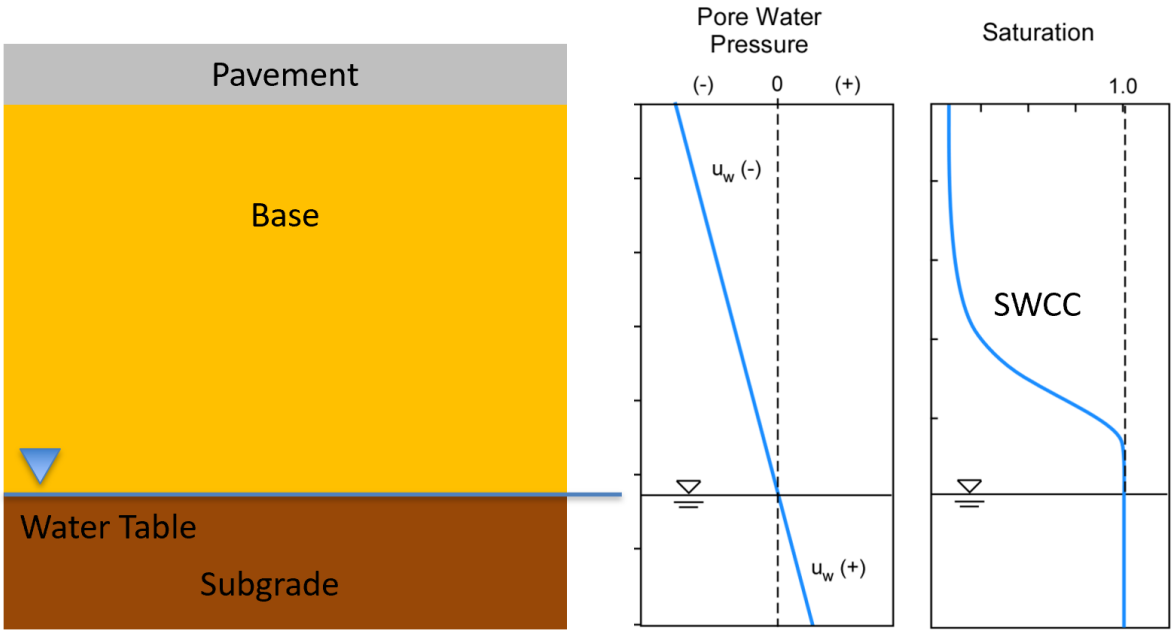

Figure 1.1 Schematic illustration of a pavement base system in the unsaturated condition. Pore pressure at hydrostatic equilibrium varies from negative values (suction) above the water table to positive values below the water table. Corresponding degree of saturation of the base material is quantified by the soil-water characteristic curve.

1.4.2 Hydraulic Conductivity and Permeability (Lu and Likos, 2004)

Darcy's law states that the discharge velocity of fluid from a porous medium, v, is linearly proportional to the gradient in the relevant driving head, ∇h, as follows:

$$v = -K\nabla h \tag{1.1}$$

where K = a proportionality term describing the conductivity of the porous medium [m/s]. The negative sign preceding the right-hand side of eq. (1.1) indicates that fluid flow occurs from a location of relatively high total head to a location of relatively low total head. Seepage velocity, v_s, which describes the average actual flow velocity through the pores of the medium, is the discharge velocity divided by the medium porosity (i.e., $v_s = v/n$).

The proportionality parameter K in eq. (1.1) describes the ability for a specific porous medium under specific conditions to transmit a specific fluid. For the flow of pore water in soil/aggregate, the driving gradient is the total hydraulic head and the constant of proportionality is the hydraulic conductivity (K).

Discharge velocity is proportional to the viscosity and density of the permeant fluid, being higher for relatively high density or low viscosity fluids. These proportionalities are captured mathematically as follows:

$$v \propto \frac{\rho g}{\mu} \tag{1.2}$$

where ρ = the fluid density [kg/m^3], g = gravitational acceleration [m/s^2], and μ = the dynamic (absolute) fluid viscosity [N·s/m^2].

Experimental results and theoretical considerations also reveal that discharge velocity is highly dependent on pore size and pore-size distribution. Following Poiseuille's law, the discharge velocity is proportional to the square of the pore diameter d, or:

$$v \propto d^2 \tag{1.3}$$

Combining the above two proportionalities with Darcy's original observation that discharge velocity is linearly proportional to the total head gradient leads to the following:

$$v = -C \frac{d^2 \rho g}{\mu} \nabla h \tag{1.4}$$

where C = a dimensionless constant related to the geometry of the soil pores. Comparing eq. (1.4) with eq. (1.1) leads to:

$$K = (Cd^2)\left(\frac{\rho g}{\mu}\right) \tag{1.5}$$

If intrinsic permeability, k, is defined as follows:

$$k = Cd^2 \tag{1.6}$$

then, together with eq. (1.5), the relationship between intrinsic permeability and hydraulic conductivity becomes:

$$K = \frac{\rho g}{\mu} k \tag{1.7}$$

Intrinsic permeability, or simply permeability, has units of length squared (m^2) and is dependent only on the pore size, pore geometry, and pore-size distribution. Permeability is the same for any porous material regardless of the properties of the fluid being transmitted as long as the pore structure remains unaltered.

1.4.3 Soil Water Characteristic Curve (Lu and Likos, 2004)

The soil-water characteristic curve (SWCC) is a fundamental constitutive relationship in unsaturated soil mechanics. In general terms, the SWCC describes the relationship between soil suction and soil water

content. More specifically, the SWCC describes the thermodynamic potential of the soil pore water relative to that of free water as a function of the amount of water adsorbed by the soil system. At relatively low water content, the pore water potential is relatively low compared with free water and the corresponding soil suction is high. At relatively high water content, the difference between the pore water potential and the potential of free water decreases and the corresponding soil suction is relatively low. When the potential of the pore water is equal to the potential of free water, the soil suction is equal to zero. For soil with negligible amount of dissolved solutes, suction approaches zero as the degree of saturation approaches unity.

The SWCC can describe either an adsorption (i.e., wetting) process or a desorption (i.e., drying) process. Differentiation between wetting characteristic curves and drying characteristic curves is typically required in order to account for the significant hysteresis that can occur between the two branches of behavior. In general, more water is retained by a soil during a drying process than adsorbed by the soil for the same value of suction during a wetting process.

Figure 1.2 conceptualizes the SWCC for a typical coarse-grained unsaturated soil (e.g., sand). As shown, there are three general regimes of saturation: (1) a capillary regime where the soil remains saturated under negative pore water pressure; (2) a funicular regime characterized by an unsaturated yet continuous water phase; and (3) a pendular regime characterized by an isolated, discontinuous water phase. Boundaries between the capillary and funicular regime and the funicular and pendular regime are approximated by the air-entry and residual suction conditions, respectively.

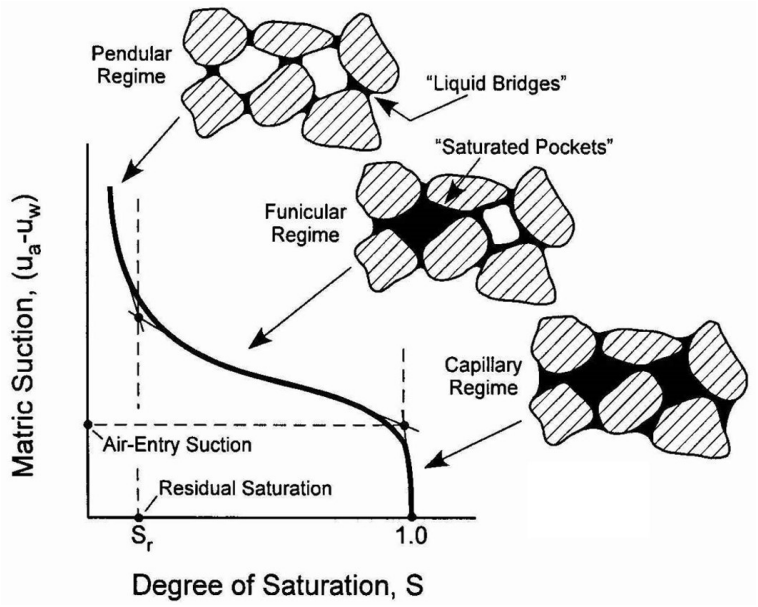

Figure 1.2 Conceptual SWCC for coarse soil showing capillary, funicular, and pendular saturation regimes (Lu and Likos, 2004).

1.4.4 Soil Water Characteristic Curve Modeling (Lu and Likos, 2004)

Experimental techniques for direct measurement of the SWCC provide a series of discrete data points comprising the relationship between soil suction and water content. Subsequent application of these measurements for predicting flow, stress, and deformation phenomena, however, typically requires that measured characteristic curves be described in continuous mathematical form. Direct measurements also remain a relatively demanding, and often expensive, endeavor. Due to the costs and complexities associated with sampling, transporting, and preparing laboratory specimens or installing, maintaining, and monitoring field instrumentation, the number of measurements which may be obtained for a given site is often too small to adequately capture the spatial variability of soil properties and stress conditions in the field. The available measurements often comprise only a small portion of the soil-water characteristic curve over the wetness range of interest in practical applications. For all these reasons, alternatives to direct measurements are desirable.

Numerous approaches have been proposed for mathematical representation (i.e., fitting) of the soil-water characteristic curve. Commonly adopted approaches for geotechnical engineering applications include the Brooks and Corey (1964) model, the van Genuchten (1980) model, and the Fredlund and Xing (1994) model. Detailed reviews and analyses of these and several other models are also provided by Leong and Rahardjo (1997), Singh (1997) and Sillers et al. (2001).

Parameters used in mathematical models for the SWCC include fixed points pertaining to water content or suction at specific conditions (e.g., saturation, residual saturation, air-entry pressure) and two or more empirical or semi-empirical fitting constants that are used to capture the general shape of the curve between these fixed points. As illustrated on Figure 1.3, the saturated water content, θ_s, describes the point where all of the available pore space in the soil matrix is filled with water, usually corresponding to the desorption branch of the curve. The air-entry, or "bubbling," pressure, ψ_b, describes the suction on the desorption branch where air first starts to enter the soil's largest pores and desaturation commences. The residual water content, θ_r, describes the condition where the pore water resides primarily as isolated pendular menisci and extremely large changes in suction are required to remove additional water from the system. A consistent way to quantify the air-entry pressure and residual water content is to construct pairs of tangent lines from inflection points on the characteristic curve, as shown on the figure.

For modeling purposes, a dimensionless water content variable, Θ, may be defined by normalizing volumetric water content with its saturated and residual values as follows:

$$\Theta = \frac{\theta - \theta_r}{\theta_s - \theta_r} \tag{1.8}$$

Note that as volumetric water content θ approaches θ_r, the normalized water content Θ approaches zero. As volumetric water content θ approaches θ_s, the normalized water content Θ approaches unity. If the residual water content θ_r is equal to zero, then the normalized water content Θ is equal to the degree of saturation S.

An "effective" degree of saturation, S_e, may also be normalized by the complete saturation condition (S = 1) and the residual saturation condition, S_r, in a similar manner:

$$S_e = \frac{S - S_r}{1 - S_r} \tag{1.9}$$

where

$$\Theta = S_e \tag{1.10}$$

If the residual saturation S_r is equal to zero, then the effective degree of saturation S_e is equal to the degree of saturation S.

Fitting constants used in the various SWCC models are related to physical characteristics of the soil such as pore size distribution and air-entry pressure. Models may be differentiated in terms of the number of fitting constants used, most commonly being either two or three. Models incorporating three fitting constants tend to sacrifice simplicity in their mathematical form, but generally offer a greater amount of flexibility in their capability to accurately represent characteristic curves over a realistically wide range of suction. Some form of iterative, non-linear regression algorithm is typically used to optimize the fitting constants to measured data comprising the characteristic curve (e.g., van Genuchten et al., 1991; Wraith and Or, 1998). Many of the two-constant models may be effectively optimized by visual observation. At least five to ten measured $\psi-\theta$ pairs are typically required for a meaningful mathematical representation. The accuracy of the models may be checked by calculating the root-mean-square deviation (RMSD) between the measured and modeled values.

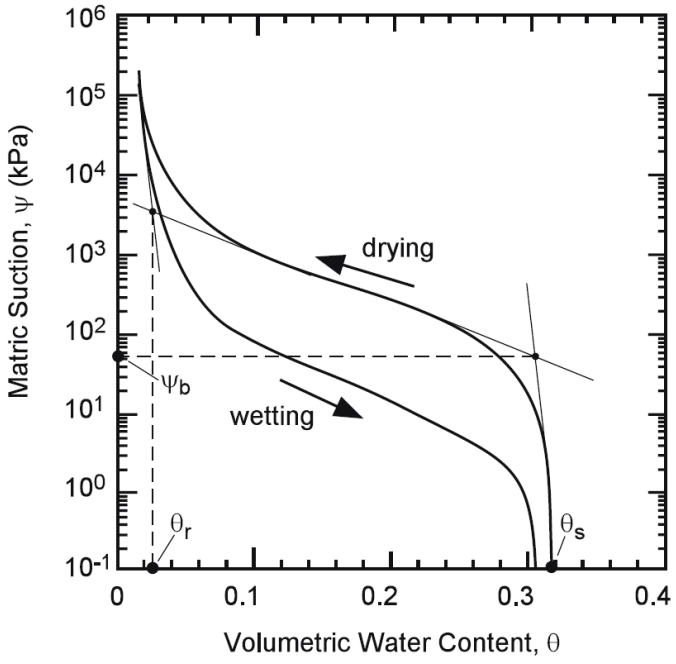

Figure 1.3 Conceptual SWCC along hysteretic wetting and drying paths showing key points on the curve used for modeling.

1.4.5 The van Genuchten (1980) SWCC Model (Lu and Likos, 2004)

van Genuchten (1980) proposed a smooth, closed-form, three-parameter model for the soil-water characteristic curve in the following form:

$$\Theta = S_e = \left[\frac{1}{1+(a\psi)^n}\right]^m \tag{1.11}$$

where a, n, and m are fitting parameters. The mathematical form of the VG model, which accounts for an inflection point, allows flexibility over a wide range of suction and captures the sigmoidal shape of the curve. Smooth transitions at the air-entry pressure and approaching the residual condition are more effectively captured.

The suction term appearing on the right-hand-side of eq. (1.11) may be expressed in either units of pressure (i.e., ψ = kPa, as shown) or head (i.e., h = m). In the former case, the a parameter is designated more specifically as α, where α has inverse units of pressure (kPa^{-1}). In the latter case, the a parameter is designated β, where β has inverse units of head (m^{-1}). Both α and β are related to the air-entry condition, where α approximates the inverse of the air-entry pressure, and β approximates the inverse of the air-entry head (or the height of the capillary fringe.) The n parameter is related to the pore size distribution of the soil and the m parameter is related to the overall symmetry of the characteristic curve. The m parameter is frequently constrained by a direct relation to the n parameter as follows:

$$m = 1 - \frac{1}{n} \tag{1.12a}$$

or

$$m = 1 - \frac{1}{2n} \tag{1.12b}$$

Either of these constraints on the m parameter significantly reduces the flexibility of the VG model but significantly simplifies it, thus resulting in greater stability during parameter optimization and permitting closed-form solution of the hydraulic conductivity function (van Genuchten et al., 1991).

1.4.6 The Hydraulic Conductivity Function (Lu and Likos, 2004)

The hydraulic conductivity of unsaturated soil is a function of material variables describing the pore structure (e.g., void ratio, porosity), the pore fluid properties (e.g., density, viscosity), and the relative amount of pore fluid in the system (e.g., water content, degree of saturation). The “unsaturated hydraulic conductivity function” specifically describes this characteristic dependence on the amount of pore fluid in the unsaturated soil system.

Consider the conceptual model illustrated as Figure 1.4, which shows a series of cross-sectional areas for a rigid mass of relatively coarse-grained soil (e.g., sand). The soil is initially saturated at condition (a) and allowed to drain under increasing suction through conditions (b) and (c) to a residual condition at point

(d). The soil-water characteristic curve and hydraulic conductivity function corresponding to the four saturation conditions are conceptualized as Figures 1.5(a) and (b), respectively. At condition (a), the soil matrix is completely saturated and matric suction is zero. The saturated volumetric water content is equal to about 0.34 and the saturated hydraulic conductivity is equal to about 2 X 10^{-3} cm/s, both reasonable values for sand. The saturated hydraulic conductivity is a maximum for the system because the cross-sectional area of pore space available for the conduction of water is at its maximum. Conversely, the air conductivity at condition (a) is effectively zero. Between points (a) and (b), the soil matrix sustains a finite amount of suction prior to desaturation at the air-entry pressure. The soil remains saturated within this regime and the hydraulic conductivity may decrease only slightly as the air-entry pressure is approached. Condition (b) represents the air-entry pressure, corresponding to the point where air begins to enter the largest pores. A further increase in suction from this point results in continued drainage of the system. At point (c), drainage under increasing suction has resulted in a significant decrease in both the water content and hydraulic conductivity. The reduction in conductivity continues with increasing suction as the paths available for water flow continue to decrease. The reduction is initially relatively steep because the first pores to empty are the largest and most interconnected and, consequently, the most conductive to water. At point (d), which occurs near the residual water content, the pore water exists primarily in the form of disconnected menisci among the soil grains. Here, the hydraulic conductivity reduces essentially to zero and pore water is transported primarily through the vapor phase. Typical of many soils, the total change in the magnitude of hydraulic conductivity from point (a) to point (d) is over six orders of magnitude.

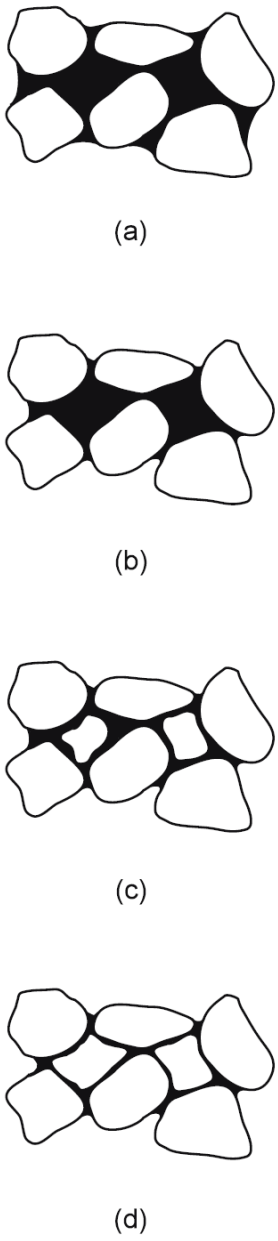

Figure 1.4 Conceptual distributions of pore water and pore air in a cross-sectional area of rigid soil matrix during incremental desaturation process (Lu and Likos, 2004)

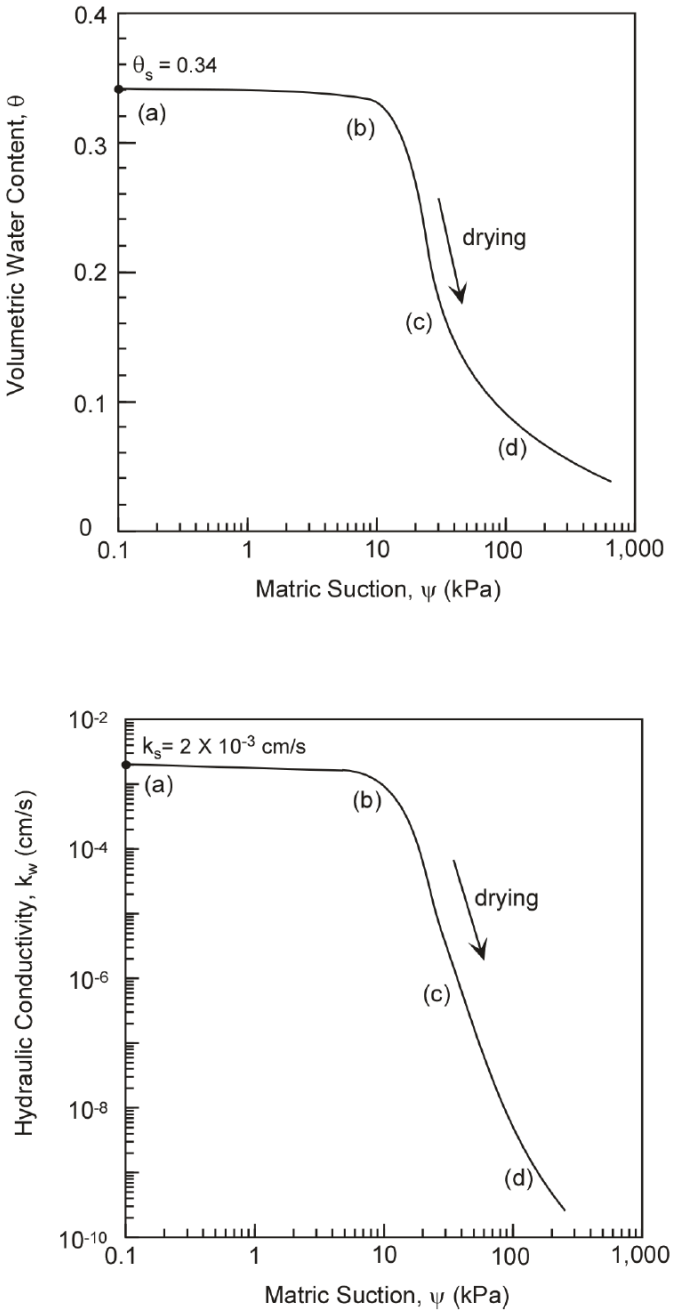

Figure 1.5 (a) Conceptual soil-water characteristic curve and (b) hydraulic conductivity function corresponding to saturation conditions for a rigid soil matrix shown in Figure 1.4 (Lu and Likos, 2004).

1.4.7 Hydraulic Conductivity Function Modeling

Numerous mathematical models have also been developed to model the unsaturated hydraulic conductivity function from limited experimental data sets or predict the conductivity function from more routinely obtained constitutive functions, most notably the soil-water characteristic curve. Detailed summaries of various hydraulic conductivity models and modeling techniques include those provided by Lu and Likos (2004). van Genuchten (1980) proposed a flexible closed-form analytical equation for the relative hydraulic conductivity function as follows:

$$K_r(\psi) = \frac{\left[1-(\alpha\psi)^{n-1}[1+(\alpha\psi)^n]^{-m}\right]^2}{[1+(\alpha\psi)^n]^{m/2}} \quad (1.13)$$

which allows the conductivity function to be estimated directly from a corresponding model of the soil-water characteristic curve if the saturated hydraulic conductivity is known. Equation (1.13) may be written in terms of effective water content Θ (or effective degree of saturation S_e) as follows:

$$K_r = \Theta^{0.5}\left[1-(1-\Theta^{1/m})^m\right]^2 \quad (1.14)$$

1.4.8 Base Course Drainability

While saturated hydraulic conductivity and soil-water retention characteristics provide a baseline of material properties that govern drainability of pavement systems, the drainability of systems in the field depends on several factors:

1. Base course permeability, including both saturated hydraulic conductivity and the unsaturated hydraulic conductivity function.
2. Effective porosity (ratio of the volume of the voids that can be drained under gravity flow to the total volume of material.)
3. Drainage boundary conditions, including the cross-sectional geometry of the pavement system, depth to the water table, side-slope geometry, and any installed drainage systems.
4. Environmental conditions, including surface water, groundwater, temperature, wind speed, and relative humidity. The volume of infiltration into the pavement system will depend on factors such as type and condition of surface, length and intensity of rainfall, properties of the drainage layer, hydraulic gradient, time allowed for drainage and the drained area.

The American Association of State Highway and Transportation Officials (AASHTO) qualitatively classifies drainage quality of material used in pavement structures from “excellent” to “very poor.” Excellent drainage is achieved when 50% of the pore volume is drained within 2 hours after a cessation of a precipitation event, whereas very poor drainage indicates that the material does not drain water (AASHTO, 1998). The Federal Highway Administration (FHWA) describes drainability for an excellent quality material equivalent to 0.353 cm/sec (1,000 ft/day) (FHWA, 1992), while a base layer that has a coefficient of permeability (K_{sat}) of less than 0.017 cm/sec (48 ft/day) is practically impermeable (McEnroe, 1994). Cedergren (1994) notes that in designing drainage layers, an open-graded base layer consisting of open-graded aggregates (1.27 cm – 2.54 cm) should have a coefficient of permeability from

3.5 cm/sec (10,000 ft/day) up to 35 cm/sec (100,000 ft/day). There is also a tradeoff between strength or stability of the base course and permeability; therefore, the material for the drainage layers should have the minimum permeability for the required drainage application.

McEnroe (1994) notes that the best measure of the drainability of a granular base is the minimum degree of saturation that can be achieved through gravity drainage in the field. This is related to the so-called field capacity (θ_f), which is the volumetric water content retained in the soil after excess water has drained away under the influence of gravity and the rate of downward movement has decreased. Field capacity is often estimated as the volumetric water content measured from an SWCC along a drainage path at a suction of 33 kPa (e.g., Kern, 1995; Stephens et al., 1998; Pineda et al., 2018.) Richards and Weaver (1944) noted that moisture equivalents (i.e., field capacity) of 71 coarse- and fine-grained soils were most robustly correlated with the moisture retained at the moisture tension of 345 cmH_2O (≈ 33 kPa).

An effective (or "drainable") porosity (n_d) is the total porosity (n) minus the field capacity (θ_f):

$$n_d = n - \theta_f \tag{1.15}$$

and the lowest degree of saturation that can be achieved in the field through gravity drainage (S_{min}) (i.e., at field capacity) is:

$$S_{min} = 1 - \frac{n_d}{n} = \frac{\theta_f}{n} \tag{1.16}$$

Effective porosity and minimum saturation can be used as parameters in designing pavement structures, such as computing time for 50% drainage of the permeable base course, calculating storage capacity of the drainage layer, and estimating permeability (Guyer, 2018). Considering if a base material meets performance goals in terms of drainage, however, ideally requires a drainage analysis specific for the environmental conditions at the location (i.e.., design rainfall intensity and duration, water table location), the pavement geometry (i.e., length and slope of drainage layer), and the material properties of the base course (i.e., permeability and SWCC).

CHAPTER 2: MATERIALS AND METHODS

2.1 MATERIALS

A suite of coarse-grained samples was procured from NRRA stakeholders to represent a range of materials that have been used in (or have been considered for use in) transportation infrastructure systems. Materials included 17 discrete samples selected in partnership with NRRA representatives from the Minnesota (MnDOT), Missouri (MoDOT), and Wisconsin (WisDOT) Departments of Transportation. Materials were supplied as disturbed grab samples (transported in 5-gallon buckets or bags) that were delivered to the UW-Madison testing laboratory.

Table 2.1 summarizes nominal designations for each material. Figure 2.1 is a series of photographs that document observable features including color and general sample morphology for visual classification and classification symbols obtained by Unified Soil Classification System (USCS), which will be further described in the next section with particle-size distribution curves. In subsequent discussion, each sample is denoted by sample number provided in Table 2.1.

Table 2.1 Nominal designation and description of 17 soil samples

Sample Number	Sample
1	3149 Super Sand (MnDOT)
2	MN Class 5 (MnDOT)
3	1007 Type 5 DGB (MoDOT)
4	1007 Type 7 DGB (MoDOT)
5	1010 Man. Sand (MoDOT)
6	MCC Freeborn West Quarry Crushed Stone (WisDOT)
7	Lannon Lisbon Pit (North Ave.) Structural Backfill (WisDOT)
8	Lannon Lisbon Pit (Mukwonago) Structural Backfill (WisDOT)
9	Lannon Stone Product Chips (WisDOT)
10	Super Aggregate Pit Granular Backfill (WisDOT)
15	Bryan Redrock Class 5, MnDOT Pit 70006
16	Bryan Redrock Ball Diamond material, MnDOT Pit 70006
A1	1¼'' Base (WisDOT)
A2	¾'' Washed (WisDOT)
A3	Manufactured Sand (WisDOT)
A4	¾'' Base Cs. (WisDOT)
A5*	Breaker Run (limestone/dolomite) (WisDOT)

* Sample photo and particle-size distribution curve for A5 are available and included, but sample A5 was not used in hydraulic conductivity tests due to the sample's large-particle fraction.

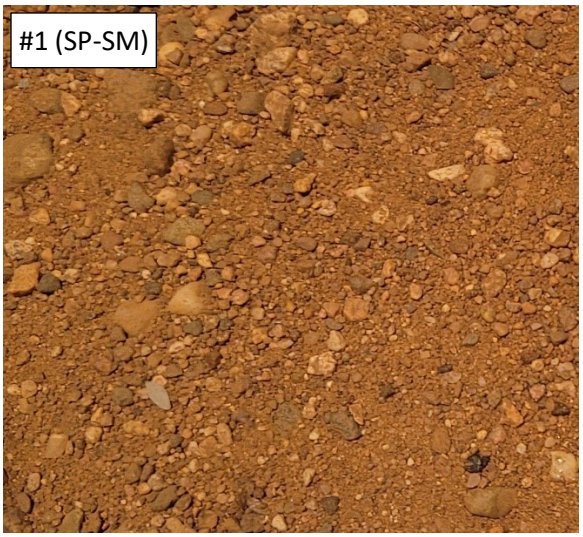

(a)

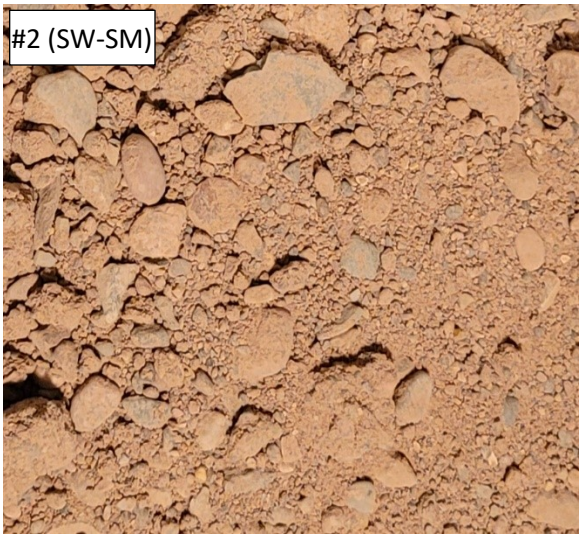

(b)

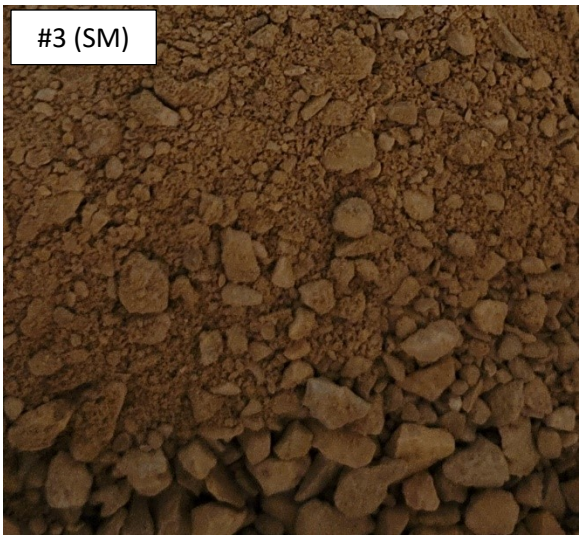

(c)

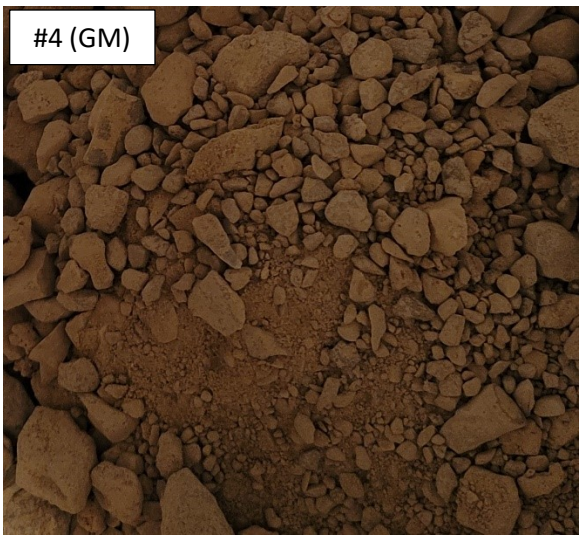

(d)

(e)

(f)

(g)

(h)

(i)

(j)

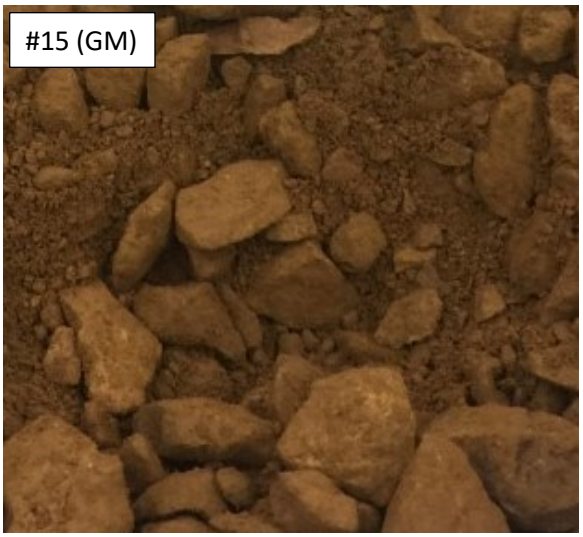

(k)

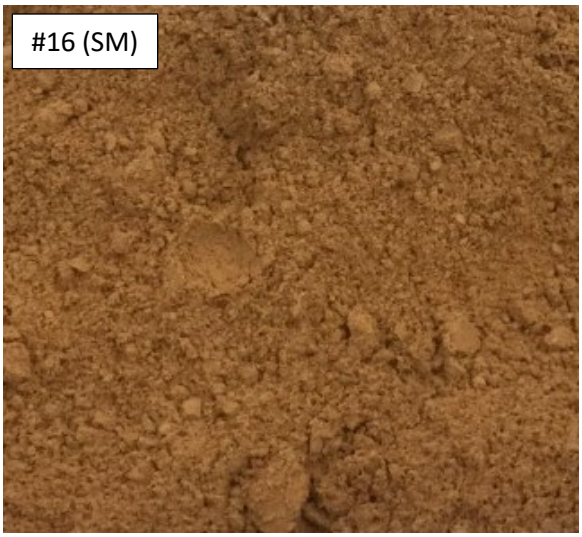

(l)

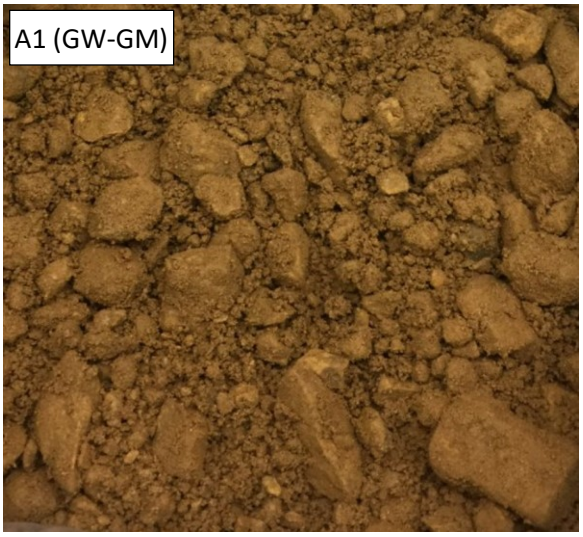

(m)

(n)

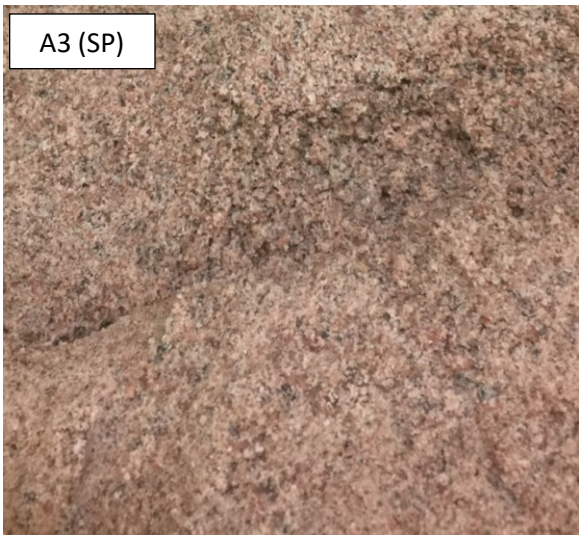

(o)

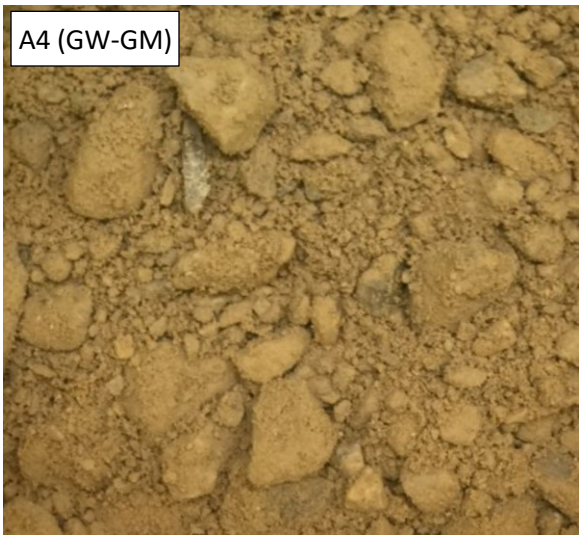

(p)

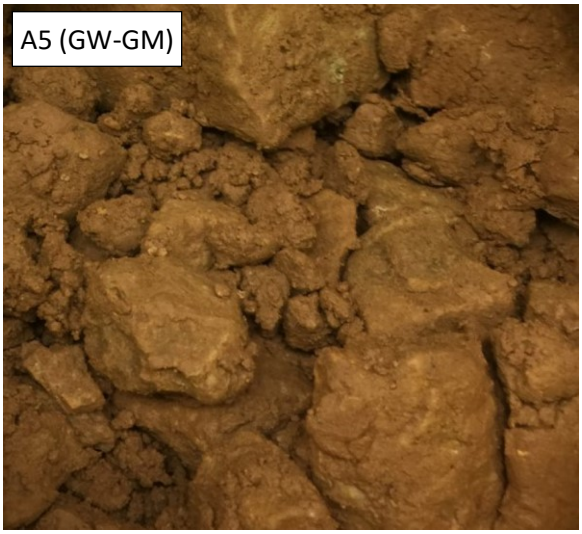

(q)

Figure 2.1 17 coarse-grained samples: (a) 1 (SP-SM), (b) 2 (SW-SM), (c) 3 (SM), (d) 4 (GM), (e) 5 (SP), (f) 6 (GP), (g) 7 (SW), (h) 8 (SP), (i) 9 (GP), (j) 10 (SP), (k) 15 (GM), (l) 16 (SM), (m) A1 (GW-GM), (n) A2 (GP), (o) A3 (SP), (p) A4 (GW-GM), and (q) A5 (GW-GM)

2.2 GRAIN SIZE ANALYSIS

Particle-size distributions were determined by standard sieve analysis (ASTM D422) and hydrometer analysis (ASTM D7928) for fractions of samples passing the #200 sieve (0.075 mm). Figure 2.2 and Table 2.2 summarize particle-size distribution curves and corresponding index properties, respectively.

Reported index properties in Table 2.2 include grain size corresponding to 10% finer by mass (D_{10}), 30% finer (D_{30}), 50% finer (D_{50}) and 60% finer (D_{60}). Coefficients of uniformity (C_u) and curvature (C_c) were calculated from the following equations:

$$C_u = \frac{D_{60}}{D_{10}} \tag{2.1}$$

$$C_c = \frac{{D_{30}}^2}{D_{60} \times D_{10}} \tag{2.2}$$

Samples were classified by the unified soil classification system (USCS) (ASTM D2487) and include eight predominantly gravel materials, specifically: silty gravel with sand (GM), poorly graded gravel (GP), and well-graded gravel with silt and sand (GW-GM). The remaining nine were predominantly sandy materials, including: poorly graded sand with silt (SP-SM), poorly graded sand with silt and gravel (SP-SM), silty sand with gravel (SM), poorly graded sand (SP), well-graded sand (SW), and silty sand (SM).

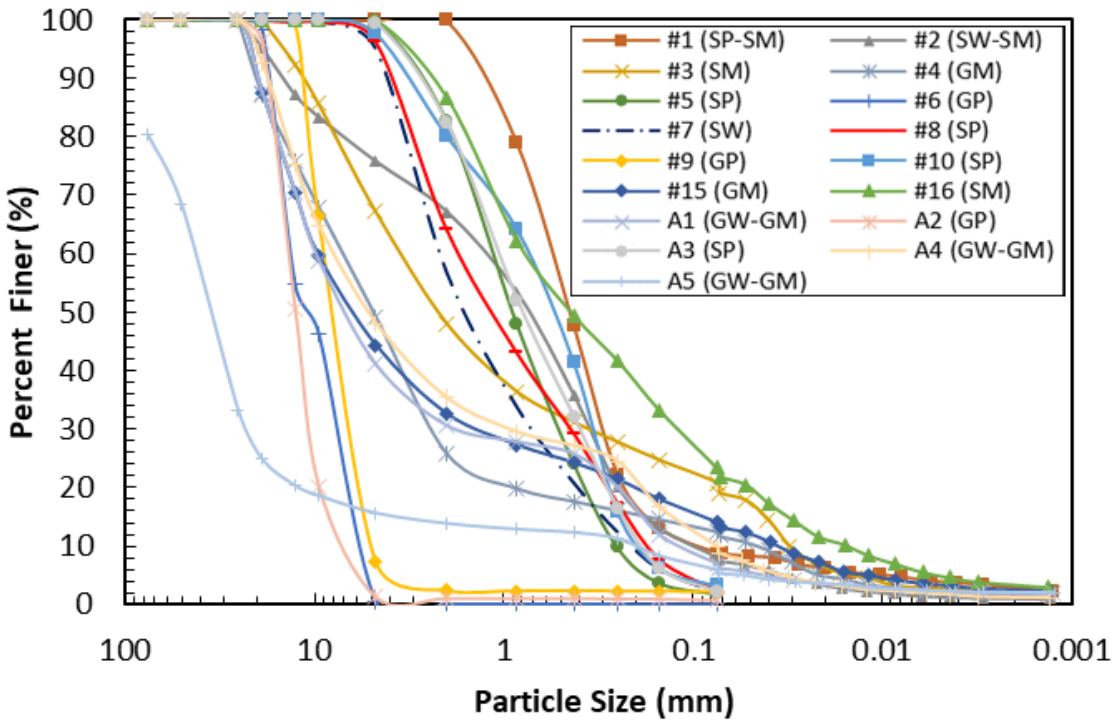

Figure 2.2 Particle-size distribution curves for 17 samples

Table 2.2 Index properties of 17 samples

Specimen	Particle Size Parameters						USCS
	D_{10} (mm)	D_{30} (mm)	D_{50} (mm)	D_{60} (mm)	C_u	C_c	
#1	0.09	0.30	0.46	0.55	5.9	1.8	SP-SM
#2	0.10	0.36	0.72	1.38	13.5	0.9	SW-SM
#3	0.03	0.36	2.28	3.65	114.8	1.1	SM
#4	0.05	2.50	4.90	7.09	154.1	19.2	GM
#5	0.27	0.52	0.90	1.26	4.8	0.8	SP
#6	5.85	7.70	10.90	14.00	2.4	0.7	GP
#7	0.22	0.72	1.70	2.20	10.1	1.1	SW
#8	0.18	0.45	1.30	1.82	10.1	0.6	SP
#9	5.00	6.60	8.05	8.95	1.8	0.97	GP
#10	0.20	0.33	0.53	0.72	3.6	0.8	SP
#15	0.04	1.58	6.35	9.50	256.8	7.1	GM
#16	0.02	0.13	0.44	0.79	46.9	1.3	SM
A1	0.13	1.82	7.00	9.92	76.3	2.6	GW-GM
A2	7.19	11.20	12.80	14.40	2	1.2	GP
A3	0.19	0.40	0.80	1.10	5.7	0.8	SP
A4	0.08	0.93	5.20	7.99	102.4	1.4	GW-GM
A5	0.20	23.00	35.80	42.50	212.5	62.2	GW-GM

Note: D_{10}, D_{30}, D_{50}, D_{60} = particle sizes corresponding to 10%, 30%, 50%, 60% finer, respectively; C_u = coefficient of uniformity; C_c = coefficient of curvature; USCS = unified soil classification system

Uniformity coefficient (C_u) is a quantitative indicator of the breadth of the particle-size distribution. A large C_u value indicates that the soil has a wide range of particle-size distribution, ranging from large to small particles (e.g., SW). A low C_u value indicates that the soil has a narrow range of particle-size distribution (e.g., SP). Some of the 17 soils had very high C_u (e.g., 256.8 C_u value for #15) primarily due to the presence of large gravels and fine particles. Nominally, soils that have high C_u values may have lower hydraulic conductivity than soils that have low C_u values, as liquid flow through the soil is predominantly governed by the finer-grained fraction for well-graded materials. The effect of high C_u on measured hydraulic conductivity is further discussed in Chapter 4.

2.3 HYDRAULIC CONDUCTIVITY TESTING

Saturated hydraulic conductivity values (K_{sat}) were determined for samples compacted in a rigid-walled permeameter using the constant head method (ASTM D2434). Figure 2.3(a) is a schematic of the constant head test apparatus, which includes a permeameter for the soil sample and water reservoir system for applying water flow driven by a constant hydraulic gradient ($i = \Delta H/L$). Figure 2.3(b) is a photograph of the apparatus used in this series of tests. The system has been specifically designed for application to relatively coarse-grained (e.g., sand or gravel) materials by using large-diameter tubing and low-head-loss fittings intended to minimize system head losses that are not attributable to flow through the (relatively low head loss) test material. The permeameter included a screen and rubber O-rings to prevent particle loss and water leakage and consisted of acrylic cell to visually observe if the soil sample includes air bubbles that can cause a potential error. Sample geometry included a height of 11.68 cm (4.6 in), diameter of 15.24 cm (6 in.), and corresponding cross-sectional flow area (A) of 182.41 cm^2. Although the permeameter is designed to measure K_{sat} for gravels and sandy soils, the permeameter was not applicable for A5 due to the predominance of large gravels (see Figure 2.1(q) and Figure 2.2). Further discussion and analysis of sample A5 is not included in this report.

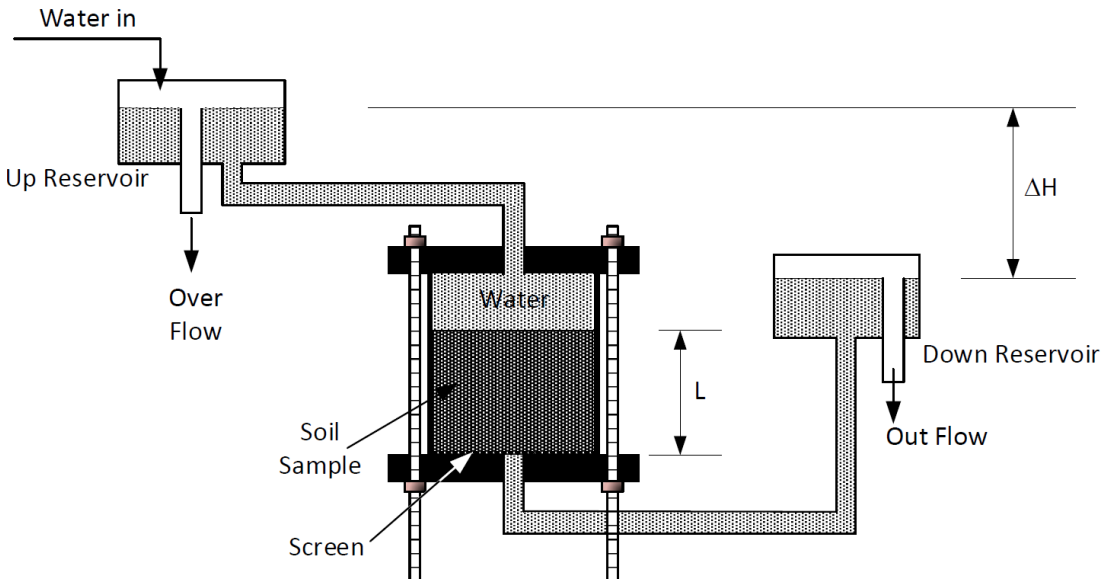

(a)

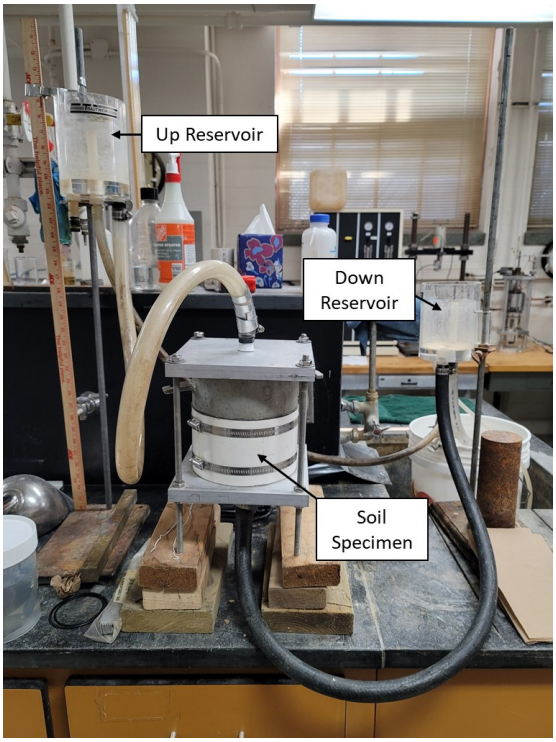

(b)

Figure 2.3 Constant head hydraulic conductivity test apparatus: (a) schematic and (b) photograph

Materials were dried in an oven at 105 °C for 24 h prior to hydraulic conductivity testing. Oven-dried soil was compacted in lifts in the permeameter, and the final weight and volume were recorded to calculate soil dry unit weight (γ_d). Table 2.3 summarizes dry unit weights for the hydraulic conductivity testing series, as well as the SWCC testing series for comparison (described subsequently). The percent difference in dry unit weight between the two tests did not exceed 0.63%, indicating that results from the two-test series could be reliably compared.

Table 2.3 Dry unit weight of the soil specimens in K_{sat} and SWCC tests

Sample	Dry Unit Weight (kN/m^3)		% Difference
	K_{sat}	SWCC	
#1 (SP-SM)	18.6	18.5	0.54%
#2 (SW-SM)	19.6	19.6	0.00%
#3 (SM)	17.8	17.8	0.00%
#4 (GM)	17.8	17.8	0.00%
#5 (SP)	15.9	16.0	0.63%
#6 (GP)	16.2	16.3	0.62%
#7 (SW)	18.7	18.6	0.54%
#8 (SP)	20.1	20.1	0.00%
#9 (GP)	16.6	16.6	0.00%
#10 (SP)	18.3	18.3	0.00%
#15 (GM)	18.7	18.7	0.00%
#16 (SM)	17.7	17.7	0.00%
A1 (GW-GM)	18.6	18.7	0.54%
A2 (GP)	15.9	16.0	0.63%
A3 (SP)	17.3	17.3	0.00%
A4 (GW-GM)	19.2	19.2	0.00%

Samples were saturated by applying bottom-to-top flow to remove air bubbles. Tap water was used as the saturation and permeant solution for all tests. After saturation, water was filled from the top of the soil to about three-quarters of the upper reservoir. The effluent spigot was placed at relative elevation H to create a constant hydraulic gradient, and the valves were opened to initiate water flow. Discharge flow rate (Q = V/t) was measured gravimetrically to calculate K_{sat} from Darcy's Law (eq. 2.3):

$$K_{sat} = \frac{V*L}{t*A*H} \tag{2.3}$$

where K_{sat} = saturated hydraulic conductivity [cm/sec], V = total quantity of water collected [cm^3], L = length of soil column [cm], t = time period of measurement [s], A = cross-sectional area of soil column [cm^2], H = constant head difference [cm].

Hydraulic conductivity testing was repeated for each sample using five hydraulic gradients (i = H/L = 0.25, 0.5, 1.0, 1.5, and 2.0) that were selected to represent a range of field scenarios for typical pavement base course applications and to quantify any effects of applied hydraulic gradient on the

measured hydraulic conductivity. Average K_{sat} values from test tests spanning the range of gradients were calculated for subsequent modeling and analysis.

2.4 SOIL-WATER CHARACTERISTIC CURVE TESTING

Soil water characteristic curves (SWCCs) for the materials were measured using a hanging column test apparatus (ASTM D6836). Figures 2.4(a) and (b) show a schematic and photograph of the testing apparatus, respectively. The apparatus includes a large-diameter cell containing the compacted specimen, a graduated outflow tube for measuring effluent water, and two reservoirs with a manometer for applying suction pressure. Specimen diameter in the cell was 30.6 cm, while the specimen height varied from 3.0 cm to 5.0 cm depending on grain size in order to maintain a representative grain size distribution.

Samples for SWCC testing were compacted directly into the test cell to dry density values within 1% of values used in the hydraulic conductivity tests (Table 2.3). The samples were saturated using tap water. SWCCs were obtained along primary drying curves initiating at zero matric suction at full saturation to matric suction of approximately 100 kPa. The highest applied suction corresponded to degree of saturation ranging from near zero to 30%, depending on the material. Suction was applied in a series of increments from 0.05 kPa to 100 kPa. The equilibrium position of the air-water interface in the graduated outflow tube was measured to determine the volume of effluent for each increment and calculate corresponding soil water content to produce the SWCC.

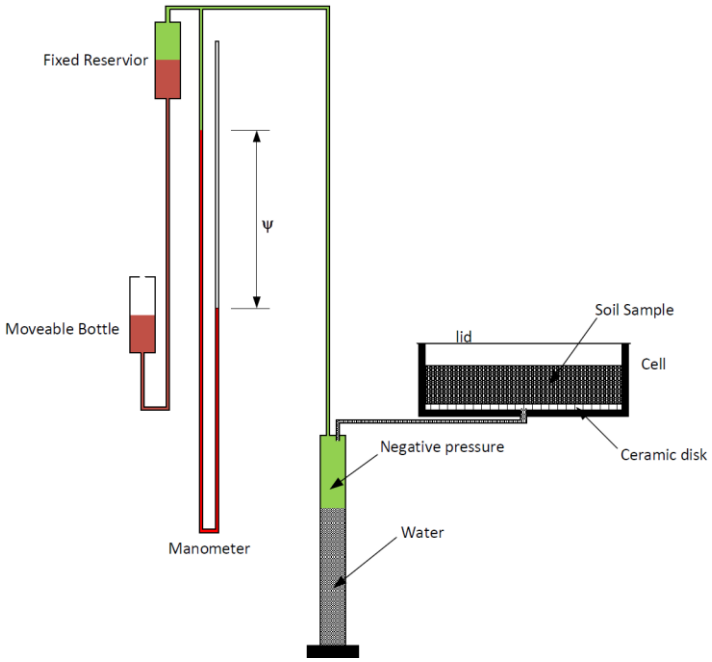

(a)

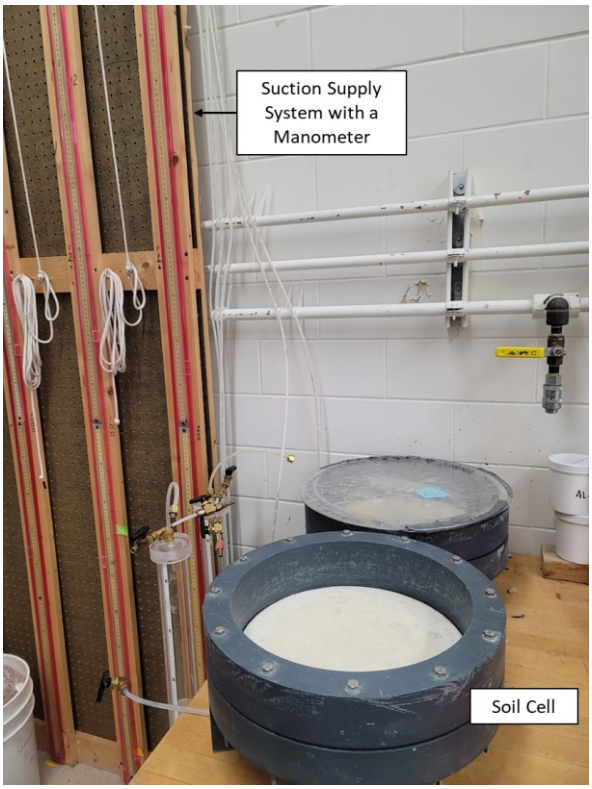

(b)

Figure 2.4 Large-scale hanging column apparatus: (a) schematic and (b) photograph

CHAPTER 3: EXPERIMENTAL RESULTS

3.1 HYDRAULIC CONDUCTIVITY

Figure 3.1 presents hydraulic conductivity results at each hydraulic gradient. Averages over the range of gradient ($K_{sat,avg}$) are represented as dashed lines. K_{sat} values for the seven gravels and nine sandy soils are tabulated in Table 3.1 and Table 3.2, respectively. Average K_{sat} for the gravels and the sandy soils were 0.324 cm/sec and 0.014 cm/sec, respectively. While there was no significant effect of hydraulic gradient on K_{sat} for the sandy soils (i.e., standard deviation was less than 1%), hydraulic gradient affected K_{sat} measurements for the gravels (i.e., average standard deviation was 11.9%). Specifically, K_{sat} values for the gravels decreased, except #15, with an increase in gradient from 0.25 to 2.0. This is potentially due to effects of turbulent flow and/or migration and clogging of fines.

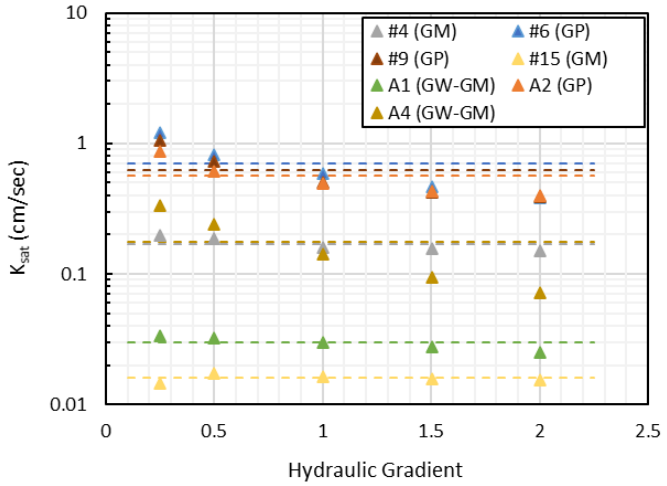

(a)

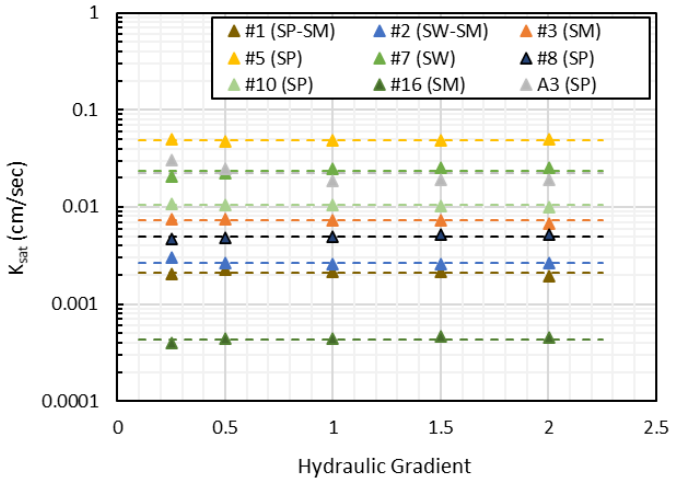

(b)

Figure 3.1 Hydraulic conductivity testing results for: (a) seven gravels and (b) nine sandy soils

Table 3.1 Hydraulic conductivity testing results for seven gravels

Sample	Saturated Hydraulic Conductivity K_{sat} (cm/sec)								Standard Deviation	Coefficient of Variation
	i = 0.25	i =0.5	i = 1.0	i = 1.5	i = 2.0	Minimum	Maximum	Average		
#4 (GM)	0.196	0.185	0.160	0.155	0.150	0.150	0.196	0.169	0.02	0.11
#6 (GP)	1.207	0.827	0.593	0.465	0.387	0.387	1.207	0.696	0.30	0.43
#9 (GP)	1.050	0.728	0.505	0.426	0.389	0.389	1.05	0.62	0.25	0.40
#15 (GM)	0.015	0.017	0.016	0.016	0.015	0.015	0.017	0.016	0.001	0.06
A1 (GW-GM)	0.034	0.032	0.030	0.028	0.025	0.025	0.034	0.03	0.003	0.10
A2 (GP)	0.874	0.612	0.493	0.434	0.396	0.396	0.874	0.562	0.17	0.31
A4 (GW-GM)	0.333	0.239	0.141	0.095	0.072	0.072	0.333	0.176	0.10	0.55

Table 3.2 Hydraulic conductivity testing results for nine sandy soils

Sample	Saturated Hydraulic Conductivity K_{sat} (cm/sec)								Standard Deviation	Coefficient of Variation
	i = 0.25	i =0.5	i = 1.0	i = 1.5	i = 2.0	Minimum	Maximum	Average		
#1 (SP-SM)	0.002	0.002	0.002	0.002	0.002	0.002	0.002	0.002	0	0.06
#2 (SW-SM)	0.003	0.003	0.003	0.003	0.003	0.003	0.003	0.003	0	0.06
#3 (SM)	0.007	0.008	0.007	0.007	0.007	0.007	0.008	0.007	0	0.04
#5 (SP)	0.050	0.048	0.048	0.049	0.050	0.048	0.05	0.049	0.001	0.01
#7 (SW)	0.021	0.023	0.024	0.025	0.025	0.021	0.025	0.024	0.002	0.08
#8 (SP)	0.005	0.005	0.005	0.005	0.005	0.005	0.005	0.005	0	0.04
#10 (SP)	0.015	0.017	0.016	0.016	0.015	0.015	0.017	0.016	0	0.02
#16 (SM)	0.0004	0.0004	0.0004	0.0005	0.0004	0.0004	0.0005	0.0004	0	0.05
A3 (SP)	0.030	0.025	0.019	0.019	0.019	0.019	0.030	0.022	0.005	0.20

3.2 SOIL-WATER CHARACTERISTIC CURVES

Figure 3.2 is a plot of soil-water characteristic curves (SWCCs) obtained from hanging column tests (represented as symbols) and van Genuchten models (represented as solid lines). As summarized in Table 3.3, fully saturated volumetric water contents (equivalent to porosity) varied from 0.23 m^3/m^3 to 0.39 m^3/m^3. As the applied suction pressure exceeded the air-entry pressure, the moisture content began to decrease. Air-entry pressures for 16 samples were determined using a pair of two tangent lines and ranged from 0.04 kPa (#4 GM) to 2.9 kPa (#2 SW-SM) with an average of 1.19 kPa (average of the seven gravels = 0.61 kPa, average of the nine sands = 1.65 kPa). The matric suction gradually increased with a decrease in the moisture. Then, the matric suction dramatically increased once the moisture content reached a residual moisture content where the moisture is adsorbed on particle surfaces as thin films due to short-ranged hydration mechanisms (Lu and Likos, 2004). Average residual water content (θ_r) for the seven gravels was 0.031, for the nine sands was 0.037, and the overall was 0.034. As described in 1.4 Background (Lu and Likos, 2004), van Genuchten α parameter is inversely proportional to the air-entry pressure and accordingly average van Genuchten α parameter for the seven gravels was remarkably higher than the average for the nine sands (average α parameter for the seven gravels = 2.99, average α parameter for the nine sands = 0.45, the overall average = 1.56). Average van Genuchten n parameter related to pore-size distribution for the seven gravels was 3.27, for the nine sands was 2.72, and for the overall was 2.96.

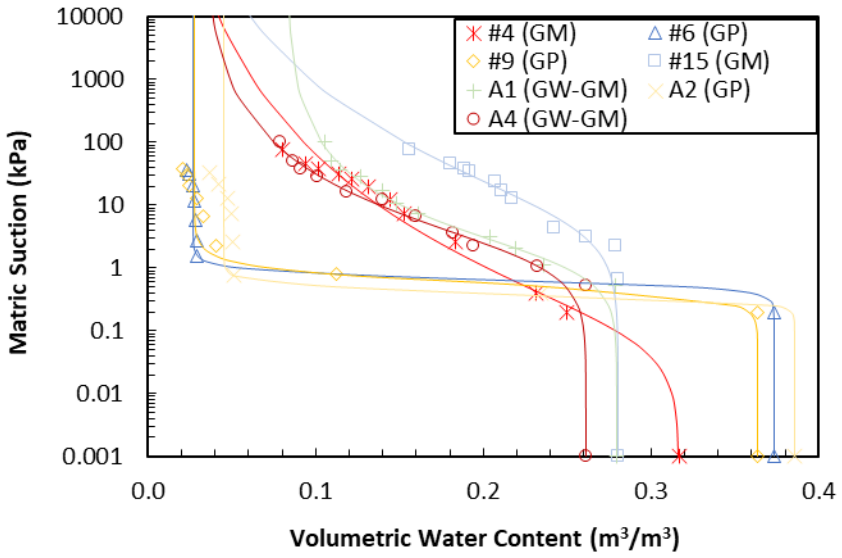

(a)

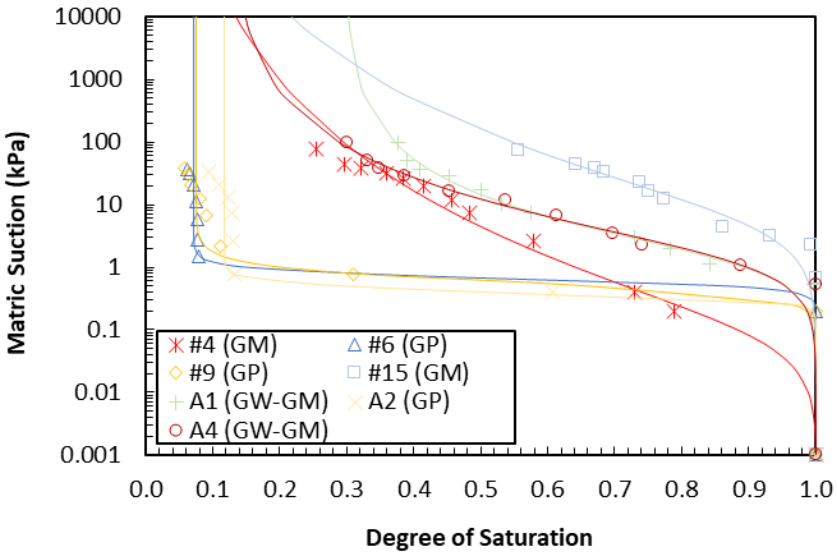
Matric Suction (kPa)
10000
1000
100
10
1
0.1
0.01
0.001
0.0
0.1
0.2
0.3
0.4
0.5
0.6
0.7
0.8
0.9
1.0
Degree of Saturation
#4 (GM)
#6 (GP)
#9 (GP)
#15 (GM)
A1 (GW-GM)
A2 (GP)
A4 (GW-GM)

(b)

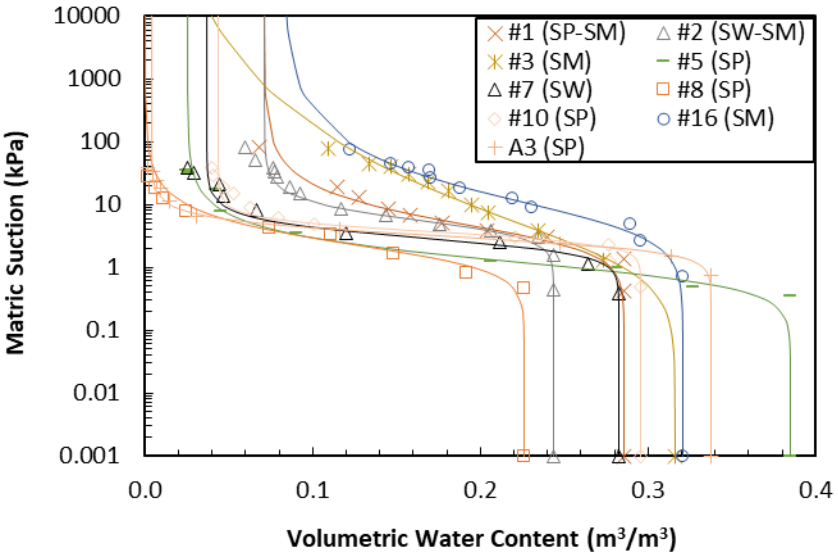
Matric Suction (kPa)
10000
1000
100
10
1
0.1
0.01
0.001
0.0
0.1
0.2
0.3
0.4
Volumetric Water Content (m³/m³)
#1 (SP-SM)
#2 (SW-SM)
#3 (SM)
#5 (SP)
#7 (SW)
#8 (SP)
#10 (SP)
#16 (SM)
A3 (SP)

(c)

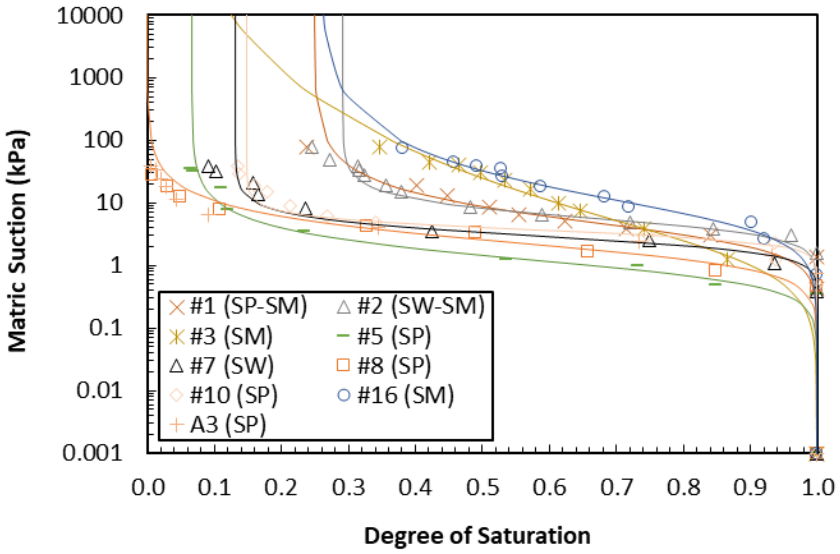

(d)

Figure 3.2 Soil-water characteristic curves for: (a) gravels regarding volumetric water content, (b) gravels regarding degree of saturation, (c) sandy soils regarding volumetric water content, and (d) sandy soils regarding degree of saturation.

Table 3.3 Summary of SWCC parameters

Sample	γ_d (kN/m^3)	Air-Entry Pressure (kPa)	van Genuchten (1980) SWCC Parameters			
			θ_r	θ_s	α	n
#1 (SP-SM)	18.5	1.80	0.07	0.29	0.29	2.09
#2 (SW-SM)	19.6	2.90	0.07	0.24	0.20	3.16
#3 (SM)	17.8	0.59	0.00	0.32	0.77	1.23
#4 (GM)	17.8	0.04	0.00	0.32	13.26	1.17
#5 (SP)	16	0.45	0.03	0.38	1.07	2.31
#6 (GP)	16.3	0.46	0.03	0.37	1.57	6.48
#7 (SW)	18.6	1.70	0.04	0.28	0.38	3.45
#8 (SP)	20.1	0.80	0.00	0.23	0.57	2.24
#9 (GP)	16.6	0.30	0.03	0.36	1.93	3.97
#10 (SP)	18.3	2.10	0.04	0.30	0.29	4.62
#15 (GM)	18.7	2.10	0.00	0.28	0.20	1.20
#16 (SM)	17.7	2.60	0.08	0.32	0.16	1.65
A1 (GW-GM)	18.7	0.51	0.08	0.28	0.74	1.52
A2 (GP)	16	0.23	0.05	0.39	2.54	7.18
A3 (SP)	17.3	1.90	0.004	0.34	0.34	3.74
A4 (GW-GM)	19.2	0.60	0.03	0.26	0.65	1.40

CHAPTER 4: ANALYSIS

4.1 HYDRAULIC CONDUCTIVITY AND INDEX PROPERTIES

Index properties including D_{10}, D_{30}, D_{50}, D_{60}, % fines, % gravel, and C_u obtained from the particle-size distribution curves were used along with as-compacted dry unit weights (γ_d) used during constant head testing to evaluate relationships between these properties and measured K_{sat} values. K_{sat} for these relationships is reported as $K_{sat,avg}$, representing an average of K_{sat} values under the five hydraulic gradients. Table 4.1 summarizes $K_{sat,avg}$ and the index properties for 16 samples.

Table 4.1 Index properties and dry unit weight (γ_d) of the soil specimens in permeameter

Sample	$K_{sat,avg}$ (cm/sec)	D_{10} (mm)	D_{30} (mm)	D_{50} (mm)	D_{60} (mm)	% Fines	% Retained Gravels	C_u	γ_d (kN/m^3)
#1 (SP-SM)	0.002	0.09	0.30	0.46	0.55	8.8	0	5.9	18.6
#2 (SW-SM)	0.003	0.10	0.36	0.72	1.38	8.2	24.3	13.5	19.6
#3 (SM)	0.007	0.03	0.36	2.28	3.65	20.8	32.8	114.8	17.8
#4 (GM)	0.169	0.05	2.50	4.90	7.09	12.5	50.8	154.1	17.8
#5 (SP)	0.049	0.27	0.52	0.90	1.26	1.9	0.3	4.8	15.9
#6 (GP)	0.696	5.85	7.70	10.90	14.00	0.2	99.4	2.4	16.2
#7 (SW)	0.024	0.22	0.72	1.70	2.20	2	4.8	10.1	18.7
#8 (SP)	0.005	0.18	0.45	1.30	1.82	2.4	3.6	10.1	20.1
#9 (GP)	0.62	5.00	6.60	8.05	8.95	2.2	92.6	1.8	16.6
#10 (SP)	0.01	0.20	0.33	0.53	0.72	3.2	2.3	3.6	18.3
#15 (GM)	0.016	0.04	1.58	6.35	9.50	14.1	55.6	256.8	18.7
#16 (SM)	0.0004	0.02	0.13	0.44	0.79	23.4	0.1	46.9	17.7
A1 (GW-GM)	0.03	0.13	1.82	7.00	9.92	7.1	59	76.3	18.6
A2 (GP)	0.562	7.19	11.20	12.80	14.40	0.8	98.6	2	15.9
A3 (SP)	0.022	0.19	0.40	0.80	1.10	2.3	0.7	5.7	17.3
A4 (GW-GM)	0.176	0.08	0.93	5.20	7.99	9.9	51.9	102.4	19.2

Figure 4.1 plots relationships between $K_{sat,avg}$ values and particle diameters corresponding to 10%, 30%, 50%, and 60% finer in each particle-size distribution curve. This includes a multivariable regression (Figure 4.1d) on both D_{10} and D_{30}. Even though there was a large gap of D_{10} data between the suite of sandy soils and gravels, [Figure 4.1(a)] for D_{10} showed the most consistent single-variable regression trend (i.e., the highest R-squared value). As the percent finer increased from D_{10} to D_{60}, the gap in particle diameters reduced with a decrease in the R-squared value. Generally, the relationships between particle size and $K_{sat,avg}$ showed similar trends. $K_{sat,avg}$ increased with increases in the particle-size parameters, due to general increases in pore sizes, particularly when the particle size was smaller than 4.75 mm. In other words, the presence of sands was more significant to $K_{sat,avg}$ than gravels.

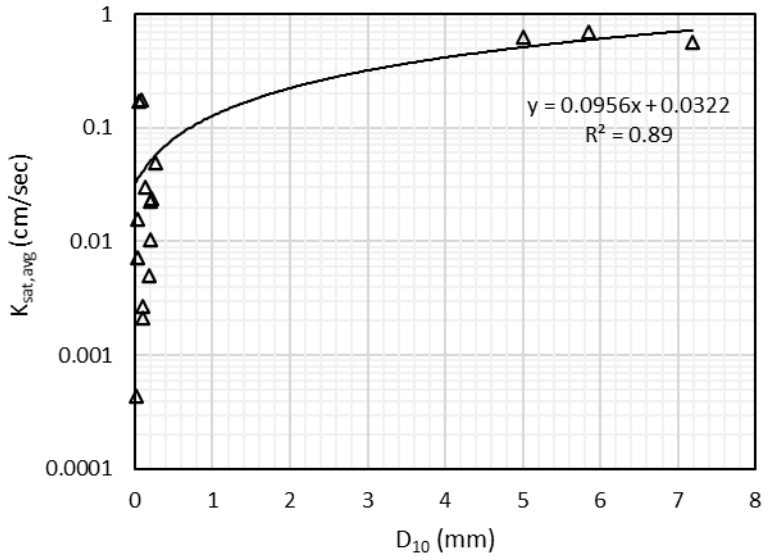
y = 0.0956x + 0.0322
R² = 0.89
K_sat,avg (cm/sec)
D10 (mm)
1
0.1
0.01
0.001
0.0001
0
1
2
3
4
5
6
7
8

(a)

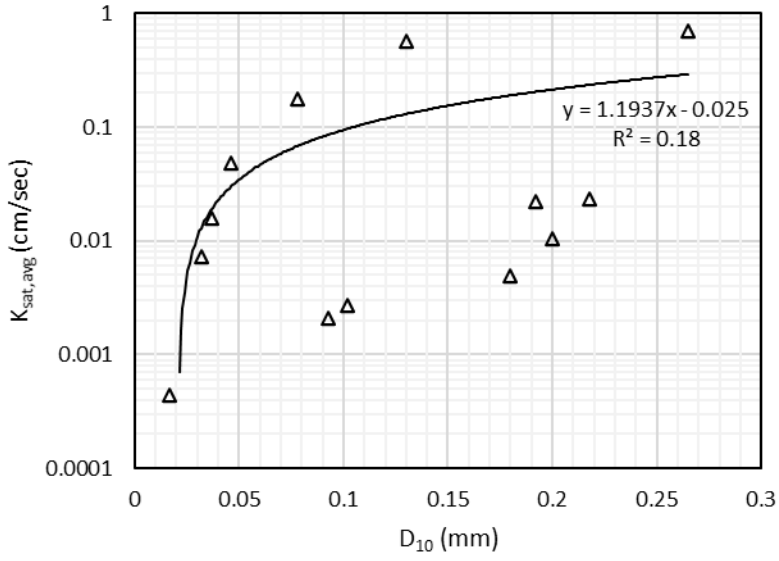
y = 1.1937x - 0.025
R² = 0.18
K_sat,avg (cm/sec)
D10 (mm)
1
0.1
0.01
0.001
0.0001
0
0.05
0.1
0.15
0.2
0.25
0.3

(b)

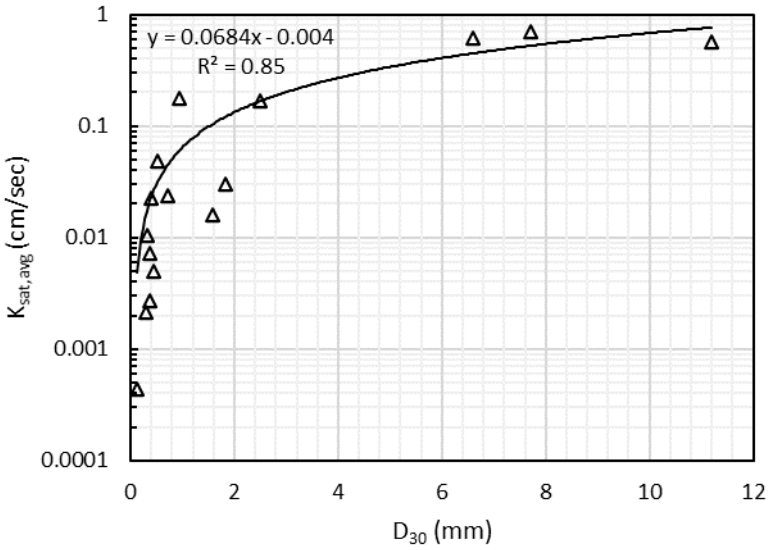
y = 0.0684x - 0.004
R² = 0.85
1
0.1
0.01
0.001
0.0001
$K_{sat,avg}$ (cm/sec)
0
2
4
6
8
10
12
D_{30} (mm)

(c)

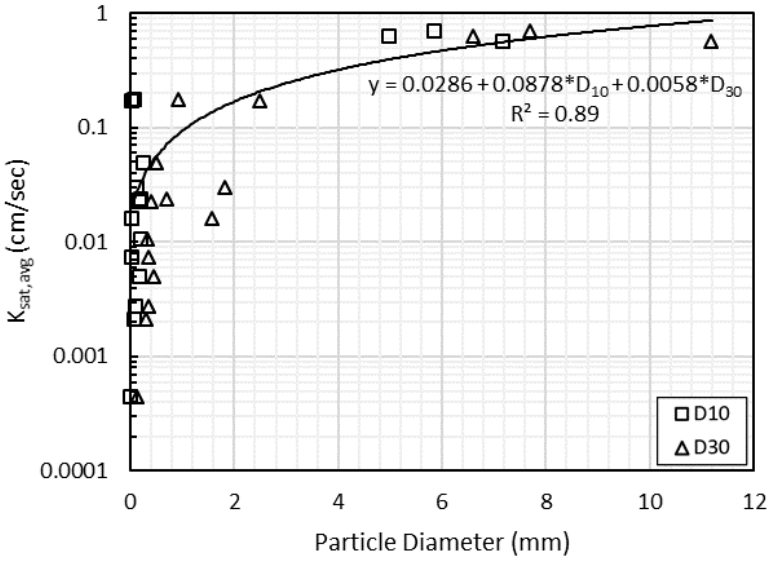
y = 0.0286 + 0.0878*D_{10} + 0.0058*D_{30}
R² = 0.89
1
0.1
0.01
0.001
0.0001
$K_{sat,avg}$ (cm/sec)
D10
D30
0
2
4
6
8
10
12
Particle Diameter (mm)

(d)

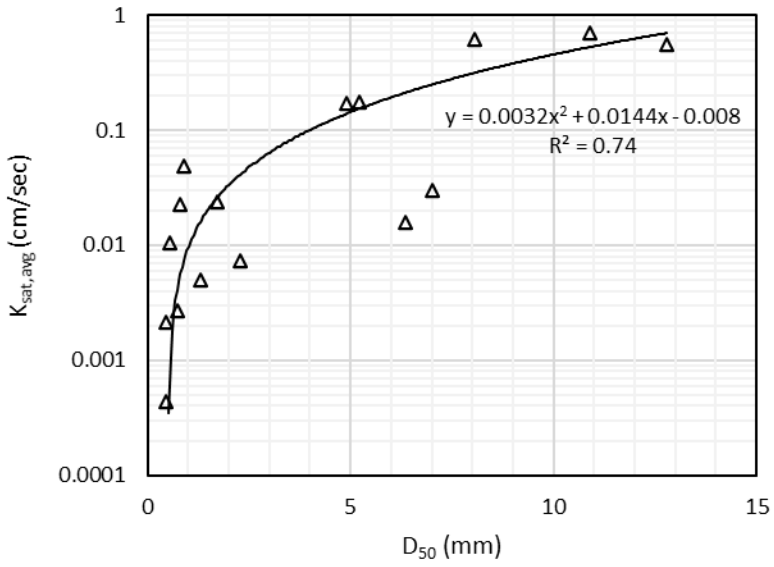

(e)

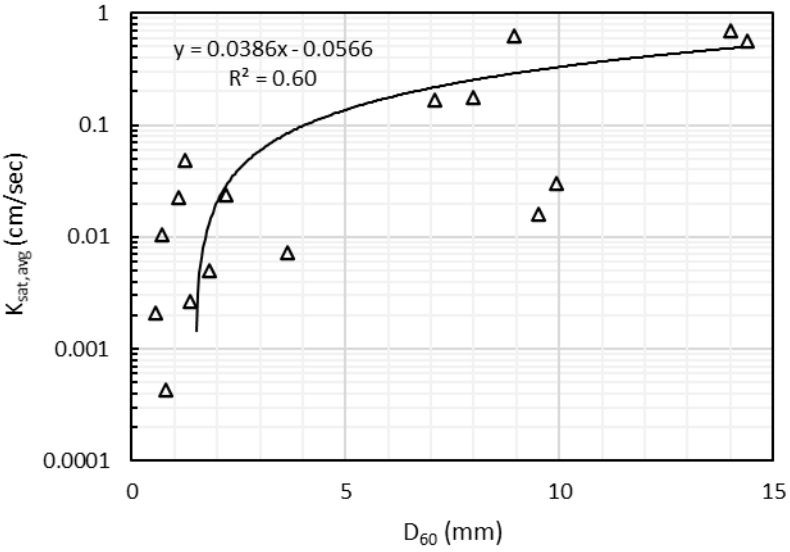

(f)

Figure 4.1 Relationships between experimentally obtained $K_{sat,avg}$ values and (a) D_{10} in full range, (b) D_{10} in small range except three outliers, (c) D_{30}, (d) multivariable on D_{10} and D_{30}, (e) D_{50}, and (f) D_{60}

Figure 4.2 is a series of relationships between K_{sat} and other index properties. In addition to the particle size effects on $K_{sat,avg}$, % gravels, fines content, C_u, and dry unit weights correlated to $K_{sat,avg}$ reflecting pore structure changes. With a decrease in % gravels and increases in fines content and dry unit weight,

the pore space where liquid flow occurs can be expected to generally decrease, resulting in the decrease in K_{sat} evident in the results. However, $K_{sat,avg}$ only slightly decreased with an increase in C_u. That is, C_u was not significantly correlated with $K_{sat,avg}$ since samples including a significant percentage of small particles can have both high and low C_u values depending on overall particle-size distribution.

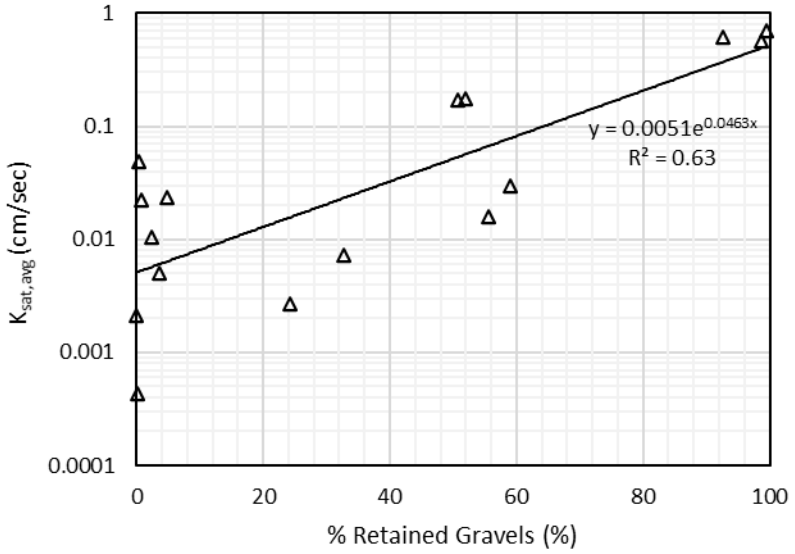

(a)

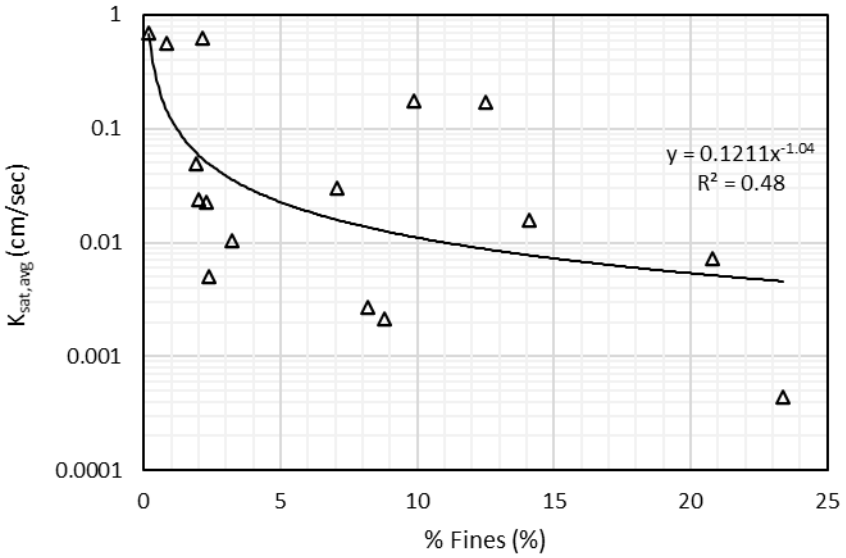

(b)

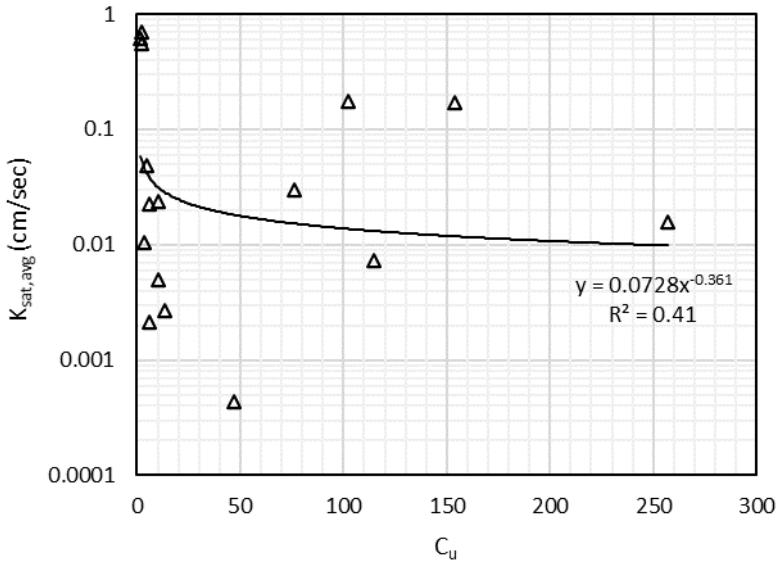

(c)

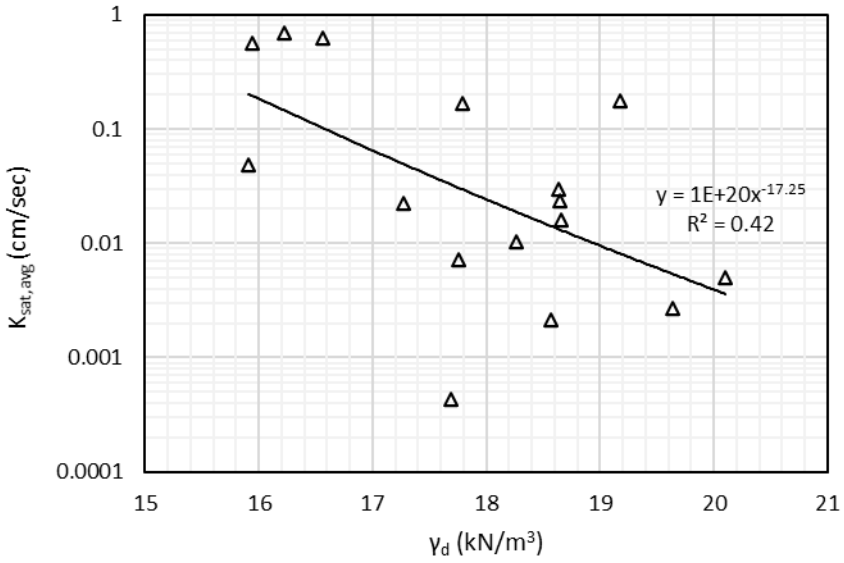

(d)

Figure 4.2 Relationships between experimentally measured $K_{sat,avg}$ and (a) %retained gravels, (b) % fines, (c) C_u, and (d) γ_d

4.2 SOIL WATER CHARACTERISTIC CURVES AND INDEX PROPERTIES

As described in the literature (e.g., Tinjum et al., 1997), shapes of the 16 SWCCs were dependent on the particle-size distributions. For example, as shown in the experimentally obtained SWCCs (Figure 3.2), matric suctions of #4, #15, A1, and A4 gravels, which had high C_u values (see Table 4.1), significantly

increased with a decrease in the moisture content (i.e., steep gradient of the SWCC slope), while only a little matric suction increases (i.e., gentle slope) were required to remove the moisture in #6, #9, and A2 gravels, which had low C_u values. As well as the effect of C_u on the SWCC shape, the air-entry pressures increased with an increase in C_u (Figure 4.3). These findings are interpreted to indicate that small particles among the gravels (i.e., samples with high C_u) decreased the pore size, thus increasing air-entry pressure and the matric suction at a given moisture content.

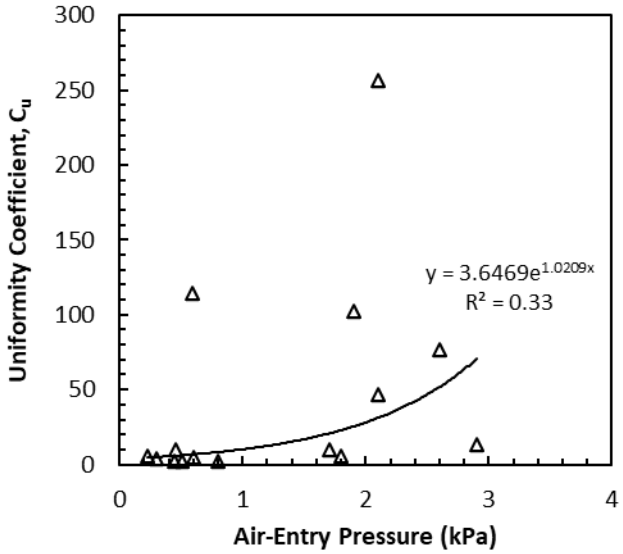

Figure 4.3 Relationship between air-entry pressure and uniformity coefficient

The van Genuchten (1980) fitting parameter α is inversely proportional to the air-entry pressure, and van Genuchten fitting parameter n is related to pore size distribution (i.e., breadth of SWCC slope). Figure 4.4 shows relationships between these two van Genuchten fitting parameters and air-entry pressures obtained from the experimentally measured SWCCs (Table 3.3). In the analysis, #4 sample, which had exceptionally higher α parameter (potentially due to experimental limitations), was excluded to analyze the relationship in detail with a rescaled y-axis. Although R-squared values of the two relationships were low, the trendlines were aligned well with the literature (e.g., Benson et al., 2014). As the air-entry pressure increased, the parameters decreased.

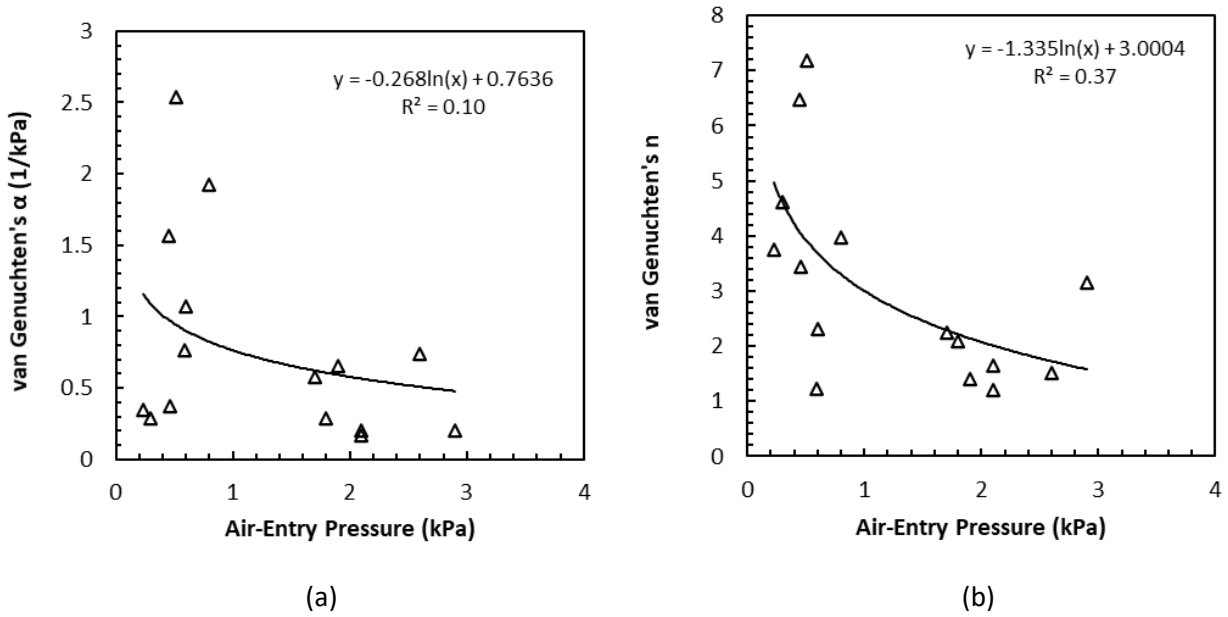

(a) (b)

Figure 4.4 Relationships between air-entry pressure and van Genuchten parameters: (a) α and (b) n

4.3 FIELD CAPACITY, EFFECTIVE POROSITY AND MINIMUM SATURATION

Table 4.2 summarizes total porosity (n), field capacity (θ_f), effective (drainable) porosity (n_d), and minimum saturation (S_{min}) for the 16 base materials used in this project. Field capacities were determined using the SWCCs as volumetric moisture contents measured at 33 kPa (see background section). Total porosity values were taken as saturated volumetric water contents (θ_s) determined from fitting the SWCCs with the van Genuchten (1980) model. Effective porosity and minimum saturation were calculated using equations 1.15 and 1.16, respectively.

Tables A3 and A4 (Appendix A) represent typical effective porosities for a wider range of materials, indicating a range from about 0.001 to 0.50 depending on soil type. Although the effective porosity for #15 GM was exceptionally lower than other samples and the typical ranges, the 15 effective porosities estimated here were generally in reasonable ranges. Minimum, maximum, and average effective porosities for the 16 samples were 0.09 (#15 GM), 0.36 (#5 SP), and 0.24, respectively, and there was no significant difference between averages for the seven gravels and the nine sands (average for the seven gravels = 0.24, average for the nine sands = 0.23).

Table 4.2 Field capacities, effective porosities, and minimum saturations for 16 samples

Sample	Total Porosity ($n = \theta_s$)	Field Capacity (θ_f)	Effective Porosity (n_d)	Minimum Saturation (S_{min})
#1 (SP-SM)	0.29	0.09	0.2	0.32
#2 (SW-SM)	0.24	0.08	0.17	0.31
#3 (SM)	0.32	0.15	0.16	0.48
#4 (GM)	0.32	0.11	0.2	0.35
#5 (SP)	0.38	0.03	0.36	0.08
#6 (GP)	0.37	0.03	0.35	0.07
#7 (SW)	0.28	0.03	0.25	0.10
#8 (SP)	0.23	0.002	0.22	0.01
#9 (GP)	0.36	0.02	0.34	0.06
#10 (SP)	0.3	0.04	0.26	0.14
#15 (GM)	0.28	0.19	0.09	0.69
#16 (SM)	0.32	0.17	0.15	0.53
A1 (GW-GM)	0.28	0.12	0.16	0.41
A2 (GP)	0.39	0.04	0.35	0.09
A3 (SP)	0.34	0.005	0.33	0.01
A4 (GW-GM)	0.26	0.10	0.17	0.36

Figure 4.5 presents a relationship between minimum saturation and % fines (%F) for the 16 samples. A linear equation capturing this relation is in the form:

$$S_{min} = 0.025(\%F) + 0.062 \ (\mathrm{R}^2 = 0.75) \tag{4.1}$$

As fines content increased, minimum saturation increased, due to potential decreases in pore sizes (i.e., increases in the matric suction), resulting in a decrease in the drainability of base materials. Similar correlations between minimum saturation and index properties (D_{10}, D_{30}, D_{50}, D_{60}, C_u, % retained gravels) were also explored, and these results are plotted in Appendix B. Minimum saturations decreased with increases in D_{10}, D_{30}, and D_{50} and a decrease in C_u due to increases in pore spaces (i.e., a decrease in the matric suction). Among the index properties, minimum saturations had relatively significant correlations with D_{10} ($R^2 = 0.66$) and C_u ($R^2 = 0.72$). Overall, minimum saturations decreased (i.e., an increase in the drainability) with decreases in % fines and C_u and an increase in D_{10}.

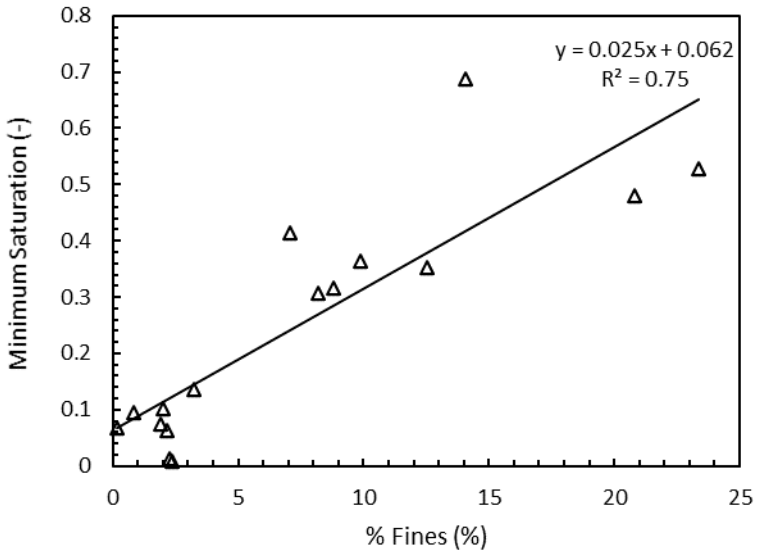

Figure 4.5 Relationship between 16 minimum saturations and % fines

4.4 HYDRAULIC CONDUCTIVITY AND SWCC PARAMETERS

Experimentally measured $K_{sat,avg}$ and van Genuchten parameters (α and n) of 15 samples (#4 was excluded due to the exceptionally high α parameter) were compared to evaluate how the SWCC is correlated to K_{sat}. The K_{sat} testing results and the two van Genuchten fitting parameters are summarized in Table 4.3. Figure 4.6 presents relationships between the $K_{sat,avg}$ and the two fitting parameters. When the α and n parameters increased, K_{sat} increased. As described above, the high α and n parameters indicate low air-entry pressure and SWCC breadth, respectively. Namely, K_{sat} increased with decreases in the air-entry pressure and SWCC breadth (i.e., the decreased matric suction).

Table 4.3 Summary of $K_{sat,avg}$ testing results and van Genuchten fitting parameters

Sample	$K_{sat,avg}$ (cm/sec)	van Genuchten (1980) SWCC Parameters			
		θ_r	θ_s	α	n
#1 (SP-SM)	0.002	0.07	0.29	0.29	2.09
#2 (SW-SM)	0.003	0.07	0.24	0.20	3.16
#3 (SM)	0.007	0.00	0.32	0.77	1.23
#4 (GM)	0.169	0.00	0.32	13.26	1.17
#5 (SP)	0.049	0.03	0.38	1.07	2.31
#6 (GP)	0.696	0.03	0.37	1.57	6.48
#7 (SW)	0.024	0.04	0.28	0.38	3.45
#8 (SP)	0.005	0.00	0.23	0.57	2.24
#9 (GP)	0.62	0.03	0.36	1.93	3.97
#10 (SP)	0.01	0.04	0.30	0.29	4.62
#15 (GM)	0.016	0.00	0.28	0.20	1.20
#16 (SM)	0.0004	0.08	0.32	0.16	1.65
A1 (GW-GM)	0.03	0.08	0.28	0.74	1.52
A2 (GP)	0.562	0.05	0.39	2.54	7.18
A3 (SP)	0.022	0.004	0.34	0.34	3.74
A4 (GW-GM)	0.176	0.03	0.26	0.65	1.40

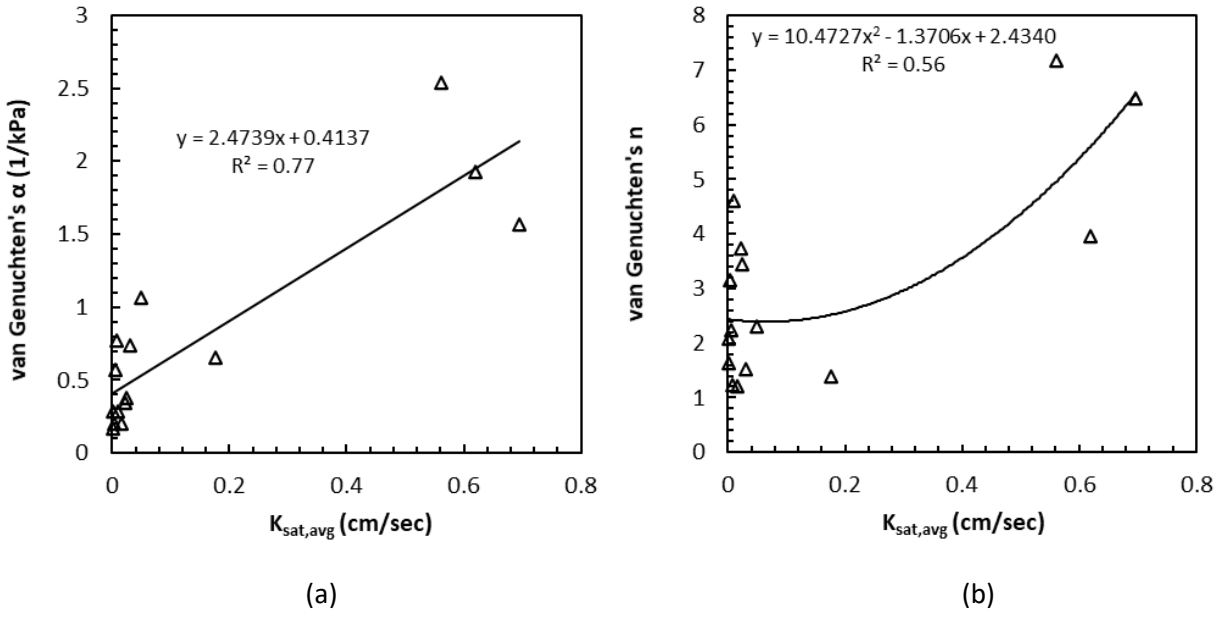

(a) (b)

Figure 4.6 Relationships between van Genuchten parameters of $K_{sat,avg}$ for 15 samples: (a) relationship between van Genuchten parameter α and average $K_{sat,avg}$ and (b) relationship between van Genuchten parameter n and average $K_{sat,avg}$

4.5 HYDRAULIC CONDUCTIVITY FUNCTIONS

The unsaturated hydraulic conductivity function proposed by van Genuchten (1980) is one of the most widely used equations in geotechnical engineering practice (Lu and Likos, 2004). The equation proposed by van Genuchten (1980) describes a relationship between matric suction (ψ) and relative hydraulic conductivity (K_r), which is defined as a ratio of unsaturated (K_U) to saturated hydraulic conductivity (K_{sat}), as described in 1.4.7 Hydraulic Conductivity Function Modeling chapter. Unsaturated hydraulic conductivity functions for the 16 samples were calculated using eq. (1.13) and the experimentally obtained data for K_{sat} and van Genuchten fitting parameters.

Figure 4.7 summarizes hydraulic conductivities as a function of the matric potential for the 16 samples. Hydraulic conductivities of the samples that have a relatively high n fitting parameter were significantly decreased (e.g., n parameter for #6 GP = 6.48, n parameter for #9 GP = 3.97, n parameter for #10 SP = 4.62, n parameter for A2 GP = 7.18) as the high n parameter indicates a narrow distribution of pore sizes (Benson et al., 2014).

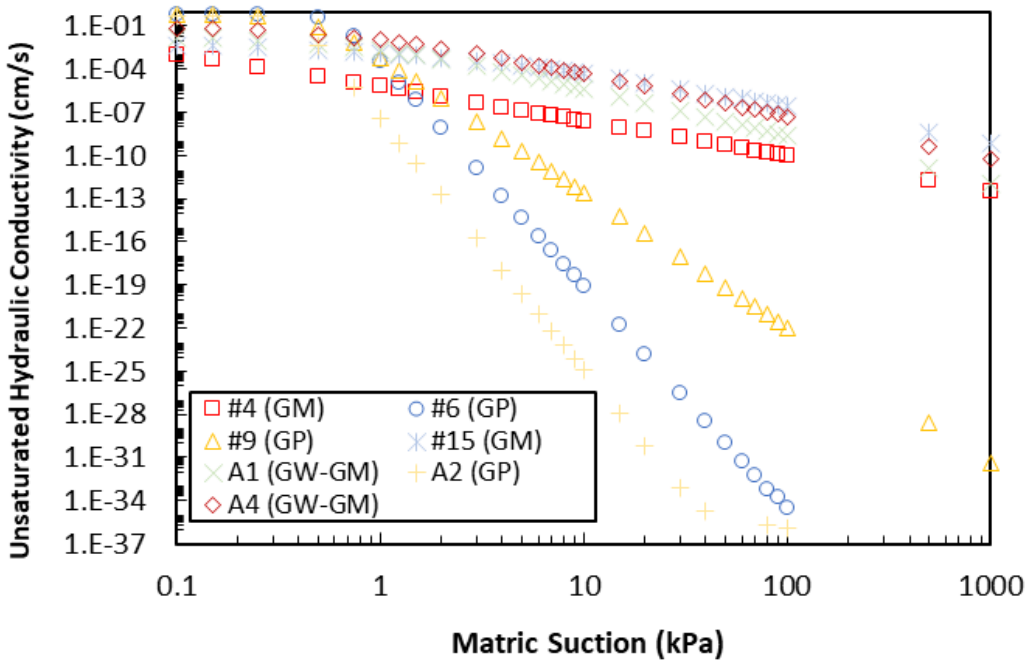

(a)

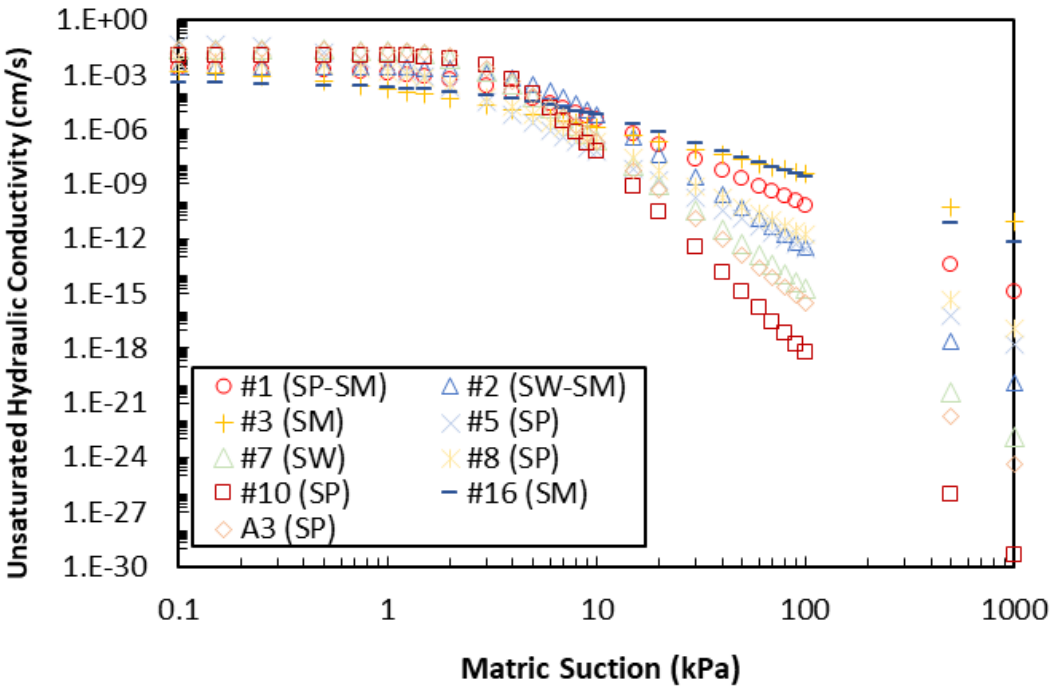

(b)

Figure 4.7 Hydraulic conductivity functions using van Genuchten (1980) approach: (a) unsaturated hydraulic conductivity functions for six gravels, and (b) unsaturated hydraulic conductivity functions for nine sandy soils.

4.6 SATURATED HYDRAULIC CONDUCTIVITY MODELS

4.6.1 Models from the Literature

As summarized in Appendix C, there are a large number of empirical equations that may be used to estimate K_{sat}. Most of the equations are based on soil physical properties, particularly particle-size distributions (e.g., D_{10}) that can be readily obtained by the sieve test.

13 applicable model equations were selected among the empirical equations described in Appendix C to estimate K_{sat} values for the 16 samples. The selected empirical equations were primarily based on soil porosity and index properties directly obtained from a particle-size distribution curve. The equations used in this study were as follows: Alyamani and Sen (Equation C.21), Beyer (Equation C.12), Harleman et al. (Equation C.11), original Hazen (Equation C.1a), modified Hazen (Equation C.1b), Kozeny (Equation C.9), Kozeny-Carman (Equation C.10), Sauerbrei (Equation C.19), Slichter (Equation C.3), Terzaghi (Equation C.5), U.S. Bureau of Reclamation (Equation C.20), Salarashayeri and Siosemarde (Equation C.25), and Chapuis (Equation C.28).

Table 4.4 summarizes measured and estimated K_{sat} values for the 16 samples. K_{sat} values estimated for #6, #9 and A2 gravels (poorly graded gravels, GP), only except two K_{sat} values estimated using Original

Hazen (C.1a) and Salarashayeri and Siosemarde (Equation C.25), were significantly higher than the experimentally measured K_{sat} values. The three GPs had higher D_{10} values (D_{10} for #6 = 5.85 mm, D_{10} for #9 = 5.00 mm, D_{10} for A2 = 7.19 mm) than other gravels (D_{10} values were less than 2.5 mm), and the high D_{10} values caused the overestimations. Except the three GPs, the K_{sat} estimations were in reasonable ranges showing low standard deviations (less than 3%).

Averages of K_{sat} values estimated using the empirical equations for each sample (i.e., Avg. row in Table 4.4) were compared to averages of the experimentally measured K_{sat} values under the five hydraulic gradients (Figure 4.8). The solid line in the figure denotes 1:1 correspondence and the dashed lines denote correspondence plus or minus 10%. The three GPs, #6, #9, and A2, were excluded in the analysis. K_{sat} values for #4 and A4 gravels (GM and GW-GM, respectively) were significantly underestimated, as highlighted in red [Figure 4.8(a)]. This suggests that the empirical equations considered may not be applicable for estimating K_{sat} of gravels as estimation results for the five gravels out of total seven gravel samples (#4, #6, #9, A2, A4) were exceptionally out of range. The two gravels, as well as the three GPs, were excluded and the axes were rescaled in Figure 4.8(b) to compare the results in detail. Although #15 and A1 gravels (GM and GW-GM, respectively) were still underestimated as highlighted in red [Figure 4.8(b)], the estimations for #15 and A1 were in reasonable ranges compared to the estimations for other five gravels as described above.

In addition to the comparisons of average K_{sat} values obtained from experiments and estimations, K_{sat} values estimated using each of the empirical equations for the 11 samples that excluded the five outliers (i.e., #4, #6, #9, A2, and A4 gravels) were individually compared to averages of experimentally measured k_{sat} values obtained under the five hydraulic gradients (Figure 4.9). The K_{sat} values were underestimated when K_{sat} values were estimated using original Hazen (1892), Kozeny (1953), Kozeny-Carman (Kozeny, 1953; Carman, 1956), Slichter (1899), Terzaghi (1925), and U.S. Bureau of Reclamation, while the K_{sat} values were overestimated when they were estimated using Alyamani and Sen (1993). Furthermore, when K_{sat} values were estimated using Alyamani and Sen (1993), Beyer (1964), modified Hazen (1892), Salarashayeri and Siosemarde (2012), the estimated k_{sat} values were scattered. Overall, the K_{sat} estimations were relatively well aligned with the experimentally measured K_{sat} values for aggregate base and sand when K_{sat} values were estimated using Chapuis (2004), Harleman et al. (1963), and Sauerbrei (1932).

Table 4.4 Summary of saturated hydraulic conductivity estimated using 13 applicable empirical equations

Method	Saturated Hydraulic Conductivity (cm/sec)															
	#1	#2	#3	#4	#5	#6	#7	#8	#9	#10	#15	#16	A1	A2	A3	A4
M1	0.008	0.009	0.007	0.028	0.063	39.539	0.046	0.033	31.235	0.047	0.042	0.0004	0.071	60.103	0.038	0.037
M2	0.010	0.010	0.000	0.001	0.083	46.499	0.047	0.032	35.815	0.050	0.000	0.0002	0.008	72.582	0.042	0.002
M3	0.006	0.004	0.001	0.003	0.075	8.565	0.021	0.008	5.972	0.021	0.001	0.0005	0.009	12.985	0.029	0.003
M4	0.006	0.007	0.001	0.001	0.045	21.833	0.030	0.021	15.949	0.026	0.001	0.0002	0.011	32.981	0.024	0.004
M5	0.007	0.006	0.001	0.002	0.001	0.442	0.000	0.000	0.304	0.000	0.000	0.0000	0.000	0.701	0.000	0.000
M6	0.009	0.010	0.001	0.002	0.070	34.223	0.048	0.032	25.000	0.040	0.001	0.0003	0.017	51.696	0.037	0.006
M7	0.000	0.000	0.000	0.000	0.009	3.985	0.002	0.001	2.514	0.002	0.000	0.0000	0.001	6.782	0.003	0.000
M8	0.002	0.002	0.000	0.001	0.062	26.658	0.012	0.004	16.817	0.012	0.000	0.0001	0.004	45.370	0.018	0.001
M9	0.013	0.004	-	-	0.024	0.538	-	0.002	0.505	0.025	-	0.0009	-	0.691	0.017	-
M10	0.008	0.005	0.001	0.030	0.069	22.092	0.020	0.005	14.761	0.015	0.003	0.0004	0.008	47.376	0.024	0.003
M11	0.001	0.001	0.000	0.000	0.032	13.960	0.008	0.003	9.091	0.008	0.000	0.0001	0.003	23.122	0.010	0.001
M12	0.002	0.001	0.000	0.001	0.040	17.614	0.009	0.002	11.399	0.009	0.000	0.0001	0.003	29.295	0.013	0.001
M13	0.002	0.003	0.000	0.045	0.007	4.930	0.008	0.003	3.524	0.003	0.001	0.0001	0.002	10.459	0.003	0.001
Avg.	0.006	0.005	0.001	0.008	0.047	17.499	0.021	0.012	12.613	0.021	0.004	0.0003	0.011	28.449	0.021	0.005
STDV	0.003	0.003	0.002	0.014	0.026	13.763	0.016	0.012	10.526	0.015	0.011	0.0002	0.017	21.717	0.013	0.009
$K_{sat,test}$	0.002	0.003	0.007	0.169	0.049	0.696	0.024	0.005	0.620	0.010	0.016	0.0004	0.030	0.562	0.022	0.176
% Diff.	93%	55%	148%	181%	5%	185%	10%	80%	181%	66%	123%	47%	93%	192%	8%	190%
Closest to K_{sat}	M13	M13	M1	M13	M4	M9	M3	M10	M9	M12	M10	M10	M6	M9	M4	M1

Note: M1 = Alyamani and Sen (1993), M2 = Beyer (1964), M3 = Chapuis et al. (2005), M4 = Harleman et al. (1963), M5 = Hazen-Original (1892), M6 = Hazen-Modified, M7 = Kozeny (1953), M8 = Kozeny-Carman (Kozeny 1927, 1953; Carman1937, 1956), M9 = Salarashayeri and Siosemarde (2012), M10 = Sauerbrei (1932), M11 = Slichter (1899), M12 = Terzaghi (1925), M13 = U.S. Bureau of Reclamation, STDV = Standard deviation, $K_{sat,test}$ = Saturated hydraulic conductivity obtained from constant head tests, % Diff. = percentage difference between average of estimations obtained using 13 equations and average of measurements under five hydraulic gradients, Closest to K_{sat} = model which is the closest to experimentally obtained K_{sat} for each sample.

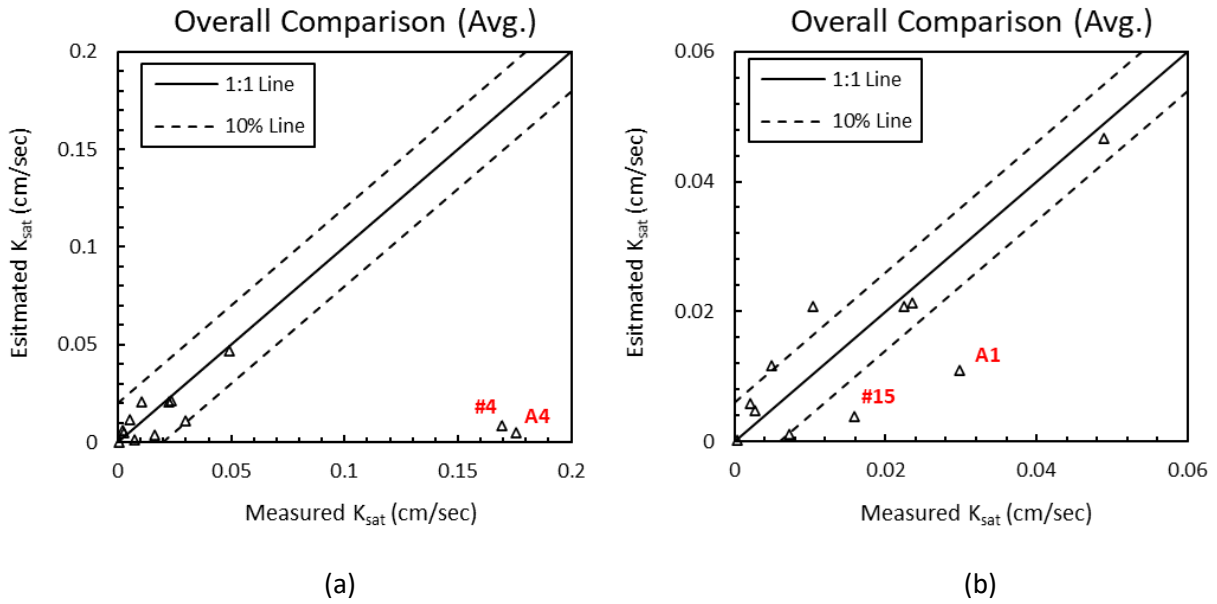

Figure 4.8 Comparisons of experimentally measured and estimated K_{sat} values for (a) 13 samples and (b) 11 samples

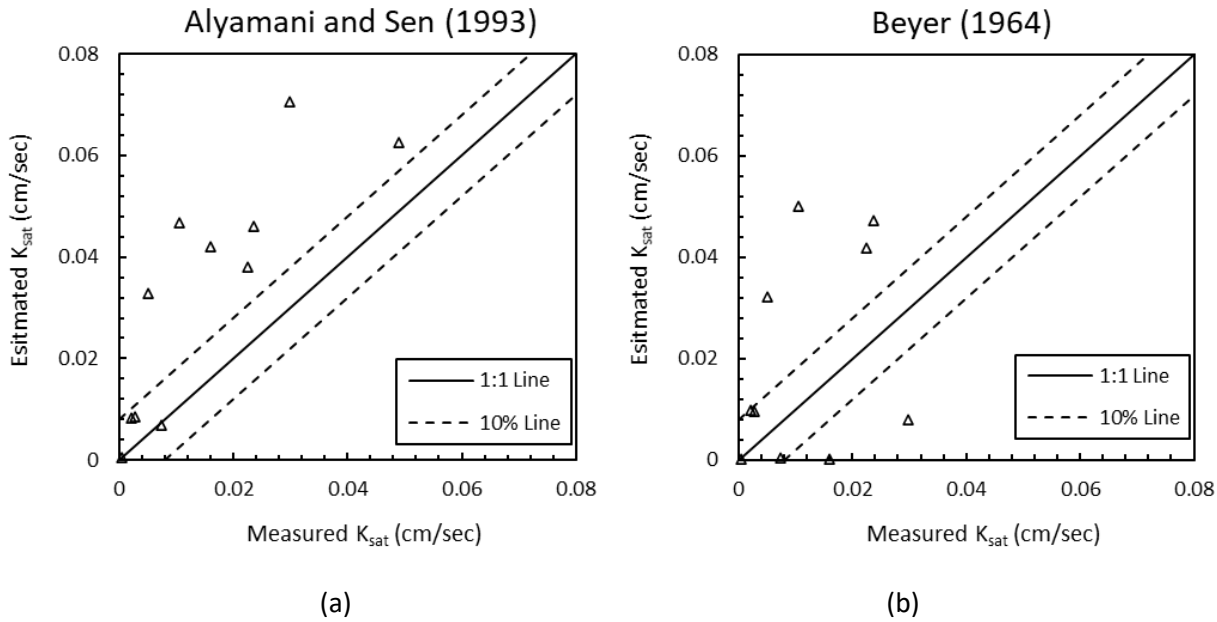

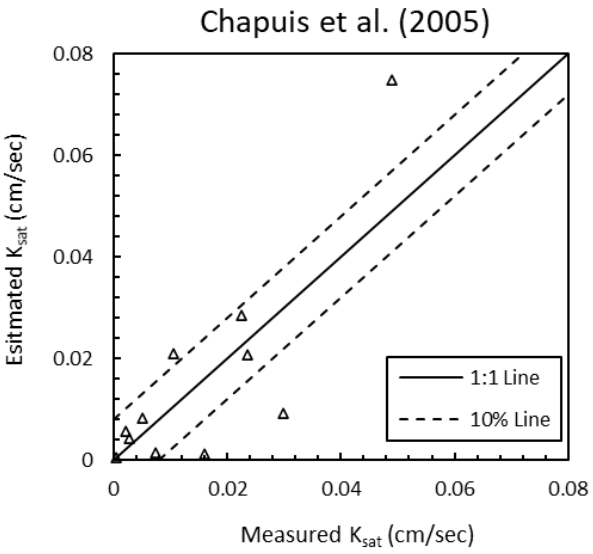
Chapuis et al. (2005)
Esitmated K_{sat} (cm/sec)
Measured K_{sat} (cm/sec)
0
0.02
0.04
0.06
0.08
1:1 Line
10% Line

(c)

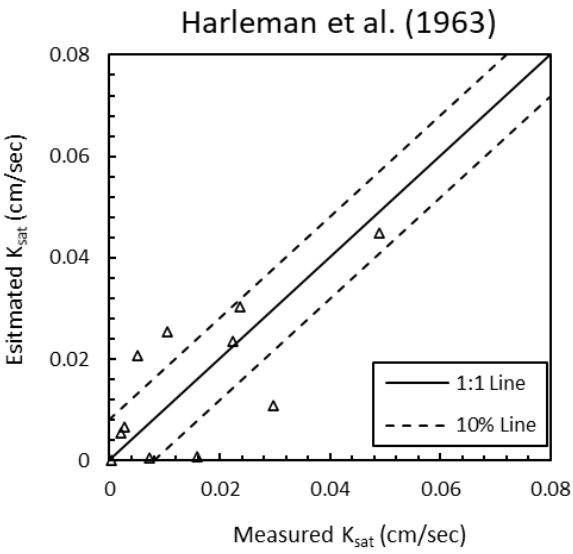
Harleman et al. (1963)
Esitmated K_{sat} (cm/sec)
Measured K_{sat} (cm/sec)
0
0.02
0.04
0.06
0.08
1:1 Line
10% Line

(d)

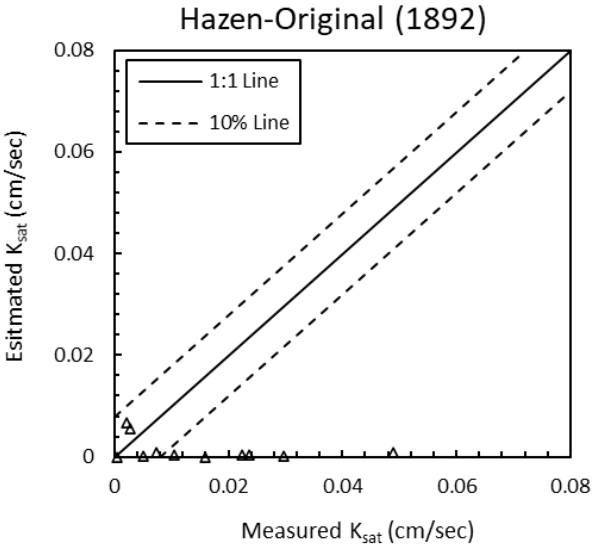
Hazen-Original (1892)
Esitmated K_{sat} (cm/sec)
Measured K_{sat} (cm/sec)
0
0.02
0.04
0.06
0.08
1:1 Line
10% Line

(e)

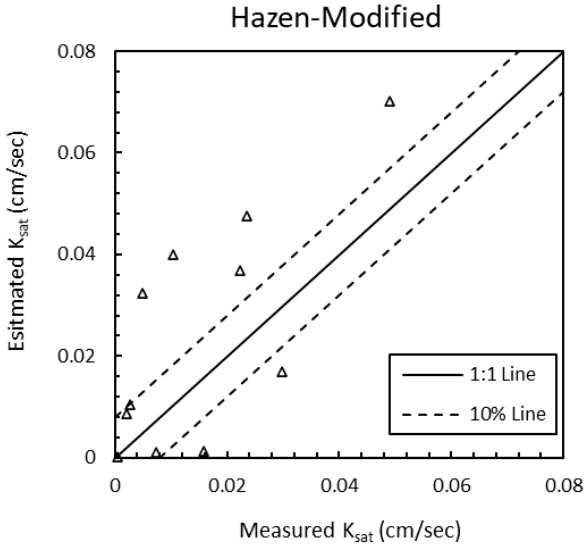
Hazen-Modified
Esitmated K_{sat} (cm/sec)
Measured K_{sat} (cm/sec)
0
0.02
0.04
0.06
0.08
1:1 Line
10% Line

(f)

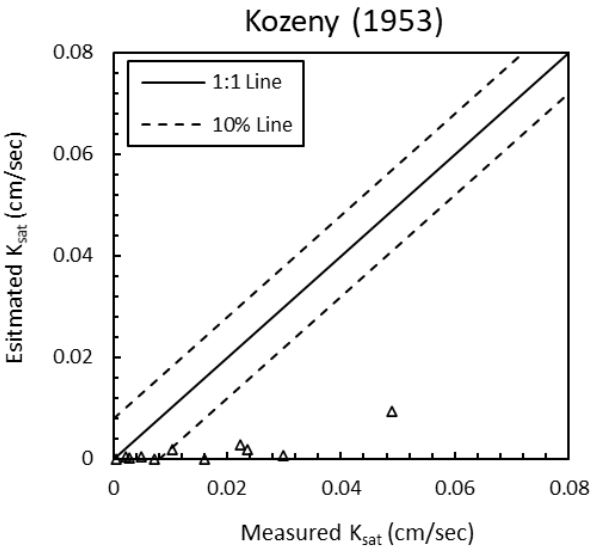
Kozeny (1953)
1:1 Line
10% Line
Esitmated K_{sat} (cm/sec)
Measured K_{sat} (cm/sec)
0
0.02
0.04
0.06
0.08

(g)

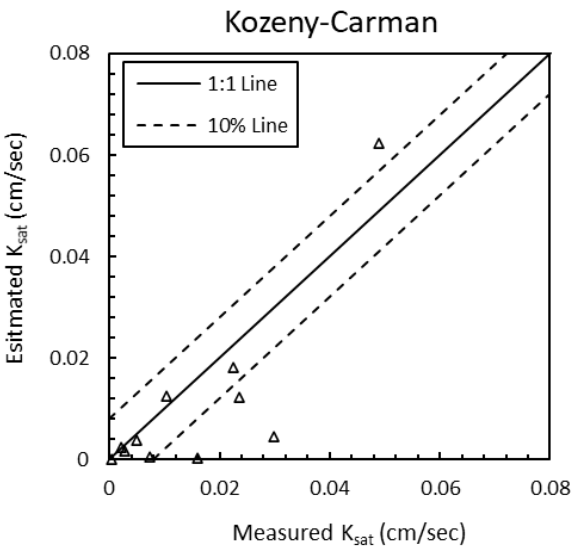
Kozeny-Carman
1:1 Line
10% Line
Esitmated K_{sat} (cm/sec)
Measured K_{sat} (cm/sec)
0
0.02
0.04
0.06
0.08

(h)

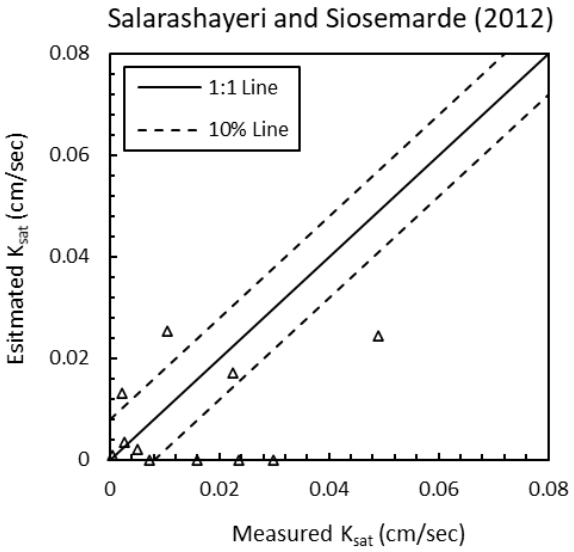
Salarashayeri and Siosemarde (2012)
1:1 Line
10% Line
Esitmated K_{sat} (cm/sec)
Measured K_{sat} (cm/sec)
0
0.02
0.04
0.06
0.08

(i)

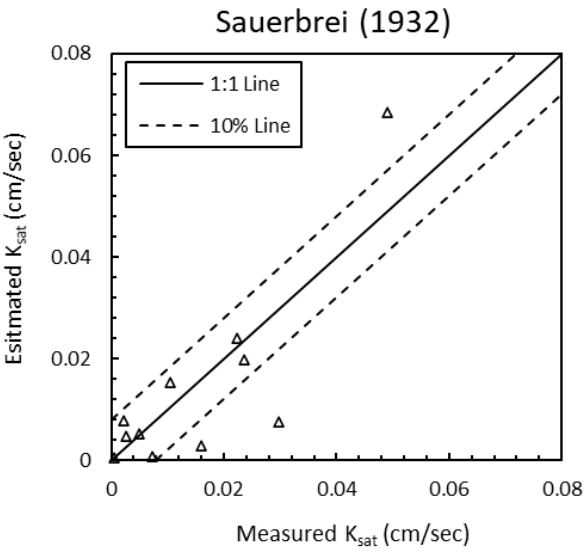
Sauerbrei (1932)
1:1 Line
10% Line
Esitmated K_{sat} (cm/sec)
Measured K_{sat} (cm/sec)
0
0.02
0.04
0.06
0.08

(j)

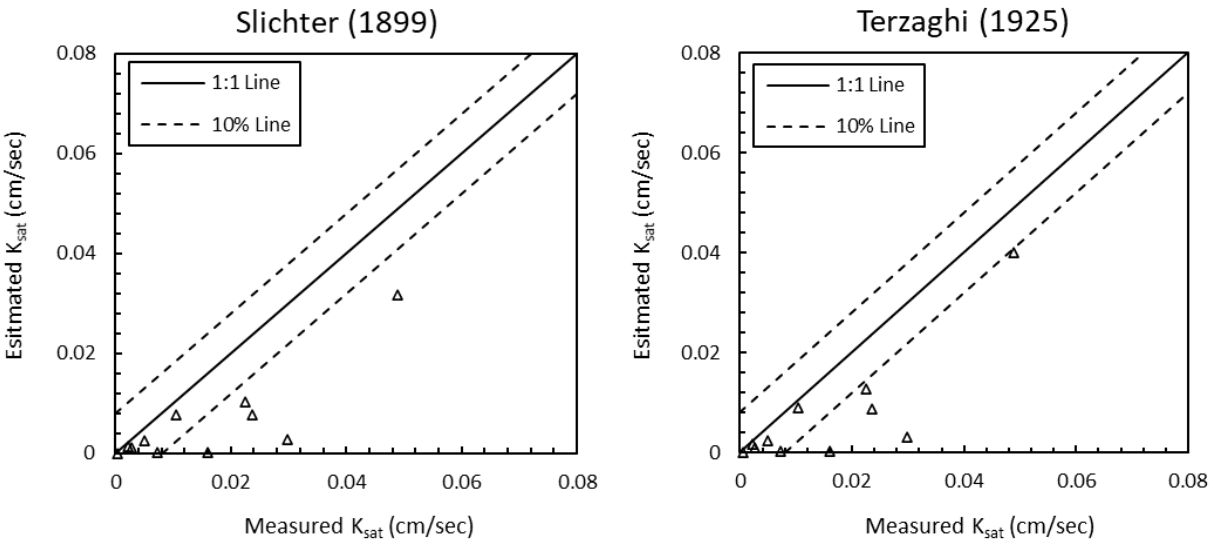

(k)

(l)

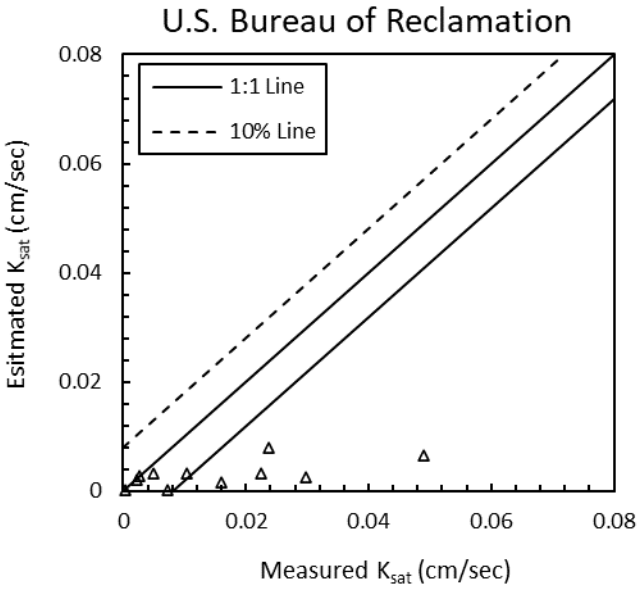

(m)

Figure 4.9 Comparisons of estimated and measured K_{sat} for 11 samples excluding #4, #6, #9, A2, and A4 using (a) Alyamani and Sen (1993), (b) Beyer (1964), (c) Chapuis et al. (2005), (d) Harleman et al. (1963), (e) Hazen-Original (1892), (f) Hazen-Modified, (g) Kozeny (1953), (h) Kozeny-Carman (Kozeny 1927, 1953; Carman1937, 1956), (i) Salarashayeri and Siosemarde (2012), (j) Sauerbrei (1932), (k) Slichter (1899), (l) Terzaghi (1925), and (m) U.S. Bureau of Reclamation

4.6.2 Dataset Specific Models

As most K_{sat} values estimated using the 13 existing empirical equations for gravels did not reveal ideal correspondence, regression equations shown with trendlines in Figure 4.1 from the specific dataset considered here were used to estimate K_{sat} values for the 16 samples. The equations developed from Figure 4.1 are as follows:

$$K_{sat} = 0.0956 \times D_{10} + 0.0322 \ (R^2 = 0.89) \quad (4.2)$$

$$K_{sat} = 0.0684 \times D_{30} - 0.004 \ (R^2 = 0.85) \quad (4.3)$$

$$K_{sat} = 0.0286 + 0.0878 \times D_{10} + 0.0058 \times D_{30} \ (R^2 = 0.89) \quad (4.4)$$

$$K_{sat} = 0.0032 \times {D_{50}}^2 + 0.0144 \times D_{50} - 0.008 \ (R^2 = 0.74) \quad (4.5)$$

$$K_{sat} = 0.0386 \times D_{60} - 0.0566 \ (R^2 = 0.60) \quad (4.6)$$

where, K_{sat} = saturated hydraulic conductivity [cm/sec], D_{10}, D_{30}, D_{50}, D_{60} = particle sizes corresponding to 10%, 30%, 50%, 60% finer, respectively, in particle-size distribution curve [mm].

Figure 4.10 compares the estimated K_{sat} values from these equations and the experimentally measured K_{sat} values. Outliers above the 10% lines are highlighted in red. While K_{sat} values estimated using the existing empirical equations obtained from the literature showed unrealistic overestimations for the three GPs (#6, #9, and A2) as described in Table 4.4, K_{sat} values estimated using the five dataset specific regression equations demonstrated reasonable estimation results for the three samples, particularly when they were estimated using the equation based on D_{10}, D_{30}, and the multivariable regression on D_{10} and D_{30} (i.e., the closest to the one-to-one line). However, #9 GP was greatly underestimated when using the regression equations based on D_{50} and D_{60}, and A2 GP.

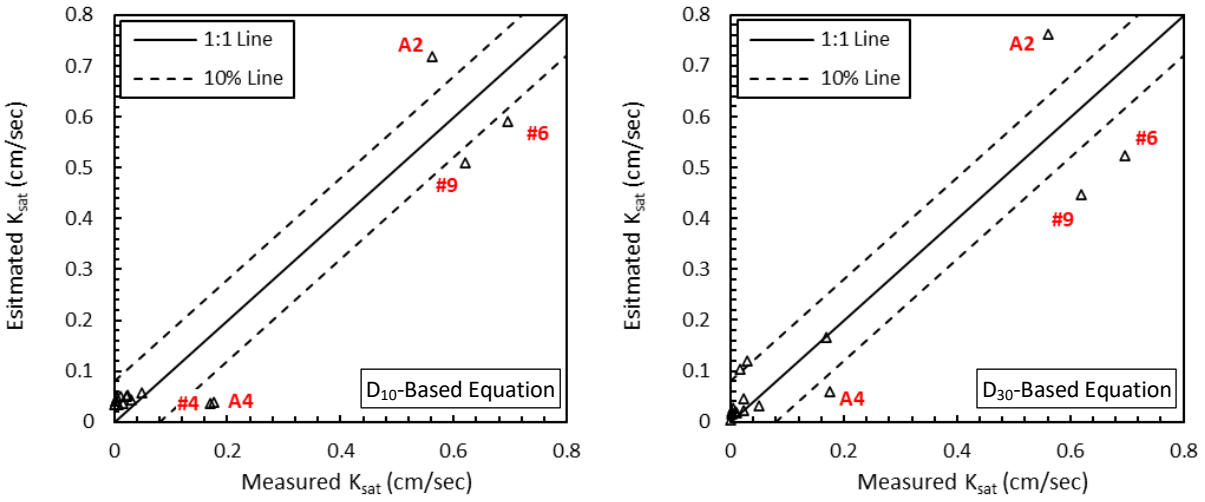

(a) (b)

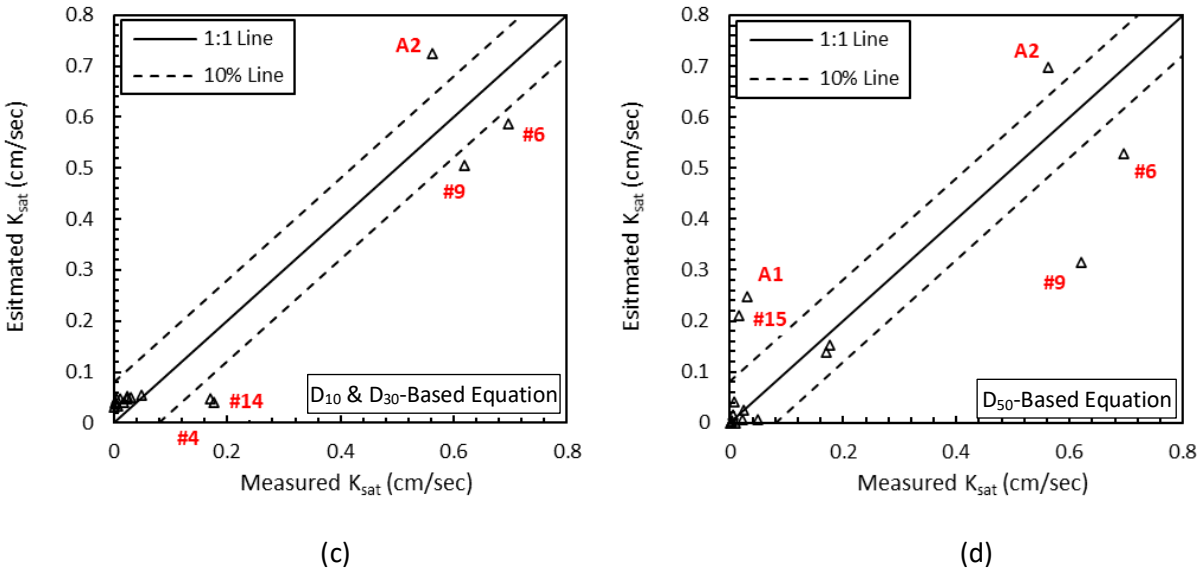

(c)

(d)

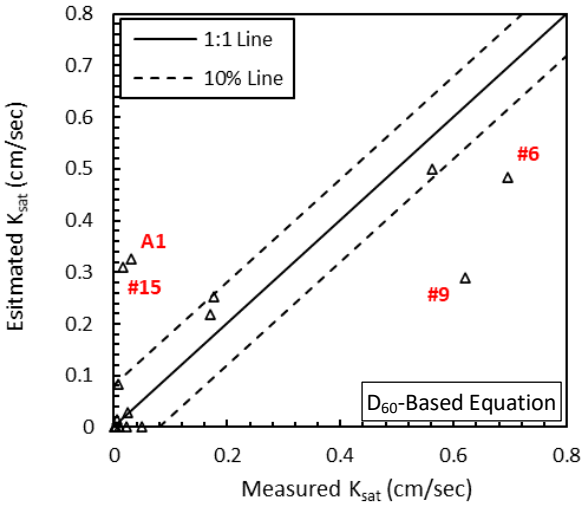

(e)

Figure 4.10 Comparisons of K_{sat} values obtained from experiments and estimations using regression equations based on (a) D_{10}, (b) D_{30}, (c) multivariable on D_{10} and D_{30}, (d) D_{50}, and (e) D_{60}

In addition to the improved K_{sat} estimations for the three GPs, the estimation results for #4 and A4 gravels, which were considerably underestimated with the existing model equations from the literature [Figure 4.8(a)], were improved with the regression equations based on D_{30}, D_{50}, and D_{60}. In contrast, the equations based on D_{10} still underestimated K_{sat} values for #4 and A4 gravels, as well as #6 and #9 gravels, while other soils were slightly overestimated. As described in Appendix C, most of the existing empirical equations were derived based on D_{10} (or less than D_{30}). That is, K_{sat} values for #4 and A4 gravels were underestimated when the K_{sat} estimation equations were derived based on D_{10} (or less than D_{30}). These results suggest that pore structures of #4 and A4 gravels were not represented and governed

by the particle diameter corresponding to 10% and 30% finer in entire particle-size distributions of the two gravels.

Although the dataset specific K_{sat} estimations improved the estimation results for #4 and A4 gravels, at the same time, results were overestimated for #15 and A1 gravels. Moreover, the overall estimations using the two equations based on D_{50}, and D_{60} were scattered due to low R-squared values: 1) R-squared value for relationship between K_{sat} and D_{10} = 89.4%, 2) R-squared value for relationship between K_{sat} and D_{30} = 85.3%, 3) R-squared value for relationship between K_{sat} and multivariable on D_{10} and D_{30} = 89.4%, 4) R-squared value for relationship between K_{sat} and D_{50} = 74.0%, and 5) R-squared value for relationship between K_{sat} and D_{60} = 60.1%. Consequently, among the regression equations, the equations based on D_{10} and D_{30}, particularly D_{10} that is one of the most broadly used parameters in the literature to estimate K_{sat}, provided reasonable estimation results for gravels (i.e., aggregate base). The equation based on D_{30} provided generally reasonable estimation results and the equation based on D_{10} showed the best estimation performance for large-sized gravels.

4.6.3 Performance Evaluation and Improvement of D_{10}-Based Equation using Data from the Literature

In this section, performance of eq. (4.2), which showed the most reliable estimation results (i.e., the closest to the one-to-one line), was evaluated using K_{sat} and D_{10} data for a wider range of experimental data. This included various recycled base materials obtained from the literature (Trzebiatowski and Benson 2015, Cetin et al., 2021, Klink, 2021). In these three studies, laboratory tests were conducted to measure K_{sat} values of recycled asphalt pavement (RAP) and recycled concrete aggregate (RCA) materials widely used in pavement systems. Table 4.5 summarizes K_{sat} and D_{10} data obtained from the literature.

Figure 4.11 compares the experimentally measured K_{sat} and K_{sat} estimated using eq. (4.2) for the 16 samples used in this study and including the recycled base materials obtained from the literature. In the full scale [Figure 4.11(a)], even though K_{sat} estimations for the recycled base materials were located above the one-to-one line (i.e., overestimations), the estimation results were in reasonable ranges (e.g., inside the 10% lines). On the other hand, in the small scale [Figure 4.11(b)] excluding the three GPs, most of estimation results particularly for the recycled base materials were located above 10% line. The 16 samples and recycled base materials had similar D_{10} values, but K_{sat} values of the recycled base materials were generally lower than those of the 16 samples potentially due to different compaction efforts and particle-size distributions (e.g., different % retained gravels). This difference in K_{sat} measurements correspondingly results in the overestimations notwithstanding similar D_{10}.

Table 4.5 Experimentally measured K_{sat} and D_{10} data of recycled base materials obtained from the literature

Source	Sample	D_{10} (mm)	K_{sat} (cm/s)	Note
Trzebiatowski and Benson 2015	PDF RAP	0.316	0.009	Compacted with standard Proctor effort in compaction-mold permeameter
	PDV RAP	0.4	0.0038	
	WSP RAP	0.16	0.0024	
	Lodi Gravel	0.089	0.000058	
Cetin et al. 2021	Coarse RCA	0.37	0.000488	Compacted using light hammering method (degree of compaction of 95%)
	Fine RCA	0.135	0.00099	
	Limestone	0.038	0.000191	
	RCA+RAP	0.1	0.000479	
	Class 6 Aggregate	0.175	0.000491	
	Class 5Q Aggregate	0.4	0.000733	
	Sand Subgrade	0.048	0.000715	
Klink (2021)	RCA DC-10	0.14	0.000412	Hand tampered in flexible wall permeameter
	RCA DC-1	0.20	0.000731	
	RCA DC-7	0.13	0.000111	
	RCA MC-1	0.25	0.001422	
	RCA DC-6	0.16	0.00036	
	RCA DC-8	0.56	0.005822	
	RCA RC-1	0.24	0.000502	
	RCA RC-2	0.23	0.002492	
	RAP DRAP-1	0.72	0.128839	
	RAP DRAP-2	0.61	0.117	

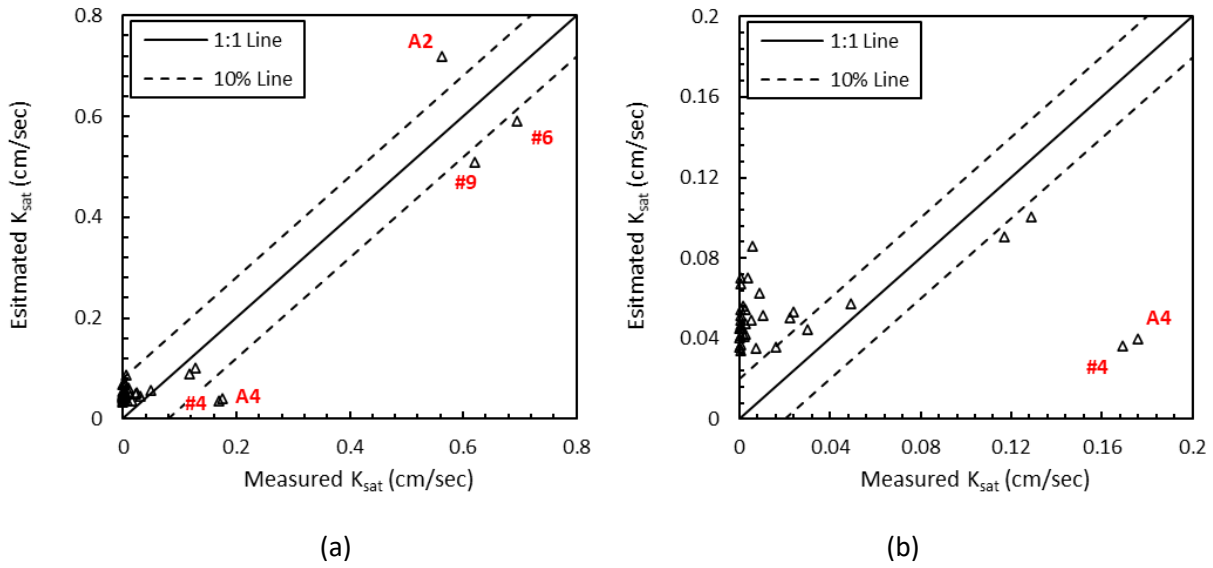

Figure 4.11 Comparisons of K_{sat} measurements and estimations obtained using eq. (4.2) for base materials: (a) in full range and (b) in small range excluding #6, #9, and A2

To improve the estimation performance, eq. (4.2) was incorporated with K_{sat} and D_{10} data of the recycled base materials. As mentioned above, most of the recycled base materials had similar D_{10} values between 0 mm and 1 mm and lower K_{sat} values (Figure 4.12). With the additional data set of recycled base materials, overall trend was same showing a slight change in the equation (eq. 4.7).

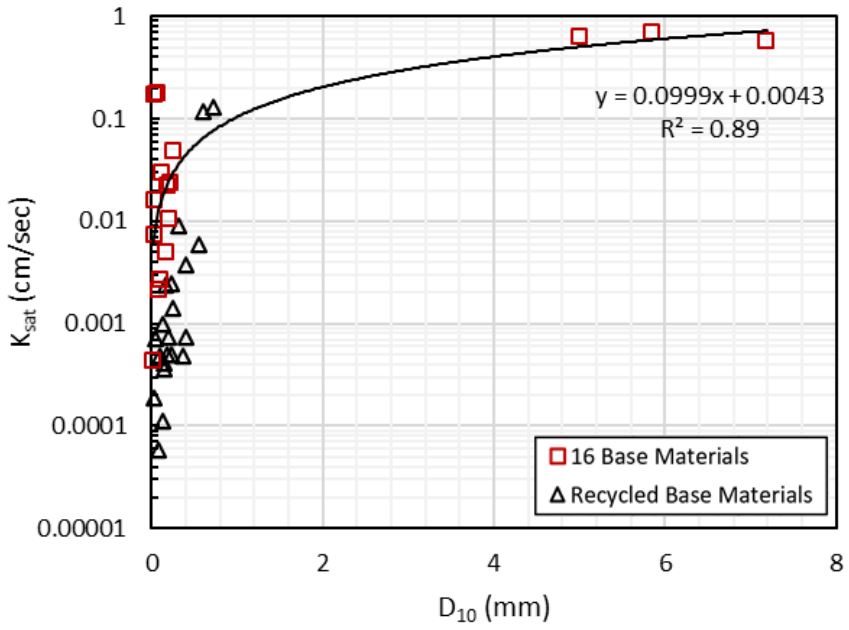

Figure 4.12 Relationship between K_{sat} and D_{10} of 16 samples and recycled base materials

$$K_{sat} = 0.0999 \times D_{10} + 0.0043 \ (\mathrm{R}^2 = 0.89) \tag{4.7}$$

where, K_{sat} = saturated hydraulic conductivity [cm/sec], D_{10} = particle diameter corresponding to 10% finer on the cumulative particle-size distribution curve [mm]. K_{sat} values for the 16 samples and recycled base materials obtained from experiments and estimated using eq. (4.7) were compared in Figure 4.13. Despite K_{sat} estimations for the #4 and A4 gravels were even lower when using eq. (4.7), overall estimations for the recycled base materials were moved to the one-to-one line. Future, additional tests are recommended to collect more K_{sat} data for the medium-sized gravels that have D_{10} between 2 mm and 8 mm and accordingly improve reliabilities of the equation.

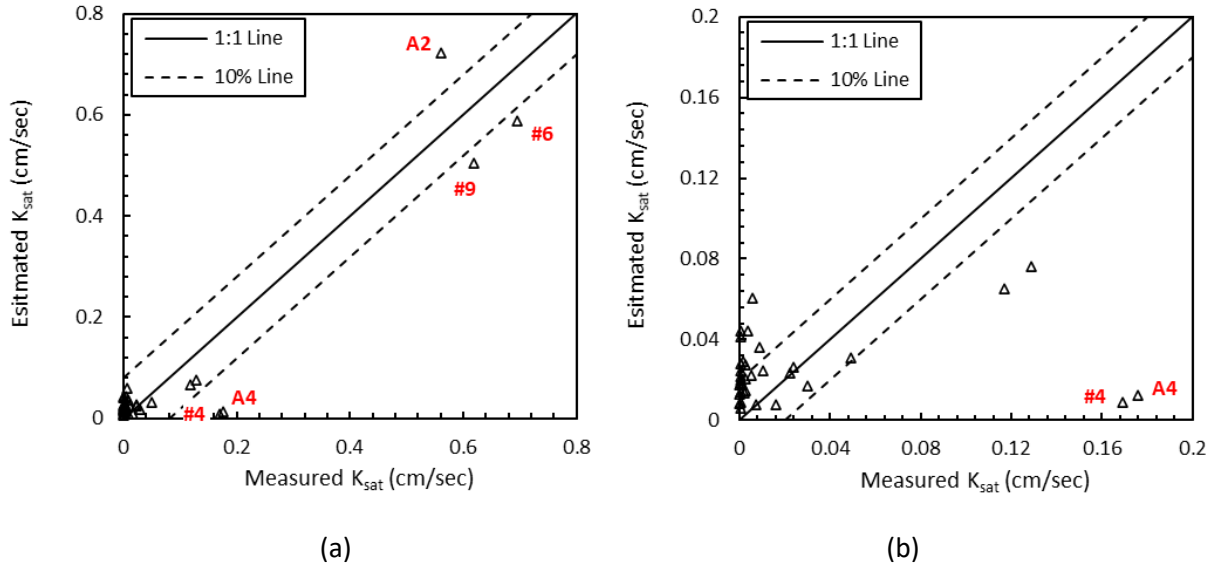

Figure 4.13 Comparisons of K_{sat} measurements and estimations obtained using eq. (4.7) for base materials: (a) in full range and (b) in small range excluding #6, #9, and A2

4.7 SOIL-WATER CHARACTERISTIC CURVE MODELS

4.7.1 Benson et al (2014)

Benson et al. (2014) performed hanging column tests (ASTM D6836) to measure SWCCs of sands having a wide range of D_{50} and C_u and proposed pedotransfer functions (PTF) to estimate the van Genuchten parameters α and n. For fitting parameters corresponding to drying SWCCs (i.e., those measured here). Equations to estimate α were proposed as:

$$\alpha = \alpha_1 N_\alpha \tag{4.8a}$$

where, α_1 = derived from regression with grain size parameter D_{60}, N_α = a normalized α value derived from regression with C_u. For the clean and uniform sands in Benson et al (2014):

$$\alpha_1 = 1.354 D_{60} \tag{4.8b}$$

$$N_\alpha = 0.99 C_u^{-0.54} \tag{4.8c}$$

Equations to estimate n were proposed as:

$$n = n_1 N_n \tag{4.9a}$$

where, n_1 = derived from regression with grain size parameter D_{60}, N_n = a normalized n value derived from regression with C_u. For the clean and uniform sands in Benson et al (2014):

$$n_1 = 14.4 \exp(-0.434 D_{60}) \tag{4.9b}$$

$$N_{n,Cu<2.2} = -0.542 C_u + 1.542 \tag{4.9c}$$

$$N_{n,Cu\geq 2.2} = -0.0033 C_u + 0.379 \tag{4.9d}$$

Equations for estimating van Genuchten parameters were rederived using the procedures described in Benson et al. (2014) with the experimental results for the 15 base aggregates and sands in this study. Procedures for deriving the equations were as follows:

1) Experimentally obtained D_{60} and van Genuchten parameters α and n were plotted to derive regression equations. Sample #4 was excluded due to the exceptionally high α.
2) Uniformity coefficients C_u were plotted with normalized van Genuchten parameters. Normalized parameters are defined as ratios of the α or n parameter for a given C_u to the α or n parameter for a nominally uniformly graded soil. In this study, Sample #9 (GP), which has the lowest C_u value (C_u = 1.79), was used as the uniformly graded sample for normalizing the parameters.

Figure 4.14(a) and Figure 4.14(b) show relations between the α and n parameters and D_{60} and corresponding regression equations. Figure 4.14(c) and Figure 4.14(d) show relations between the normalized α and n parameters and C_u.

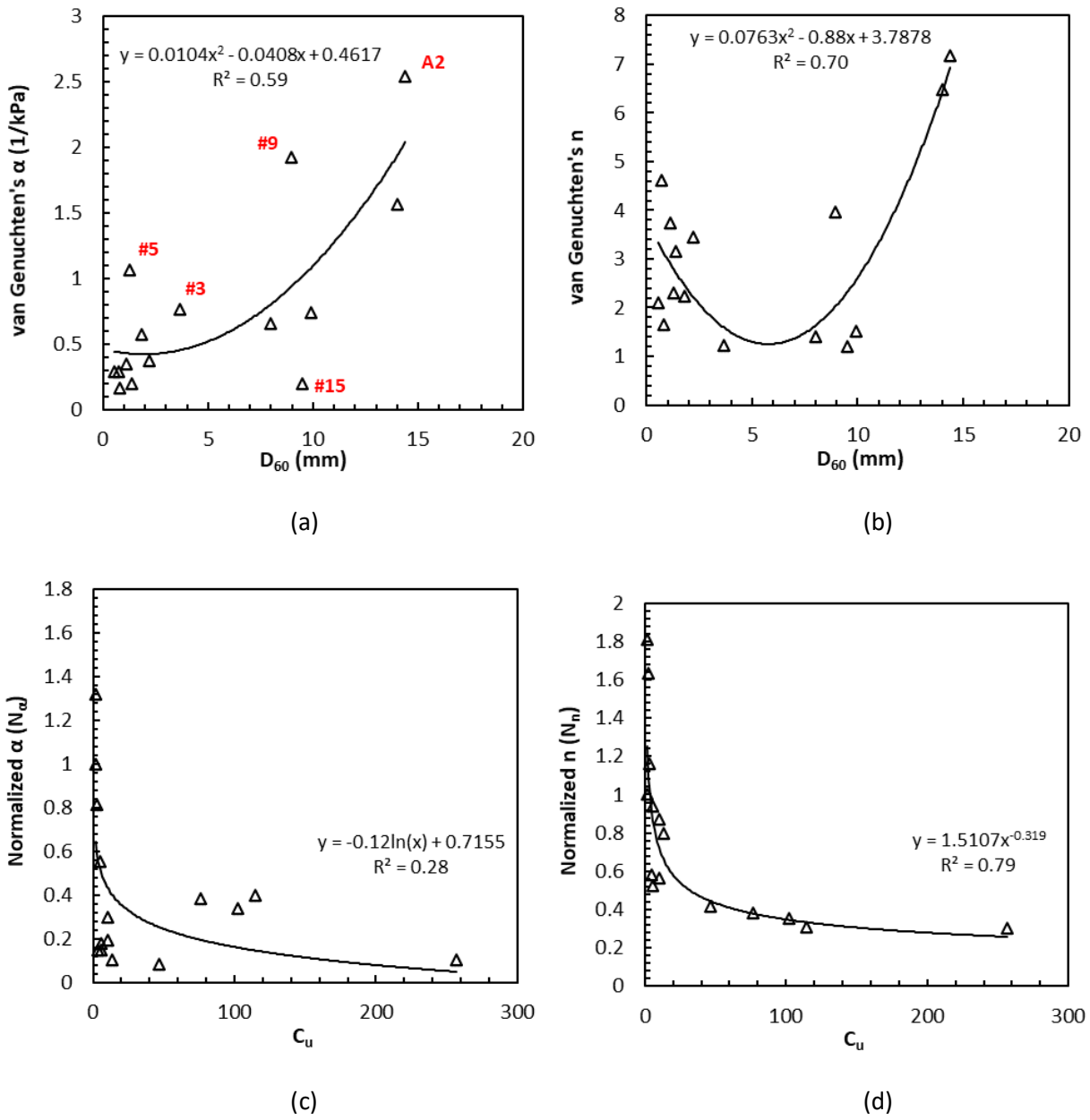

Figure 4.14 Deriving new regression equations using experimental results of 15 samples: (a) relationship between D_{60} and van Genuchten parameter α, (b) relationship between D_{60} and van Genuchten parameter n, (c) relationship between C_u and normalized α, and (d) relationship between C_u and normalized n

Resulting equations to estimate α based on the materials in this study are:

$$\alpha = \alpha_1 N_\alpha \tag{4.10}$$

where

$$\alpha_1 = 0.0104 \times {D_{60}}^2 - 0.0408 \times D_{60} + 0.4617 \ (\mathrm{R}^2 = 0.59)$$

$$N_\alpha = -0.12 \ln(C_u) + 0.7155 \ (\mathrm{R}^2 = 0.28)$$

Resulting equations to estimate n based on the materials in this study are:

$$n = n_1 N_n \tag{4.11}$$

where

$$n_1 = 0.0763 \times {D_{60}}^2 - 0.88 \times D_{60} + 3.7878 \ (\mathrm{R}^2 = 0.70)$$

$$N_n = 1.5107 \times {C_u}^{-0.3187} \ (\mathrm{R}^2 = 0.79)$$

Figure 4.15 compares 15 sets of the van Genuchten parameters estimated using the new equations (equations 4.10 and 4.11). As highlighted in Figure 4.14(a), some D_{60} values were not robustly correlated with the experimentally obtained α, and these led to significant underestimations for α parameters of #3, #5, #9, and A2, as well as general underestimations for other samples [Figure 4.15(a)]. In other words, the air-entry pressure related to the α parameter may not be correlated well with D_{60}. On the other hand, even though n parameters for some samples were underestimated below the 10% line, the estimated n parameters were generally well aligned with the experimentally obtained n parameters [Figure 4.15(b)]. Namely, breadth of SWCC slope (related to the n parameter) was well represented with D_{60}.

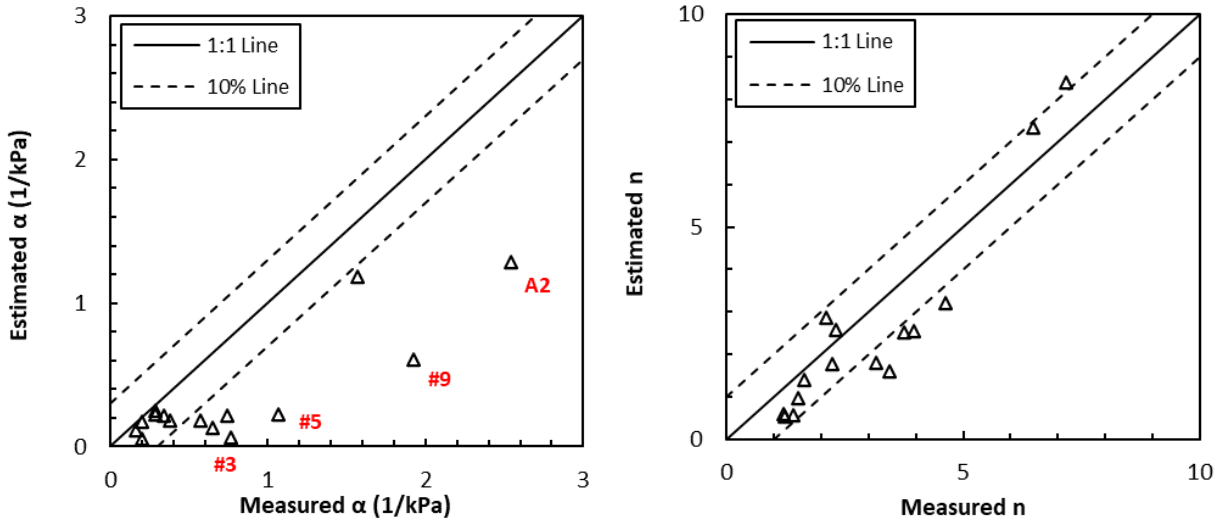

(a) (b)

Figure 4.15 Comparisons of van Genuchten parameters obtained from experiments and estimations: (a) comparison of α parameters, (b) comparison of n parameters.

4.7.2 Dataset Specific Models

Additional regression equations were derived with D_{10}, D_{30}, D_{50} and dry unit weight (γ_d) data for the 15 samples. To derive the equations, experimentally obtained van Genuchten parameters and the index properties were plotted with trendlines (Figure 4.16). Figure 4.16 demonstrates that both α and n parameters increased as the particle size (i.e., D_{10}, D_{30}, D_{50}) increased and γ_d decreased. That is, the increased pore sizes (caused by increases in D_{10}, D_{30}, and D_{50} and a decrease in γ_d) resulted in decreases in the air-entry pressure and the gradient of SWCC (i.e., increases in α and n parameters).

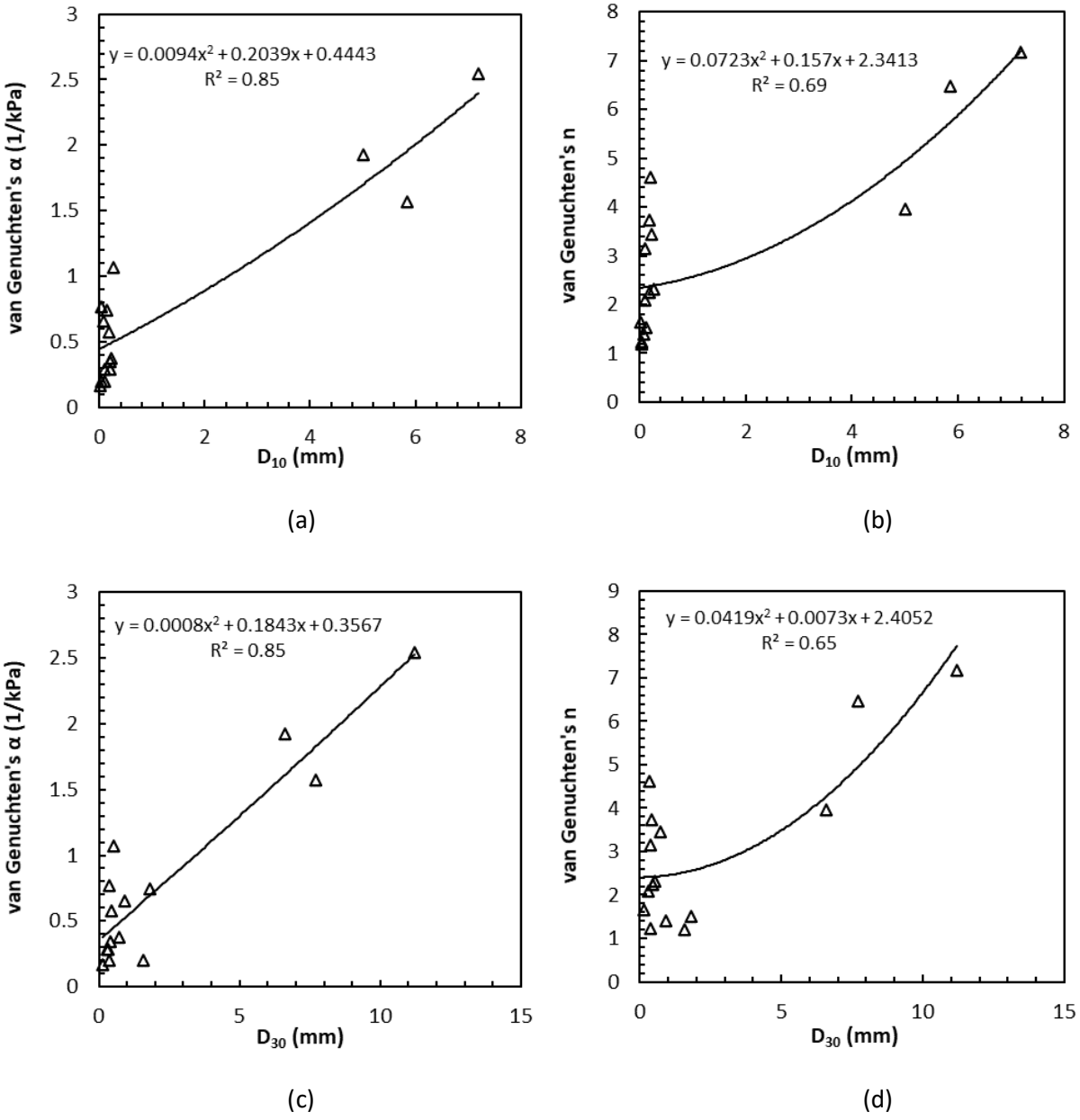

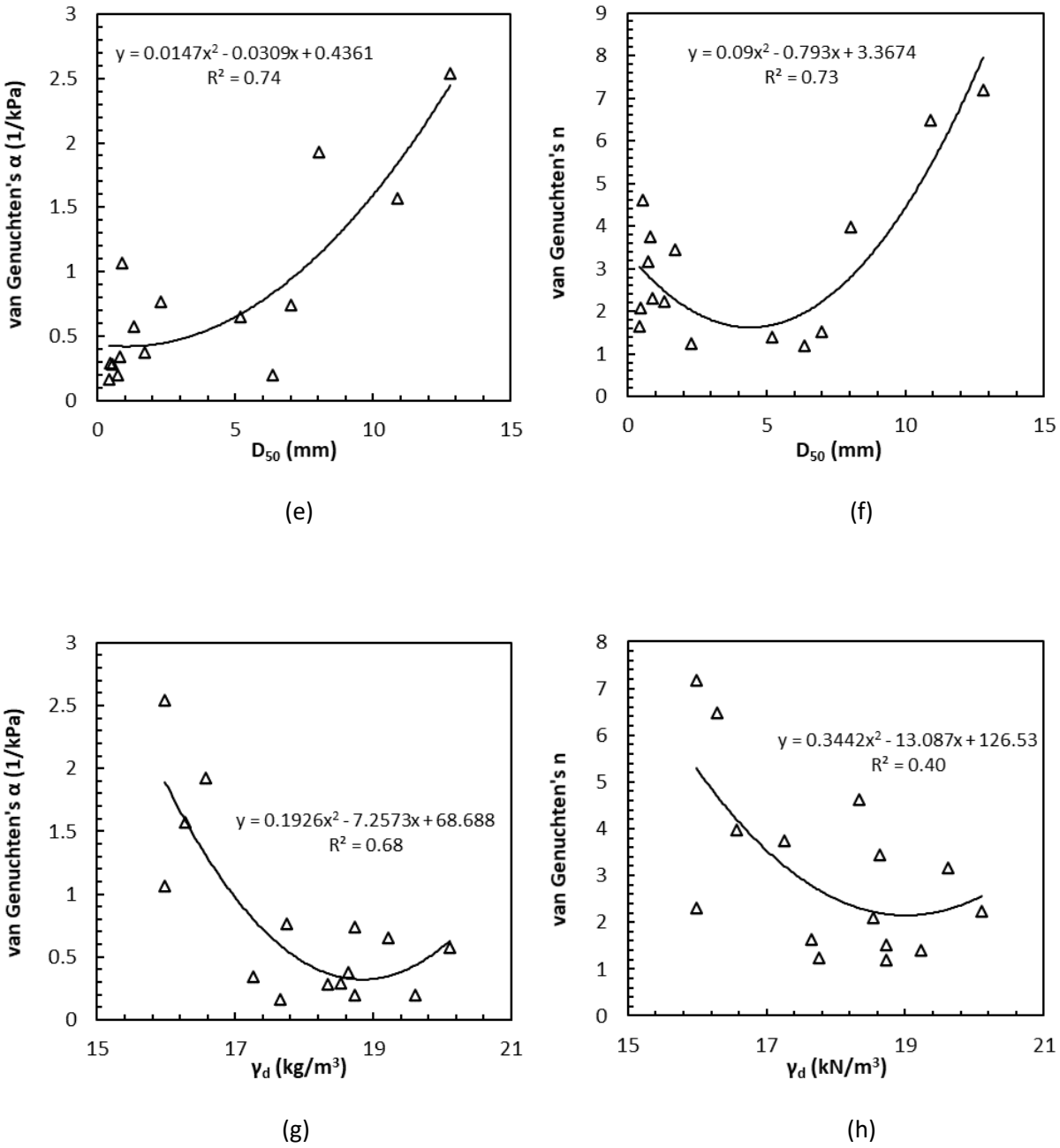

Figure 4.16 Relationships between experimentally obtained van Genuchten fitting parameters and index properties: (a) relationship between α and D_{10}, (b) relationship between n and D_{10}, (c) relationship between α and D_{30}, (d) relationship between n and D_{30}, (e) relationship between α and D_{50}, (f) relationship between n and D_{50}, (g) relationship between α and γ_d, and (h) relationship between n and γ_d

The regression equations for estimating α are as follows:

$$\alpha = 0.0094 \times {D_{10}}^2 + 0.2039 \times D_{10} + 0.4443 \ (R^2 = 0.85) \quad (4.12)$$

$$\alpha = 0.0008 \times {D_{30}}^2 + 0.1843 \times D_{30} + 0.3567 \ (R^2 = 0.85) \quad (4.13)$$

$$\alpha = 0.0147 \times {D_{50}}^2 - 0.0309 \times D_{50} + 0.4361 \ (R^2 = 0.74) \quad (4.14)$$

$$\alpha = 0.1926 \times {\gamma_d}^2 - 7.2573 \times \gamma_d + 68.6876 \ (R^2 = 0.68) \quad (4.15)$$

The regression equations for estimating n are as follows:

$$n = 0.0723 \times {D_{10}}^2 + 0.1570 \times D_{10} + 2.3413 \ (R^2 = 0.69) \quad (4.16)$$

$$n = 0.0419 \times {D_{30}}^2 + 0.0073 \times D_{30} + 2.4052 \ (R^2 = 0.65) \quad (4.17)$$

$$n = 0.09 \times {D_{50}}^2 - 0.793 \times D_{50} + 3.3674 \ (R^2 = 0.73) \quad (4.18)$$

$$n = 0.3442 \times {\gamma_d}^2 - 13.087 \times \gamma_d + 126.53 \ (R^2 = 0.40) \quad (4.19)$$

where, D_{10}, D_{30}, and D_{50} = particle diameters in mm corresponding to 10%, 30%, and 50% finer in the particle-size distribution curve, respectively, γ_d = dry density in kN/m^3. Using the equations above and the 15-sample data, van Genuchten parameters were estimated. Similar to Figure 4.15(a), almost all estimation results for α parameters were located below the one-to-one line (i.e., underestimation), while estimation results for n parameters were in reasonable ranges. Among the n parameter estimation results, the equations based on D_{30} showed the best performance (i.e., the estimated van Genuchten parameters were the closest to the one-to-one line), and these results are interpreted to reflect the highest R-squared values. That is, the performance improvements are expected with adding robust data set that can increase the R-squared values.

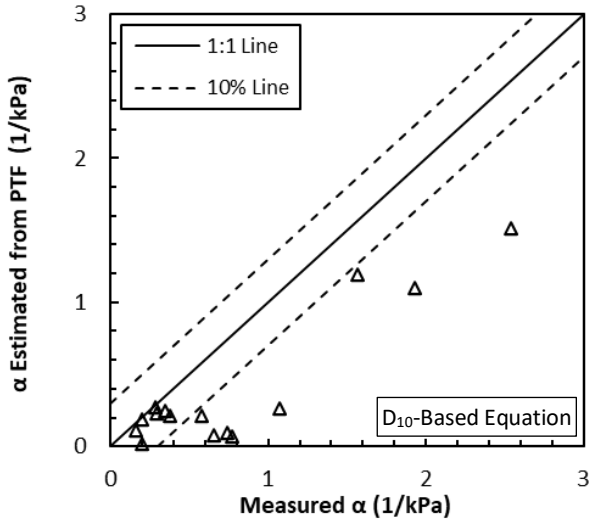
1:1 Line
10% Line
D10-Based Equation
α Estimated from PTF (1/kPa)
Measured α (1/kPa)
0
1
2
3

(a)

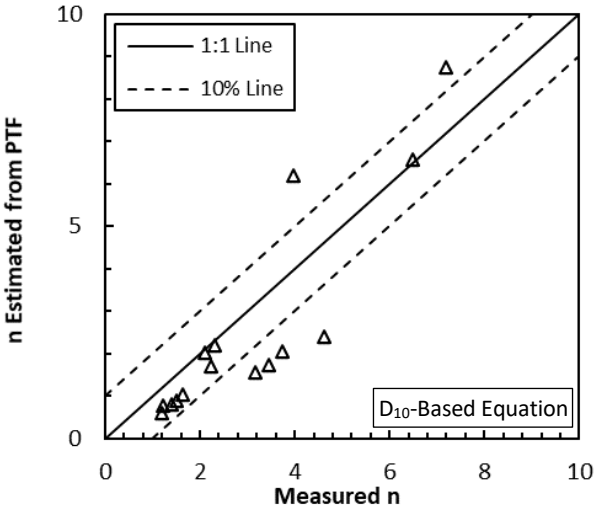
1:1 Line
10% Line
D10-Based Equation
n Estimated from PTF
Measured n
0
5
10

(b)

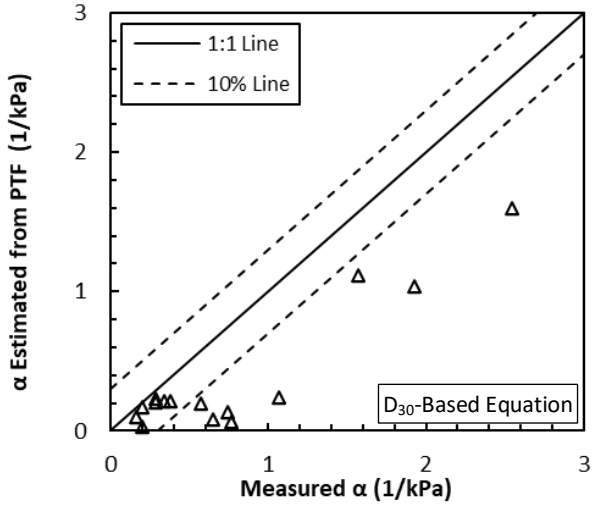
1:1 Line
10% Line
D30-Based Equation
α Estimated from PTF (1/kPa)
Measured α (1/kPa)
0
1
2
3

(c)

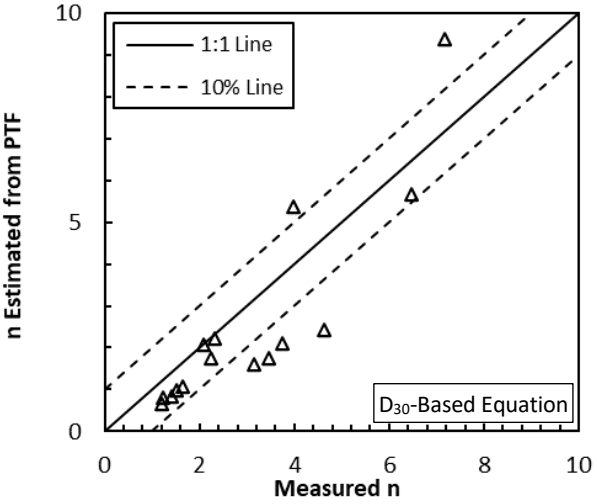
1:1 Line
10% Line
D30-Based Equation
n Estimated from PTF
Measured n
0
5
10

(d)

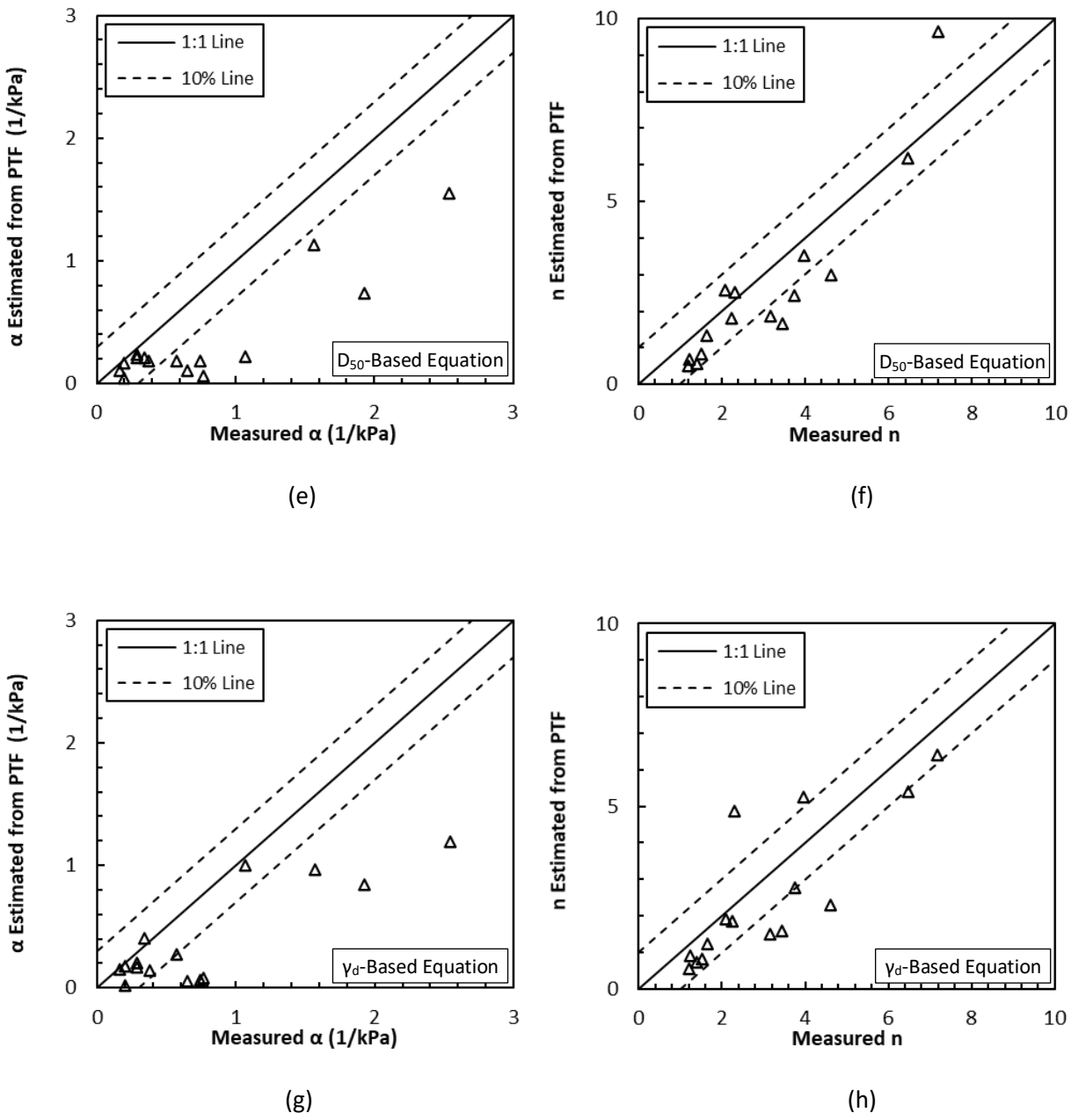

Figure 4.17 Comparisons of van Genuchten parameters obtained from experiments and pedotransfer functions based on: (a) D_{10} for α parameter, (b) D_{10} for n parameter, (c) D_{30} for α parameter, (d) D_{30} for n parameter, (e) D_{50} for α parameter, (f) D_{50} for n parameter, (g) γ_d for α parameter, and (h) γ_d for n parameter

CHAPTER 5: CONCLUSIONS AND RECOMMENDATIONS

5.1.1 Summary and Key Findings

The objective of this project is to assess the drainability of coarse soil/aggregate materials applicable to pavement base course applications. Emphasis is placed on saturated hydraulic conductivity and water retention curves, including evaluation of existing predictive equations for indirect estimation of these properties from surrogate material properties (e.g., grain size distribution) and the development of new correlation equations from the materials examined here. Samples of 16 representative materials were obtained from NRRA stakeholders, including materials that are generally classified as gravels (7 samples) and sands (9 samples).

Laboratory tests were conducted to determine grain size distribution, grain size index properties, saturated hydraulic conductivity (K_{sat}), and soil-water characteristic curves (SWCCs). Key findings from the experimental program included the following:

1) Measured K_{sat} of the sandy materials was independent of applied hydraulic gradient (i) typical of field conditions for pavement base applications ($0.25 < i < 2.0$). Measured K_{sat} of the gravels systematically decreased with increasing hydraulic gradient, potentially due to migration of fines and the effects of turbulent flow. Average K_{sat} values over the range of applied gradient was calculated for subsequent analysis.
2) K_{sat} for all materials generally increased as % gravels and particle diameters corresponding to 10%, 30%, 50%, and 60% finer (D_{10}, D_{30}, D_{50}, and D_{60}, respectively) increased. K_{sat} generally increased as % fines and dry unit weight (γ_d) decreased.
3) K_{sat} slightly increased with a decrease in uniformity coefficient (C_u), but the relationship was not significantly correlated. Air-entry pressure on measured soil-water characteristic curves increased with an increase in C_u.
4) The van Genuchten (1980) SWCC parameters (α and n) increased with increases in D_{10}, D_{30}, D_{50}, D_{60}, and % retained gravels and with decreases in % fines, C_u, and γ_d. Comparisons among the experimentally measured K_{sat} values and the van Genuchten α and n parameters showed a proportional relationship.
5) Effective (drainable) porosities for the 16 samples ranged from 0.26 (#15 GM) to 0.59 (#5 SP) with an average of 0.42 and were comparable to typical values obtained from the literature.

Test results were analyzed to examine the accuracy and applicability of equations available in the literature for estimating K_{sat} and SWCC parameters for coarse materials and to develop dataset-specific equations for the suite of materials tested here. This analysis showed:

1) Estimated K_{sat} for materials that classified as poorly graded gravel (GP) were significantly higher than the experimentally measured K_{sat} values. Measured K_{sat} values for a subset of samples that excluded the gravels were generally well estimated using the Harleman et al. (1963), Sauerbrei (1932), and Chapuis (2004) empirical equations.
2) New dataset-specific regression equations to estimate K_{sat} were derived using the experimentally obtained K_{sat} and index properties (D_{10}, D_{30}, D_{50}, D_{60}). Measured K_{sat} values that

were overestimated using the existing equations were reasonably estimated with the new equations, particularly using single-variable equations based on D_{10} and D_{30}.

3) The van Genuchten (1980) SWCC fitting parameters α and n were estimated using regression equations obtained by following procedures developed by Benson et al. (2014). New dataset-specific equations were derived using the Benson et al., (2014) approach. Equations based on D_{30} and C_u showed the best performance.

5.1.2 Qualitative Material Rating System for Base Course Drainability

As noted in Section 1.4.8, the drainability of pavement systems in the field depends on several factors:

1) Base course permeability, including both saturated hydraulic conductivity and the unsaturated hydraulic conductivity function.
2) Effective (drainable) porosity (ratio of the volume of the voids that can be drained under gravity flow to the total volume of material.) Corresponding minimum saturation is the minimum saturation that is achieved by gravity and can be estimated from the field capacity corresponding to a suction value of 33 kPa.
3) Drainage boundary conditions, including the cross-sectional geometry of the pavement system, depth to the water table, side-slope geometry, and any installed drainage systems.
4) Environmental conditions, including surface water, groundwater, temperature, wind speed, and relative humidity. The volume of infiltration into the pavement system will depend on factors such as type and condition of surface, length and intensity of rainfall, properties of the drainage layer, hydraulic gradient, time allowed for drainage and the drained area.

Rigorous drainability analysis, therefore, requires knowledge of material properties, pavement system design, and site environmental conditions, thereby allowing site-specific time-to-drainage analyses to be conducted. In lieu of knowledge of system design parameters and site environmental conditions, however, base course material properties may be used to screen candidate materials for drainability performance. If saturated hydraulic conductivity (K_{sat}) and minimum saturation (S_{min}) are adopted as screening parameters for base course material performance, criteria must be selected to quantify acceptable ranges for these properties.

Table 5.1 summarizes recommended bounds for K_{sat} and S_{min} to meet qualitative drainability assessments of “excellent,” “marginal,” and “poor.” The criteria for K_{sat} are based on Federal Highway Administration (FHWA) guidance describing drainability for an excellent-quality material equivalent to 0.353 cm/sec (1,000 ft/day) (FHWA, 1992), while a base layer that has a coefficient of permeability (K_{sat}) of less than 0.017 cm/sec (48 ft/day) is practically impermeable (McEnroe, 1994). Criteria for S_{min} are based on characteristics of material that may be considered “freely draining” under gravity (McEnroe, 1994).

Table 5.1 Recommended material parameters for qualitative drainability assessment of pavement base course materials

Qualitative Drainability	Hydraulic Conductivity (cm/s)	Minimum Saturation
Excellent	$K_{sat} \geq 0.35$	$S_{min} \leq 0.10$
Marginal	$0.02 \leq K_{sat} < 0.35$	$0.10 < S_{min} \leq 0.30$
Poor	$K_{sat} < 0.02$	$S_{min} > 0.30$

Approaches for either direct measurement of K_{sat} and S_{min} (e.g., permeability and SWCC testing) or their indirect estimation (e.g., based on grain size indices) must be adopted to apply the qualitative rating system. Three recommendations for such approaches are summarized below.

5.1.3 Recommendation 1: Qualitative Material Rating Based on Direct Measurements of Permeability and Water Retention

Table 5.2 summarizes ratings for each material examined in this study based on direct measurements of K_{sat} and S_{min}. The experimentally obtained K_{sat} values for the 16 base aggregates and sands ranged from 0.0004 cm/sec (#16, SM) to 0.6957 cm/sec (#6, GP). The three GPs (#6, #9, and A2) satisfied the K_{sat} criterion for "excellent" quality, five materials are designated "marginal," and 8 materials are designated as "poor." Another 7 of the materials classify as "excellent" with respect to minimum water retention, four as "marginal," and five as "poor." The overall ratings reflect the combination of the permeability and water retention criteria.

Table 5.2 Qualitative performance rating of materials based on measured permeability and water retention

Sample	K_{sat} (cm/s)	Minimum Saturation	K_{sat} Criterion	S_{min} Criterion	Overall Rating
#1 (SP-SM)	0.0021	0.32	Poor	Marginal	Poor-Marginal
#2 (SW-SM)	0.0027	0.31	Poor	Marginal	Poor-Marginal
#3 (SM)	0.0073	0.48	Poor	Poor	Poor
#4 (GM)	0.1693	0.35	Marginal	Poor	Marginal
#5 (SP)	0.0489	0.08	Marginal	Excellent	Marg - Excellent
#6 (GP)	0.6957	0.07	Excellent	Excellent	Excellent
#7 (SW)	0.0236	0.10	Marginal	Excellent	Marginal
#8 (SP)	0.0050	0.01	Poor	Excellent	Marginal
#9 (GP)	0.6196	0.06	Excellent	Excellent	Excellent
#10 (SP)	0.0104	0.14	Poor	Marginal	Poor-Marginal
#15 (GM)	0.0159	0.69	Poor	Poor	Poor
#16 (SM)	0.0004	0.53	Poor	Poor	Poor
A1 (GW-GM)	0.0298	0.41	Marginal	Poor	Poor-Marginal
A2 (GP)	0.5618	0.09	Excellent	Excellent	Excellent
A3 (SP)	0.0224	0.01	Marginal	Excellent	Marg - Excellent
A4 (GW-GM)	0.1759	0.36	Poor	Marginal	Poor-Marginal

5.1.4 Recommendation 2: Qualitative Material Rating Based on Grain Size Indices

If K_{sat} and the SWCC are not directly measured, then the empirical relations developed in this study can be used to indirectly estimate K_{sat} and S_{min} and in turn be used in the qualitative rating system. Correlation equations exhibiting the best fit are recommended. For the dataset here, an equation for estimating K_{sat} using D_{30} showed an R^2 value of 0.853 over a wide range of grain sizes and is recommended:

$$K_{sat} = 0.0684 \times D_{30} - 0.004 \ (\mathrm{R}^2 = 0.85) \tag{5.1}$$

Among the relationships between grain size index properties and the van Genuchten SWCC parameters (α and n), estimations using the Benson et al. (2014) approach with D_{30} and C_u (equations 5.2 and 5.3) showed the best performance:

$$\alpha = \alpha_1 N_\alpha \tag{5.2a}$$

where

$$\alpha_1 = \ 0.0008 \times {D_{30}}^2 + 0.1843 \times D_{30} + 0.3567 \ (\mathrm{R}^2 = 0.85) \tag{5.2b}$$

$$N_\alpha = -0.12 \ln(C_u) + 0.7155 \ (\mathrm{R}^2 = 0.28) \tag{5.2c}$$

And for the SWCC n parameter:

$$n = n_1 N_n \tag{5.3a}$$

where

$$n_1 = 0.0419 \times D_{30}{}^2 + 0.0073 \times D_{30} + 2.4052 \ (\mathrm{R}^2 = 0.65) \tag{5.3b}$$

$$N_n = 1.5107 \times C_u{}^{-0.3187} \ (\mathrm{R}^2 = 0.79) \tag{5.3c}$$

Minimum saturation (S_{min}) can be estimated from the van Genuchten (1980) equation by setting matric suction ψ = 33 kPa and residual water content θ_r = 0.:

$$S_{min} = \left[\frac{1}{1+(\alpha 33)^n}\right]^{1-\frac{1}{n}} \leq 1.0 \tag{5.4}$$

Table 5.3 summarizes ratings of the 16 base course materials based on indirect estimates of K_{sat} and S_{min} following these procedures. Example calculations are provided following the table for an "excellent" and "poor" rated material. Two materials satisfy the K_{sat} criterion for "excellent" quality, 10 materials are designated "marginal," and four materials are designated as "poor." Another 10 of the materials classify as "excellent" with respect to minimum saturation, three as "marginal," and three as "poor." The overall ratings reflect the combination of the permeability and water retention criteria.

Table 5.3 Qualitative performance rating of materials based on permeability and water retention estimated from grain size distribution

Sample	K_{sat} (cm/s)	Minimum Saturation	K_{sat} Criterion	S_{min} Criterion	Overall Rating
#1 (SP-SM)	0.017	0.13	Poor	Excellent	Marginal
#2 (SW-SM)	0.021	0.35	Marginal	Excellent	Marginal
#3 (SM)	0.021	*(1.0)*	Marginal	Poor	Poor-Marginal
#4 (GM)	0.167	*(1.0)*	Marginal	Poor	Poor-Marginal
#5 (SP)	0.032	0.08	Poor	Excellent	Marginal
#6 (GP)	0.523	0.00	Excellent	Excellent	Excellent
#7 (SW)	0.045	0.22	Marginal	Excellent	Marg - Excellent
#8 (SP)	0.027	0.25	Marginal	Excellent	Marg - Excellent
#9 (GP)	0.447	0.00	Excellent	Excellent	Excellent
#10 (SP)	0.019	0.05	Marginal	Excellent	Marg - Excellent
#15 (GM)	0.005	*(1.0)*	Poor	Poor	Poor
#16 (SM)	0.120	0.78	Marginal	Marginal	Marginal
A1 (GW-GM)	0.023	*(1.0)*	Marginal	Marginal	Marginal
A2 (GP)	0.060	0.01	Marginal	Excellent	Marg - Excellent
A3 (SP)	0.017	0.12	Poor	Excellent	Marginal
A4 (GW-GM)	0.021	*(1.0)*	Marginal	Marginal	Marginal

Example for an "excellent" base course material

Considering sample #9 (GP), where D_{30} = 6.60 mm and C_u = 1.8 we have:

$$K_{sat} = 0.0684 \times D_{30} - 0.004 = 0.447 \text{ cm/s}$$

$$\alpha_1 = 0.0008 \times {D_{30}}^2 + 0.1843 \times D_{30} + 0.3567 = 1.61$$

$$N_\alpha = -0.12 \ln(C_u) + 0.7155 = 0.646$$

$$\alpha = \alpha_1 N_\alpha = 1.04$$

$$n_1 = 0.0419 \times {D_{30}}^2 + 0.0073 \times D_{30} + 2.4052 = 4.28$$

$$N_n = 1.5107 \times {C_u}^{-0.3187} = 1.25$$

$$n = n_1 N_n = 5.36$$

And thus the estimated parameters are K_{sat} = 0.447 cm/s, α = 1.04, and n = 5.36. The measured values are K_{sat} = 0.620 cm/s, α = 1.93, n = 3.97 for comparison.

Minimum saturation is then estimated as:

$$S_{min} = \left[\frac{1}{1 + (\alpha 33)^n}\right]^{1-\frac{1}{n}} = 2.05\ X\ 10^{-7}$$

Thus, the estimated K_{sat} = 0.447 cm/s and the estimated S_{min} = 2.05 X 10^{-7}, placing sample #9 into the "excellent" drainability category for both permeability and water retention.

Example for a "poor" base course material

Considering sample #15 (GM), where D_{30} = 0.13 mm and C_u = 256.8 we have:

$$K_{sat} = 0.0684 \times D_{30} - 0.004 = 0.005 \text{ cm/s}$$

$$\alpha_1 = 0.0008 \times {D_{30}}^2 + 0.1843 \times D_{30} + 0.3567 = 0.381$$

$$N_\alpha = -0.12 \ln(C_u) + 0.7155 = 0.05$$

$$\alpha = \alpha_1 N_\alpha = 0.019$$

$$n_1 = 0.0419 \times {D_{30}}^2 + 0.0073 \times D_{30} + 2.4052 = 2.407$$

$$N_n = 1.5107 \times {C_u}^{-0.3187} = 0.258$$

$$n = n_1 N_n = 0.62$$

And thus the estimated parameters are K_{sat} = 0.005 cm/s, α = 0.019, and n = 0.62. The measured values are K_{sat} = 0.016 cm/s, α = 0.198, n = 1.201 for comparison.

Minimum saturation is then estimated as:

$$S_{min} = \left[\frac{1}{1+(\alpha 33)^n}\right]^{1-\frac{1}{n}} = 1.41 \sim 1.0$$

Thus, the estimated K_{sat} = 0.005 cm/s and the estimated S_{min} = 1.0, placing sample #9 into the "poor" drainability category for both permeability and water retention.

5.1.5 Recommendation 3: Qualitative Material Rating Based on Percent Fines

In lieu of either direct measurements or estimations of K_{sat} and S_{min} from grain size indices, percent fines from mechanical grain size analysis can be used to establish acceptability bounds for "excellent," "marginal," and "poor" drainage. Figure 5.1 is a plot of measured K_{sat} and S_{min} along with measured percent fines. Boundaries for "excellent" and "marginal" drainability are established at percent fines of less than 3% and less than 5%, respectively.

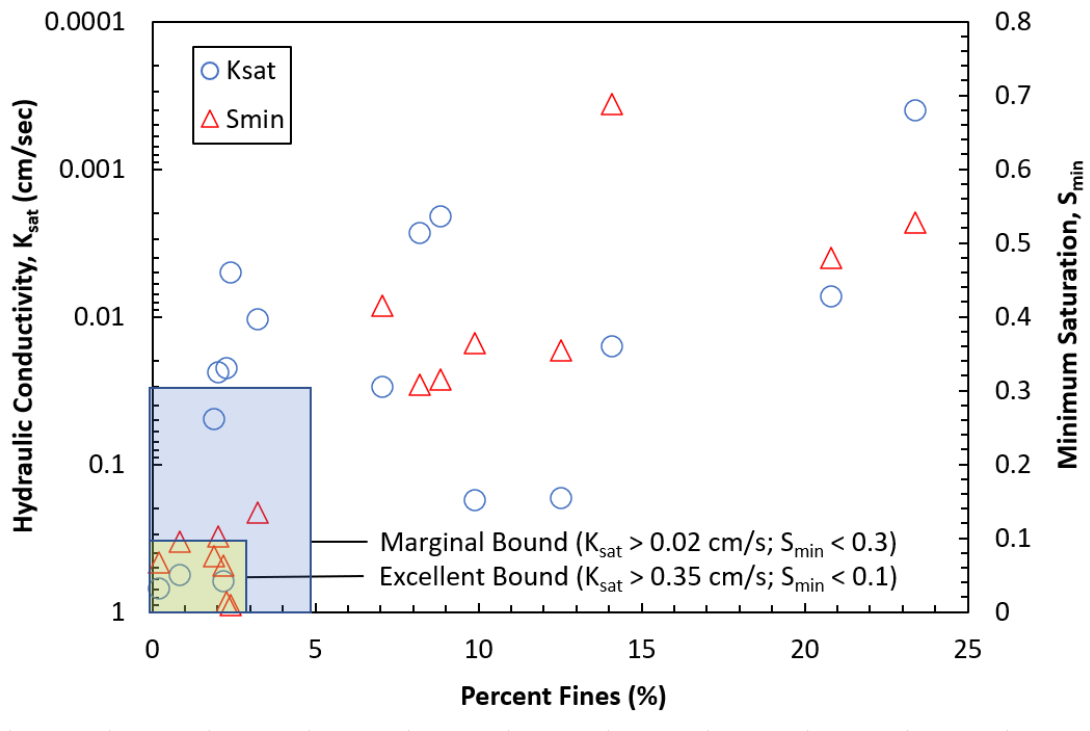

Figure 5.1 Relations among hydraulic conductivity, minimum saturation and percent fines with boundaries for "excellent" and "marginal" drainability.

Table 5.4 summarizes ratings of the 16 base course materials based on these bounds for percent fines: 7 materials satisfy criterion for "excellent" quality, 1 material is designated "marginal," and 8 materials are designated as "poor."

Table 5.4 Qualitative performance rating of materials based on percent fines

Sample	% Fines	Overall Rating
#1 (SP-SM)	8.8	Poor
#2 (SW-SM)	8.2	Poor
#3 (SM)	20.8	Poor
#4 (GM)	12.5	Poor
#5 (SP)	1.9	Excellent
#6 (GP)	0.2	Excellent
#7 (SW)	2	Excellent
#8 (SP)	2.4	Excellent
#9 (GP)	2.2	Excellent
#10 (SP)	3.2	Marginal
#15 (GM)	14.1	Poor
#16 (SM)	23.4	Poor
A1 (GW-GM)	7.1	Poor
A2 (GP)	0.8	Excellent
A3 (SP)	2.3	Excellent
A4 (GW-GM)	9.9	Poor

5.1.6 Comparison of Qualitative Drainability Approaches and Implementation

Table 5.5 is a comparison of overall ratings for each material following each of these three approaches (direct measurements, estimations from grain size, and estimations from percent fines). In the comparison of ratings obtained from the three approaches, the ratings obtained from estimations based on % fines are more conservative (e.g., more likely to result in poor classification), except the ratings for the four sands including #5, #7, #8, and A3, than the two others. The ratings obtained from estimations based on grain size are generally optimistic compared to direct measurements. That is, if ratings obtained from direct measurements are used as references, drainability of the 16 samples are optimistically rated when they are rated using the approach based on grain size while those are conservatively rated when they are rated using the approach based on % fines.

Although the two approaches based on grain size (Recommendation 2) and percent fines (Recommendation 3) are time- and cost-effective and convenient, the rating systems may include errors as shown in comparisons of experimental results and estimations in Chapter 4. Moreover, the material that include fines can have a low minimum saturation, such as #8 and A3 (see Figure 4.5 and Table 4.2). Therefore, these observations should be carefully considered when selecting assessment approaches for specific scenarios.

Additional implementation into design software may also be considered. MnPAVE Flexible, for example, consists of three design levels: basic, intermediate, and advanced. Design level is selected based on the amount and quality of information known about the material properties, progressing from only general knowledge in basic mode to advanced knowledge about material properties and environmental operating range in advanced mode. By analogy, the three qualitative drainability approaches proposed here can be considered as an input for: 1) advanced level when the rating system based on direct measurements is applicable, 2) intermediate level when the rating system based on either grain size or fines content is applicable, and 3) basic level when grain size index properties and fines content are not available.

Table 5.5 Comparison of drainability assessments following three recommended approaches

	Overall Rating		
Sample	Direct Measurement	Estimation from Grain Size	Estimation from Percent Fines
#1 (SP-SM)	Poor-Marginal	Marginal	Poor
#2 (SW-SM)	Poor-Marginal	Marginal	Poor
#3 (SM)	Poor	Poor-Marginal	Poor
#4 (GM)	Marginal	Poor-Marginal	Poor
#5 (SP)	Marg - Excellent	Marginal	Excellent
#6 (GP)	Excellent	Excellent	Excellent
#7 (SW)	Marginal	Marg - Excellent	Excellent
#8 (SP)	Marginal	Marg - Excellent	Excellent
#9 (GP)	Excellent	Excellent	Excellent
#10 (SP)	Poor-Marginal	Marg - Excellent	Marginal
#15 (GM)	Poor	Poor	Poor
#16 (SM)	Poor	Marginal	Poor
A1 (GW-GM)	Poor-Marginal	Marginal	Poor
A2 (GP)	Excellent	Marg - Excellent	Excellent
A3 (SP)	Marg - Excellent	Marginal	Excellent
A4 (GW-GM)	Poor-Marginal	Marginal	Poor

REFERENCES

AASHTO. (1998). *AASHTO guide for design of pavement structures*. Washington, DC: American Association of State Highway and Transportation Officials.

AASHTO. (2007). Chapter 14 – Culvert inspection, material selection, and rehabilitation guideline. In *Highway drainage guidelines* (Fourth edition). Washington, DC: American Association of State Highway and Transportation Officials.

Alyamani, M. S., & Sen, Z. (1993). Determination of hydraulic conductivity from complete grain-size distribution. *Ground Water, 31*(4), 551–555.

Barber, E. S., & Sawyer, C. L. (1952). Highway subdrainage. *Public Roads, 26*, 251–268.

Barr, D. W. (2001). Coefficient of permeability determined by measurable parameters. *Ground Water, 39*(3), 356–361.

Benson, C. H., Chiang, I., Chalermyanont, T., & Sawangsuriya, A. (2014). Estimating van Genuchten parameters α and n for clean sands from particle size distribution data. *Proceedings, From Soil Behavior Fundamentals to Innovations in Geotechnical Engineering*, M. Iskander, J. E.Garlanger, & M. H.Hussein (Eds.): American Society of Civil Engineers (ASCE).

Beyer, W. (1964). Zur bestimmung der wasserdurchlassigkeit von kieson und sanduen aus der kornverteilung [On the determination of hydraulic conductivity of gravels and sands from grain-size distribution]. *Wasserwirtschaft Wassertechnik, 14*, 165–169.

Bouchedid, M. B., & Humphrey, D. N. (2005). Permeability of base material for Maine roads. *Transportation Research Record, 1936*(1), 142–149.

Brooks, R. H., & Corey, A. T. (1964). Hydraulic properties of porous media (Hydrology paper No. 3, Civil Eng. Department). Fort Collins, CO: Colorado State University.

Campbell, G. S. (1985). *Soil physics with basic*. Amsterdam: Elsevier.

Campbell, G., & Shiozawa, S. (1992). Prediction of hydraulic properties of soils using particle size distribution and bulk density data. Paper presented at the *International Workshop on Indirect Methods for Estimating the Hydraulic Properties of Unsaturated Soils*, University of California Press, Berkeley, CA.

Carman, P. C. (1937). Fluid flow through granular beds. *Transactions, Institution of Chemical Engineers*, *15*, 150–166.

Carman, P. C. (1956). *Flow of gases through porous media*. London: Butterworths Scientific Publications.

Carsel, R. F., & Parrish, R. S. (1988). Variation within texture classes of soil water characteristics. *Water Resource, 24*, 755–769.

Carrier, W. D. (2003). Goodbye, Hazen; Hello, Kozeny-Carman. *Journal of Geotechnical and Geoenvironmental Engineering, 129*(11), 1054–1056.

Cedergren, H. R. (1973). *Development of guidelines for the design of subsurface drainage systems for highway pavement structural section* (FHWA-RD-73-14. Office of Research), Washington, DC: Federal Highway Administration.

Cedergren, H. R. (1974). *Drainage of highway and airfield pavements.* New York: Wiley.

Cedergren, H. R. (1977). *Seepage, drainage and flow nets*. New York: Wiley.

Cedergren, H. R. (1994). America's pavements: World's longest bathtubs. *Civil Engineering, 64*, 56–58.

Celia, M. A., Bouloutas, E. T., & Zarba, R. L. (1990). A general mass-conserved numerical solution for the unsaturated flow equation. *Water Resources Research, 26*, 1483–1496.

Cetin, B., Coban, H., Edil, T., Ceylan, H., Likos, W., Zheng, J., Buss, A., (2021). *Determining pavement design criteria for recycled aggregate base and large stone subbase* (Final Report). St. Paul, MN: Minnesota Department of Transportation.

Chu, T. Y., Davidson, D. T., & Wickstrom, A. E. (1955). *Permeability test for Sands ASTM Special Technical* (Publication No. 1.63). Philadelphia, PA: American Society for Testing Materials.

Crank, J. (1984). *Free and moving boundary value problems*. Oxford, UK: Claredon Press.

Chapuis, R. P. (2004). Predicting the saturated hydraulic conductivity of sand and gravel using effective diameter and void ratio. *Canadian Geotechnical Journal, 41*(5), 787–795.

Chapuis, R. P., Dallaire, V., Marcotte, D., Chouteau, M., Acevedo, N., & Gagnon, F. (2005). Evaluating the hydraulic conductivity at three different scales within an unconfined sand aquifer at Lachenaie, Quebec. *Canadian Geotechnical Journal, 42*, 1212–1220.

Domenico, P. A., & Schwartz, F. W. (1990). *Physical and chemical hydrogeology*. New York: Wiley.

Dungca, J. R., Galupino, J. G., Alday, J. C., Barretto, M. A. F., Bauzon, M. K. G., & Tolentino, A. N. (2018). Hydraulic conductivity characteristics of road base materials blended with fly ash and bottom ash. *International Journal of GEOMATE, 14*(44), 121–127.

Elhakim, A. F. (2016). Estimation of soil permeability. *Alexandria Engineering Journal, 55*(3), 2631–2638.

ERES. (1998). *Evaluation of Unbonded Portland Cement Concrete Overlays* (Final Report, NCHRP 10-41). Washington, DC: Transportation Research Board.

ERES. (1999). *Pavement subsurface drainage design*. (Reference manual ERES Project No. 99-035-E1). McLean, VA: U.S. Dept. of Transportation, Federal Highway Administration, National Highway Institute.

ERES. (2004). *Guide for mechanistic-empirical design of new and rehabilitated pavement structures.* Washington, DC: National Cooperative Highway Research Program, Transportation Research Board, National Research Council.

Espinoza, R. D., Bourdeau, P. L., & White, T. D. (1993). *Pavement drainage and pavement shoulder joint evaluation and rehabilitation*. *Numerical analysis of infiltration and drainage in pavement systems.* West Lafayette, IN: Purdue University.

Fair, G. M., & Hatch, L. P. (1933). Fundamental factors governing the stream-line flow of water through sand. *Journal of American Water Works Association, 25*, 1551–1565.

FHWA. (1992). *Drainable pavement systems: Participant notebook, demonstration project 87* (Publication No. FHWA-SA-92-008). Washington, DC: Federal Highway Administration (FHWA).

Fredlund, M. D., Wilson, G. W., & Fredlund, D. G. (2002). Use of the grain-size distribution for estimation of the soil-water characteristic curve. *Canadian Geotechnical Journal, 39*(5), 1103–1117.

Fredlund, D. G., & Xing, A. (1994). Equations for the soil-water characteristic curve. *Canadian Geotechnical Journal, 31*, 521–532.

Fu, H. Y., Wu, S. J., & Wang, G. Y. (2009). Experimental study of influence of compressive stress on water permeability of sands soils (in Chinese). *Rock and Soil Mechanics, 30*(12), 3677–3681.

Ghanbarian-Alavijeh, B., Liaghat, A., Huang, G.-H., & Van Genuchten, M. T. (2010). Estimation of the van Genuchten soil water retention properties from soil textural data. *Pedosphere, 20*(4), 456–465.

Green, R. E., & Corey, J. C. (1971). Calculation of hydraulic conductivity: A further evaluation of some predictive methods. *Soil Science Society of America Journal, 35*, 3–8.

Guyer, P. J. (2018). *An introduction to subsurface drainage for pavements*. El Macero CA: Guyer Partners

Hansen, V. E., Israelson, O. A., & Stingham, G. (1979). *Irrigation principles and practice*. New York: Wiley.

Harleman, D. R. F., Melhorn, P.F., & Rumer, R.R. (1963). Dispersion-permeability correlation in porous media. *Journal of the Hydraulic Division 89*(2), 67–85.

Hazen, A. (1892). *Some physical properties of sands and gravels, with special reference to their use in filtration* (24th annual report, 539–556). Boston, MA: Massachusetts State Board of Health.

James, L.G. (1988). *Principles of farm irrigation system design*. New York: Wiley.

Kern, J. S. (1995). Evaluation of soil water retention models based on basic soil physical properties. *Soil Science Society of America Journal, 59*(4), 1134–1141. https://doi.org/10.2136/sssaj1995.03615995005900040027x

Klink, T., (2021). Drainage characteristics of recycled materials for mechanically stabilized earth walls, (MS thesis). Madison, WI: University of Wisconsin-Madison.

Koerner, R. M. (1990). *Designing with geosynthetics* (Second edition). Englewood Cliffs, NJ: Prentice Hall.

Koenders, M. A., & Williams, A. F. (1992). Flow equations for particle fluid mixtures. *Acta Mechanica, 92*(1), 91–116.

Kozeny, J. (1927). Uber kapillare leitung des wassers in boden. Sitzungsber Akad (in German). *Wiss. Wien Mathematica Naturwiss K1, Abt.2a*, *136,* 271–306.

Kozeny, J. (1953). Das wasser im boden. grundwasserbewegung. *Hydraulik*, 380–445.

Kruger, E. (1918). Die grundwasserbewegung (in German). *Internationale Mitteilungen fur Bodenkunde, 8*, 105.

Krumbein, W. C., & Monk, G. D. (1943). Permeability as a function of the size parameters of unconsolidated sands. *Transactions of the American Institute of Mining, Metallurgical and Petroleum Engineers, 151*, 153–163.

Lenhard, R. J., Parker, J. C., & Mishra, S. (1989). On the correspondence between Brooks-Corey and van Genuchten models. *Journal of Irrigation and Drainage Engineering, 115*(4), 744–751.

Leong, E. C., & Rahardjo, H. (1997). Reviews of soil-water characteristic curve equations. *Journal of Geotechnical and Geoenvironmental Engineering, 123*, 1106–1117.

LRRB. (2003). *Effective methods to repair frost damaged roadways* (Research implementation series Number 27). MN: Local Road Research Board.

Lu, C., Chen, X., Cheng, C., Ou, G., & Shu., L. (2012). Horizontal hydraulic conductivity of shallow streambed sediments and comparison with grain-size analysis results. *Hydrological Processes, 26*, 454–466.

Lu, N., & Likos, W. J. (2004). *Unsaturated soil mechanics*. New York: Wiley.

Marianelli, F., & Durnford, D. S. (1998). Semi analytical solution to Richard's equation for layered porous media. *Journal of Irrigation and Drainage Engineering, 124*, 290–299.

McEnroe, B. M. (1994). Drainability of granular bases for highway pavements. *Transportation Research Record, 1434,* 23–28.

MnDOT. (1994). *Permeable aggregate base drainage systems - Design guidelines*. St. Paul, MN: Materials Engineers Committee, Minnesota Department of Transportation.

MnDOT. (1995). *Comparison of pavement drainage systems* (Research report number Mn/RD–95/28). St. Paul, MN: Minnesota Department of Transportation.

MnDOT. (2002). *Evaluation of water flow through pavement systems* (Research report number Mn/RC–2002-30). St. Paul, MN: Minnesota Department of Transportation.

MnDOT. (2003a). *Special practices for design and construction of subgrades in poor, wet and/or saturated soil conditions* (Research report number Mn/RC–2003-36). St. Paul, MN: Minnesota Department of Transportation.

MnDOT. (2003b). *Designing pavement drainage systems: The MnDRAIN Software* (Research report number Mn/RC–2003-17). St. Paul, MN: Minnesota Department of Transportation.

MnDOT. (2009a). *Evaluating roadway subsurface drainage practices* (Research report number MN/RC 2009–08). St. Paul, MN: Minnesota Department of Transportation.

MnDOT. (2009b). *Subsurface drainage manual for pavements in Minnesota* (Research report number MN/RC 2009–17). St. Paul, MN: Minnesota Department of Transportation.

MnDOT. (2012). *A Research plan and report on factors affecting culvert pipe service life in Minnesota* (Research report number MN/RC 2012–27). St. Paul, MN: Minnesota Department of Transportation.

Mokwa, R. L., & Trimble, N. R. (2008). Permeability of coarse-grain soil from void space and pore distribution. Paper presented at *GeoCongress 2008*, New Orleans, LA.

Moulton, L. K. (1980). *Highway subsurface drainage design* (FHWA-TS-80-224). Washington, DC: Office of Research and Development, Federal Highway Administration.

Navfac DM7. (1974). *Design manual—Soil mechanics, foundations and earth structures*. Washington, DC: U.S. Government Printing Office.

NYDOT. (1973). *Test procedures for specific surface analysis soil test procedures STP-1*. New York: Soil Mechanics Bureau.

Oh, Y., Hamm, S., Chung, S. Y., & Lee, B. D. (2013). Characterizing hydraulic properties by grain-size analysis of fluvial deposits depending on stream path in Korea. *Environmental Engineering Research, 18*(3), 129–137, https://doi.org/10.4491/eer.2013.18.3.129

Pineda, M. C., Viloria, J., Martínez-Casasnovas, J. A., Valera, A., Lobo, D., Timm, L. C., Pires, L. F., & Gabriels, D. (2018). Predicting soil water content at − 33 kPa by pedotransfer functions in stoniness 1 soils in northeast Venezuela. *Environmental Monitoring and Assessment, 190*(161), https://doi.org/10.1007/s10661-018-6528-3

Pravedny, G. H. (1966). *Design and selection of grain size composition of filter beds for the transition zones of large dams*. Moscow: Energiia.

Rawls, W. J., Ahuja, L. R., Brakensiek, D. L., & Shirmohammadi, A. (1992). Soil water movement and infiltration. In *Handbook of hydrology*. New York: McGraw Hill.

Ren, X., Zhao, Y., Deng, Q., Kang, J., Li, D., & Wang, D. (2016). A relation of hydraulic conductivity — void ratio for soils based on Kozeny-Carman equation. *Engineering Geology, 213*, 89–97.

Richards, L. A., & Weaver, L. R. (1944). Moisture retention by some irrigated soils as related to soil-moisture tension. *Journal of Agricultural Research, 69*(6), 215–235.

Robertson, P. K. (2010). Estimating in-situ soil permeability from CPT & CPTu. Paper presented at the 2nd International Symposium on Cone Penetration Testing, Huntington Beach, CA.

Rosas, J., Lopez, O., Missimer, T. M., Coulibaly, K. M., Dehwah, A. H. A., Sesler, K., & Mantilla, D. (2013). Determination of hydraulic conductivity from grain-size distribution for different depositional environments. *Groundwater, 52*(3), 399–413.

Salarashayeri, A. F., & Siosemarde, M. (2012). Prediction of soil hydraulic conductivity from particle-size distribution. *World Academy of Science Engineering and Technology, International Journal of Geological and Environmental Engineering, 6*(1), 16–20.

Seelheim, F. (1880). Methoden zur bestimmung der durchlässigkeit des bodens (in German). *Zeitschrift für Analytische Chemie, 19*, 387–418.

Sillers, W. S., Fredlund, D. G., & Zakerzadeh, N. (2001). Mathematical attributes of some soil-water characteristic curve models. *Geotechnical and Geological Engineering, 19*, 243–283.

Singh, V. P. (1997). *Kinematic wave modeling in water resources: Environmental hydrology*. New York: Wiley.

Slichter, C. S. (1899). *Theoretical investigation of the motion of ground waters*. (U.S. Geological Survey 19th annual report, Part 2: 322). Reston, VA: USGS.

Smith, K. D., Mueller, A. L., Darter, M. I., & Peshkin, D. G. (1990). *Performance of jointed concrete pavements, Volume II - Evaluation and modification of concrete pavement design and analysis models.* McLean, VA: Federal Highway Administration.

Stephens, D. B., Hsu, K., Prieksat, M. A., Ankeny, M. D., Blandford, N., Roth, T. L., Kelsey, J. A., & Whitworth, J. R. (1998). A comparison of estimated and calculated effective porosity. *Hydrogeology Journal*, 6, 156–165, https://doi.org/10.1007/s100400050141

Terzaghi, C. (1925). Principles of soil mechanics. *Engineering News Record, 95*, 832.

Trzebiatowski, B., & Benson, C. (2005). Saturated hydraulic conductivity of compacted recycled asphalt pavement. *Geotechnical Testing Journal, 28*(5), 514–519.

Tinjum, J., Benson, C., & Blotz, L. (1997). Soil-water characteristic curves for compacted clays. *Journal of Geotechnical and Geoenvironmental Engineering, 123*(11), 1060–1069.

van Genuchten, M. T. (1980). A closed form solution for predicting the hydraulic conductivity of unsaturated soil. *Soil Science Society of America Journal, 11*, 892–898.

van Genuchten, M. T., Leij, F. J., & Yates, S. R. (1991). *The RETC code for quantifying the hydraulic functions of unsaturated soils* (Report IAG-DW 12933934). Riverside, CA: U.S. Department of Agriculture, Agricultural Research Service.

Vauclin, M., Khanji, D., & Vachaud, G. (1979). Experimental and numerical study of a transient two dimensional unsaturated-saturated water table recharge problem. *Water Resources Research, 15*(5), 1089–1101.

Vukovic, M., & A. Soro. (1992). *Determination of hydraulic conductivity of porous media from grain-size composition*. Littleton, CO: Water Resources Publications.

Wan, L., Jiang, X. W., & Wang, X. S. (2010). A common regularity of aquifers: The decay in hydraulic conductivity with depth (in Chinese). *Geological Journal of China Universities, 16*(1), 7–12.

Wang, J. P., François, B., & Lambert, P. (2017). Equations for hydraulic conductivity estimation from particle size distribution: A dimensional analysis. *Water Resources Research, 53*(9), 8127–8134.

Wraith, J. M., & Or, D. (1998). Nonlinear parameter estimation using spreadsheet software. *Journal of Natural Resources and Life Sciences Education, 27*, 13–19.

Zhang, G. L., & Wang, Y. J. (2014). Experimental investigation of hydraulic conductivity of sand under high confining pressure (in Chinese). *Yantu Lixue/Rock and Soil Mechanics, 35*(10), 2748–2754.

Zienkiewicz, O. C., & Taylor, R. L. (1989). *The finite element method (Fourth edition)*. New York: McGraw-Hill.

APPENDIX A
CASE HISTORY REVIEW

Case histories summarized here were primarily focused on evaluating subsurface drainage systems based on literature reviews, surveys, experiments, numerical modeling, and statistical analyses. Review of these studies provides theoretical and practical background for the current research project. Emphasis is placed on research on pavement systems performed by the Minnesota Department of Transportation (MnDOT).

A.1 EVALUATION OF WATER FLOW THROUGH PAVEMENT SYSTEMS (MNDOT, 2002)

Pavement systems can be fully saturated only under very specific circumstances, such as surface ponding where positive total heads are present and distributed in such a manner that saturation of the pavement system is reached. Drainage design criteria used in the past has predominantly assumed the flow of water through pavements and the drainage of pavement layers can be represented with saturated flow. In this research project, unsaturated water flow in three testing sections, MnROAD Cell 33, Cell 34, and Cell 35, was numerically modeled using SEEP/W to represent the first step in the development of a comprehensive approach considering the unsaturated soil condition. Results of the SEEP/W modeling were compared with experimental results and analytical solutions calculated using Drainage Requirements In Pavements (DRIP) from the Federal Highway Administration (FHWA).

Prior to modeling for the testing sections, experimental results and analytical solutions in Espinoza et al. (1993) and Vauclin et al. (1979) were compared with SEEP/W predictions to evaluate use of SEEP/W for modeling the water flow through soils and simplified pavement systems. Comparison of results for three example cases showed that SEEP/W is a useful tool for the modeling of unsaturated flow through layered systems under complex boundary conditions and material characterization.

For material properties of the three testing sections used in the modeling, soil-water characteristic curves (SWCCs) and hydraulic conductivity functions (HCF) for base material, Class 6 special material, and subgrade soil, R-12 silty clay, were measured using the suction plate testing (Figure A.1). The air-entry pressures in SWCCs were shifted to 3 kPa for the modeling. A saturated hydraulic conductivity of 1.54E-6 m/s was obtained from Figure A.1(c). In addition, using automated time domain reflectometry (TDR) probes, volumetric water contents were measured in the base layer at 0.13 m (101), 0.25 m (102), and 0.38 m (103) depth. The measured TDR volumetric water contents were used as benchmarks for adjusting laboratory-based unsaturated soil hydraulic properties.

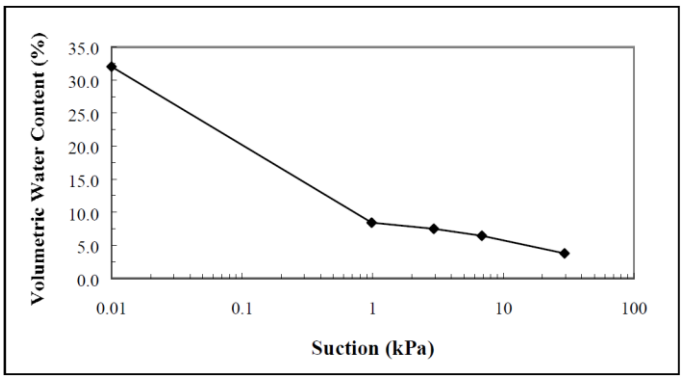
Volumetric Water Content (%)
35.0
30.0
25.0
20.0
15.0
10.0
5.0
0.0
0.01
0.1
1
10
100
Suction (kPa)

(a)

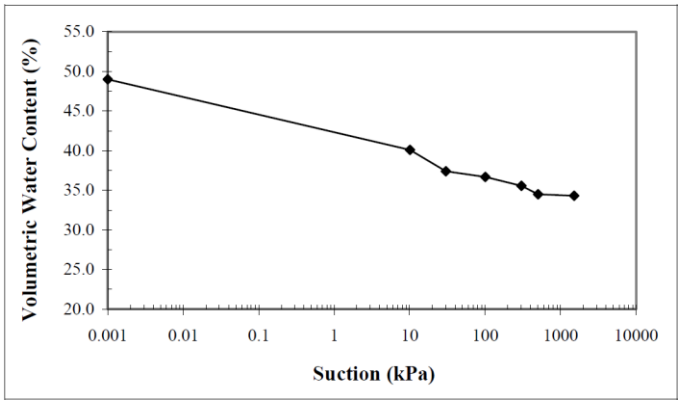
Volumetric Water Content (%)
55.0
50.0
45.0
40.0
35.0
30.0
25.0
20.0
0.001
0.01
0.1
1
10
100
1000
10000
Suction (kPa)

(b)

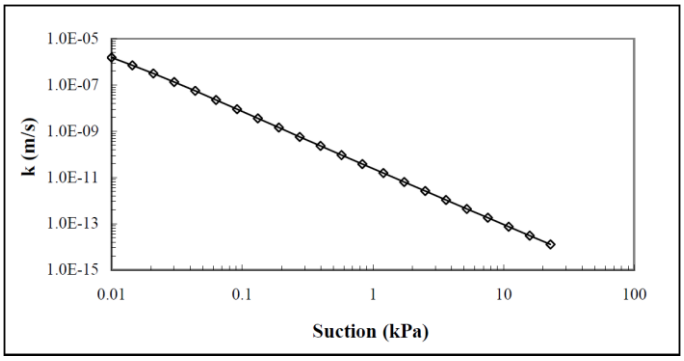
k (m/s)
1.0E-05
1.0E-07
1.0E-09
1.0E-11
1.0E-13
1.0E-15
0.01
0.1
1
10
100
Suction (kPa)

(c)

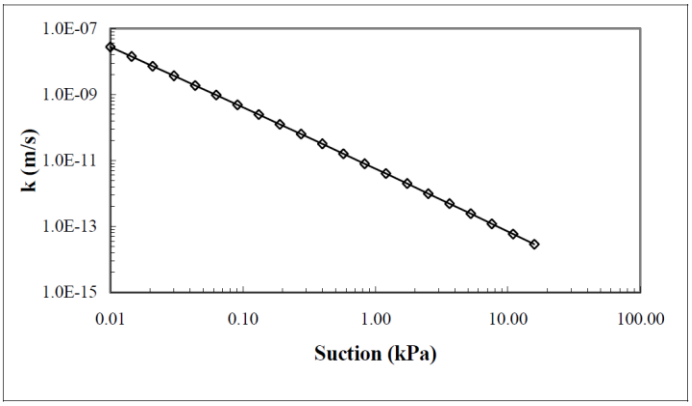

(d)

Figure A.1 Material properties used in the modeling: (a) soil-water characteristic curve for base material (Class 6 special), (b) soil-water characteristic curve for subgrade soil (R-12 silty clay), (c) hydraulic conductivity curve for base material (Class 6 special), and (d) hydraulic conductivity curve for subgrade soil (R-12 silty clay)

The three sections consisted of a layer of hot mix asphalt (i.e., impervious material), a Mn/DOT Class 6 Special base course (consisting of 100 percent crushed granite), and an R-12 silty clay subgrade (Figure A.2). A time-dependent flux boundary condition was applied on the shoulder to simulate infiltration from precipitation. Rain events (time-dependent flux condition) were applied on top of the base, and the ones underneath the hot mix asphalt represent no infiltration through this material [Figure A.2(a)]. To represent real conditions more accurately, the subgrade layer was extended laterally 10 m beyond the area covered by the asphalt and base layer [Figure A.2(b)]. To induce lateral and vertical drainage in the system, points of total head equal to 0 m were applied at the bottom corners.

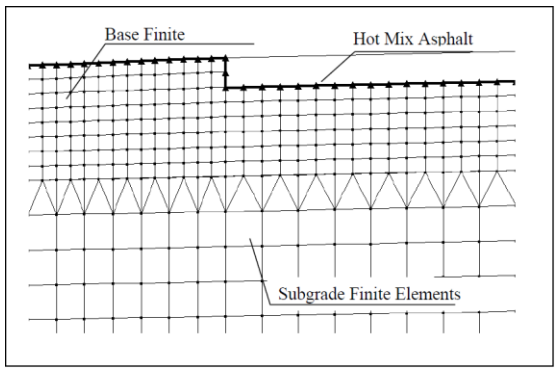

(a)

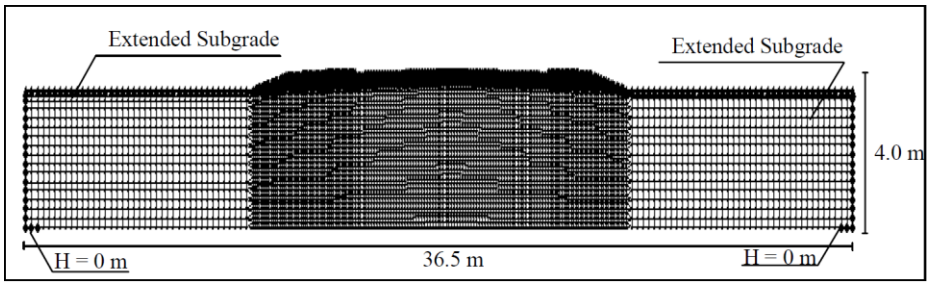

(b)

Figure A.2 Geometry and mesh used in the modeling: (a) section representing Cells 33, 34, and 35 and (b) extended subgrade layer

Figure A.3 shows the measured TDR water contents for each cell. For a more detailed and definitive comparison between measured and predicted results, the span of time from July 31st to September 30th, 2000 was chosen for this study. Although the range is 22 days shorter than the precipitation data, the first 22 days established an initial volumetric water content baseline in the model.

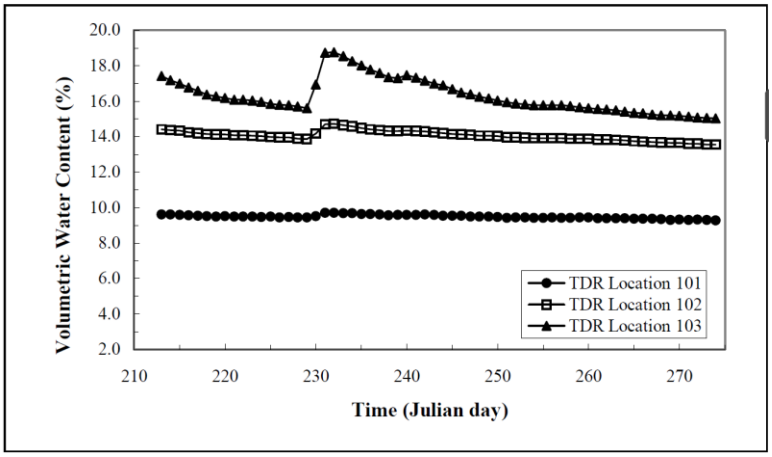

(a)

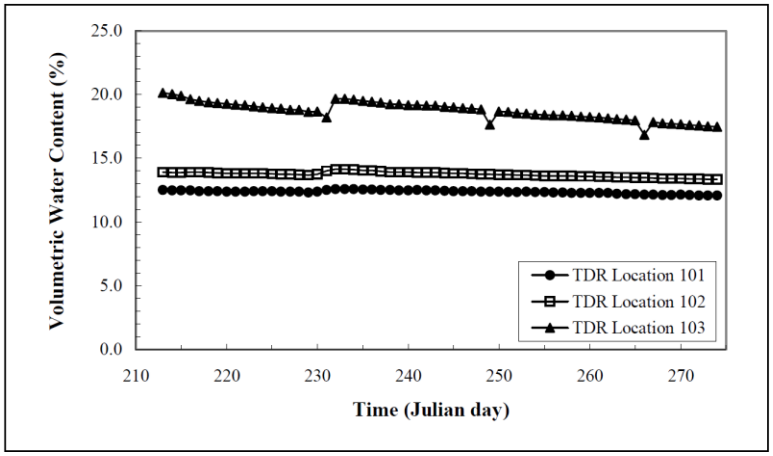

(b)

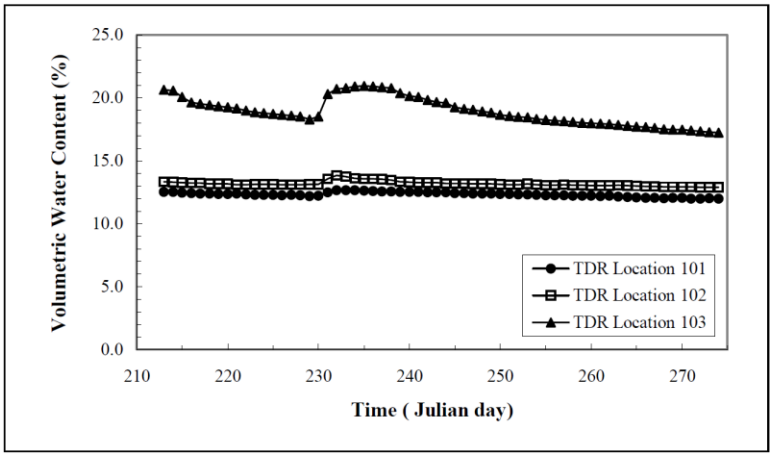

(c)

Figure A.3 Volumetric water content obtained from TDR probes: (a) at Cell 33, (b) at Cell 34, and (c) at Cell 35

As volumetric water contents predicted from SWCCs [Figures A.1(a) and (b)] were slightly different from the TDR field volumetric moisture contents due to limitations (e.g., the required empirical calibration of results, differences in field and laboratory compaction processes), SWCCs were adjusted to fit the TDR field data based on the air entry values, saturated volumetric water content, and the slope of the SWCCs. After the calibrations, hydraulic conductivity curves were generated using the Green and Corey (1971) formulation in SEEP/W. These procedures were used to simulate changes in volumetric water contents for Cells 33, 34, and 35 at TDR locations 101, 102, and 103. Figure A.4 shows Cell 34 results as examples, and the results were well aligned.

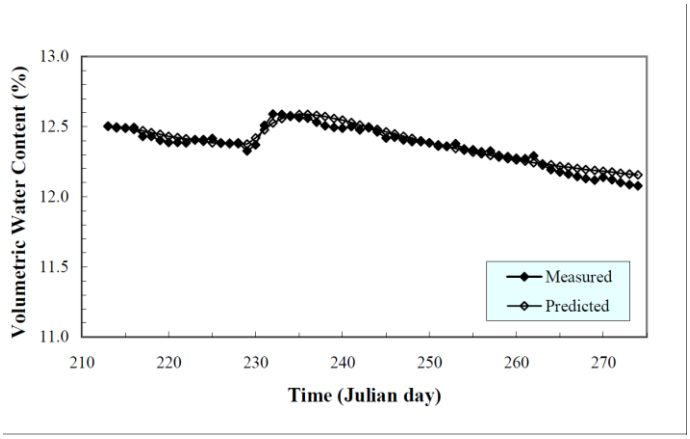

(a)

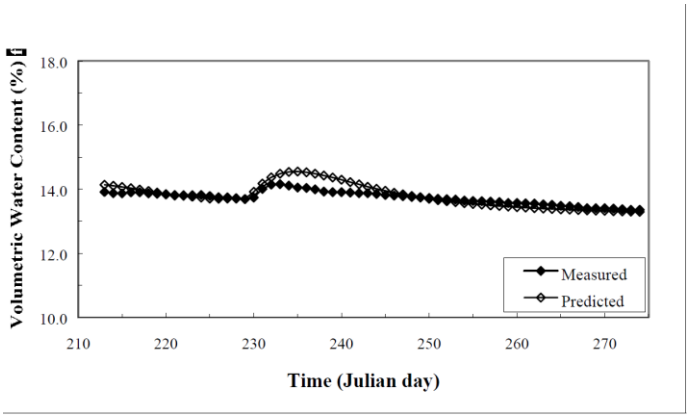

(b)

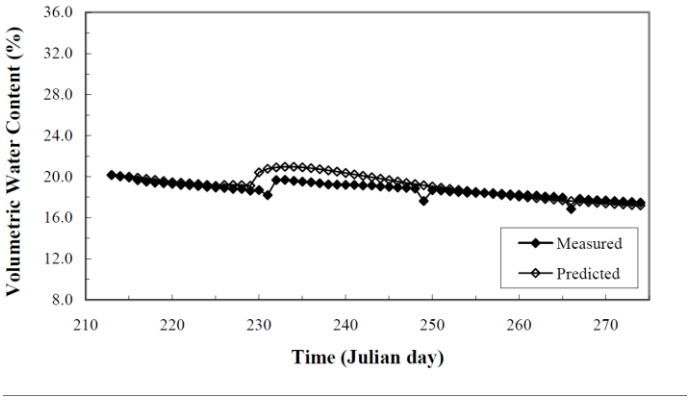

(c)

Figure A.4 Comparisons of volumetric water contents obtained at Cell 34: (a) TDR location 101, (b) TDR location 102, and (c) TDR location 103

In addition, sensitivity analyses were conducted using Cell 33 at TDR location 101 (as a representative pavement configuration) for evaluating effects of : 1) the initial slope of the soil water characteristic curve, 2) the air entry value of the Mn/DOT Class 6 Special crushed granite, 3) the saturated hydraulic conductivity of the Mn/DOT Class 6 Special crushed granite, 4) the air entry value of the R-12 silty clay subgrade soil, 5) the saturated hydraulic conductivity for the subgrade soil, 6) the type of granular base material, 7) variations in infiltration characteristics, and 8) the water table location. The results indicated that the most sensitive parameters were as follows: 1) the air entry value of the granular base course material, 2) water table location, and 3) gradation and type of Mn/DOT Class granular base material. Similarly, moderate sensitivity was observed with changes in saturated hydraulic conductivity of the subgrade and time history of infiltration. Finally, the volumetric moisture content was found to be relatively insensitive to changes in the initial slope of the soil water characteristic curve, the saturated hydraulic conductivity of the granular base material, and the air entry value for the subgrade soil.

Lastly, in this research project, effects of edge and under drains on the water flow were evaluated. The edge drain consists of coarse graded gravel surrounding a collector pipe in trench that is longitudinally placed next to the outer traffic lane under the shoulder. The under drain consists of a layer of a woven or non-woven geotextile that extends all the way under the traffic lanes to replace an equivalent sand drainage layer. The numerical modeling for Cell 33 was used as a baseline with four drainage systems: 1) the original pavement section for Cell 33 with a 0.02 m thick geotextile underdrain located between the Mn/DOT Class 6 Special crushed granite base course and the subgrade soil, 2) modification of Case 1, in which collector pipes were placed directly in the Mn/DOT Class 6 Special crushed granite coarse base material under the shoulder, 3) a typical edge drain configuration from Cell 10, and 4) a combination of an edge drain and a geotextile under drain system, in which the under drain now connects to a backfilled trench containing a collector pipe. The main difference between Case 2 and Case 4 was that the material around the collector pipe (Case 2) was Class 6 Special crushed granite, while the material around the edge drain consisted of well-draining gravel (pea gravel). The results indicated that under drains did not significantly improve the drainability of dense graded bases, while either collector pipes or edge drains in combination with under drains was very effective to reduce the amount of moisture in a Mn/DOT Class 6 Special crushed granite base course material. This was because of the effects of zero head boundary conditions around the collector pipes and edge drains, which in combination with the shortened drainage path due to the under drains affected the distribution of suctions significantly throughout the base material, thus promoting better drainage.

A.2 DESIGN AND CONSTRUCTION OF SUBGRADES IN POOR, WET, AND/OR SATURATED SOIL CONDITIONS (MNDOT, 2003A)

In constructions of pavement structures the subgrade soil helps resist the destructive effects of traffic and weather (MnDOT, 2003a). For the subgrade, naturally occurring soils have been used due to various benefits (e.g., cost-effective, easier access). However, the subgrade based on natural soil sometimes has mechanically and physically poor conditions that should be improved. In this research project, literature

review, questionnaire directed to Minnesota state, county, and city highway engineers, and interviews were thus conducted to provide enhanced methods for the subgrade.

MnDOT (2003a) summarizes various traditional subgrade enhancement choices: 1) surface (e.g., pavement) drainage of runoff and subsurface (e.g., embankment) drainage of infiltrated water, 2) compaction using heavy equipment, 3) moisture content adjustment through mechanical or chemical methods, 4) soil modification with cementing or drying agents (e.g., lime, fly ash, bituminous), 5) soil stabilization with cementing or drying agents (e.g., Portland cement, lime, fly ash), 6) reinforcement and separation using geosynthetics (e.g., geotextile, geogrid, geomembrane), and 7) substitution with natural (granular, wood) or man-made materials (shredded tires, form). Compatibility with in-service subgrade soil conditions, extent of improvement required, safety precautions or environmental concerns, and construction requirements should be considered to appropriately select the enhancement method.

Drainage refers to the removal of surface and/or subsurface water, such as drawdown of the water table, intercepting lateral seepage above an impervious pavement layer, drain of infiltrating surface water, and preventing capillary rise or collecting discharge from other drainage systems. Proper drainage helps maintain the pavement strength due to a decrease in pore water pressure (i.e., increased inter-particle friction) and minimizes frost heave and thaw weakening. The surface drainage is achieved using storm sewers, ditches, culverts, or bridges, and the subsurface drainage is accomplished through uses of permeable base, pipes, drains, and geosynthetics.

There are two common drainage systems for subgrade enhancement: longitudinal edge drains and permeable base layer. Effectiveness and performance of the longitudinal drains and the permeable base are dependent on filter materials, pipes, location of seepage area within the system, and soil permeability. For example, permeable asphalt stabilized base (PASB), which has a permeability coefficient of 300 m/day, drained the most water within 2 hours of the end of rainfall (MnDOT, 1995). According to MnDOT (2003a), permeable bases may be treated with asphalt (2 – 5 % by weight) or Portland cement (2 – 3 bags/cubic yard) for strength in construction. A separator layer should be installed a minimum depth of 4 in. (102 mm) below the permeable base to prevent the migration of fine aggregate particles. Aggregate should have a dense gradation, and there are uniformity requirements as follows:

$$\frac{D_{15}}{D_{85}} \text{ of } \frac{filter}{subgrade} \text{ and } \frac{base}{filter} \leq 5 \tag{A.1}$$

$$\frac{D_{50}}{D_{50}} \text{ of } \frac{filter}{subgrade} \text{ and } \frac{base}{filter} \leq 25 \tag{A.2}$$

$$20 \leq \frac{D_{60}}{D_{10}} \leq 40 \tag{A.3}$$

where D_{15} = Maximum particle size at which 15 percent of the aggregate is finer, D_{50} = Maximum particle size at which 50 percent of the aggregate is finer, D_{85} = Maximum particle size at which 85 percent of the aggregate is finer.

For pavement applications in Minnesota, various geosynthetics are used as a separation of dissimilar materials, a subgrade enhancement, a drainage application, and for filtration in the drainage system. Specifically, geomembrane, which is a relatively impermeable barrier due to the low permeability of water vapor for geomembrane (5×10^{-11} to 5×10^{-14} cm/s), is used for the separation between an underlying fine-grained soil and an aggregate base or granular subbase. Geogrid is commonly used to reduce deformation and improve the durability and lifespan of paved roads, primarily due to an increase in stiffness and the load spreading ability of geogrids. Geonet, which is similar to the geogrid except larger apertures, is used for drainage application. The drainage performance is dependent on the thickness (ASTM D1777) and can be degraded over time due to clogging of soil particles, destruction at a high temperature, and damages caused by chemical reactions. Lastly, in the drainage system, small aperture of the geotextiles keeps large particles from entering the drainage layer or pipe, allowing some of the small, suspended particles to pass without clogging.

There are three major design components for a geosynthetic drainage system: 1) maximum flow rate necessary to drain area, 2) percent and size of fine-grained material, and 3) type of drain system to be implemented. The maximum aperture of the geosynthetic must be smaller than the larger particles in the soil, retaining a majority of the soil, and use of transmissivity values will help ensure adequate flow with proper soil retention.

Table A.1 Typical values of transmissivity (in-plane drainage capability) of geotextiles (Koerner, 1990)

Type of Geotextile	Transmissivity (m^2/s)	Permeability (m/s)
Nonwoven, heat-bonded	3.0×10^{-9}	6×10^{-6}
Woven, slit-film	1.2×10^{-8}	2×10^{-5}
Woven, monofilament	3.0×10^{-8}	4×10^{-5}
Nonwoven, needle-punched	2.0×10^{-6}	4×10^{-4}
*Values taken at applied normal stress of 40 kPa		

In addition to the geosynthetics, shredded tires have been used as a lightweight fill and drainage layers (hydraulic conductivity of tire shreds is 1 cm/sec). As tire shreds have a compacted dry density of one-third to one-half of the compacted dry density of a typical soil, the tires are attractive lightweight fill for construction on weak and compressible soils where slope stability or excessive settlement is concerned. Due to the low thermal conductivity of tire shreds, the tires can be used as an insulating layer of 6 in. (150 mm) to 18 in. (450 mm) thickness.

A.3 DESIGNING PAVEMENT DRAINAGE SYSTEMS: THE MNDRAIN SOFTWARE (MNDOT, 2003B)

Edge drain is a drainage used in a road system to remove moisture from the granular base through pipes placed in a gravel trench. To evaluate a quality of the edge drain, for the first step, time to drain the moisture from 100% to 85% saturation is calculated. The calculations are then used to evaluate the drainage quality based on pavement rehabilitation manual guidance of federal highway administration (e.g., excellent = less than 2 hours, good = 2 to 5 hours).

In this research project, MnDrain codes were outlined for a design of the edge drain. Figure A.5 shows the drainage system used for developing MnDrain codes. The system consisted of two materials: fine material that has a low saturated hydraulic conductivity and coarse material that has a relatively higher saturated hydraulic conductivity.

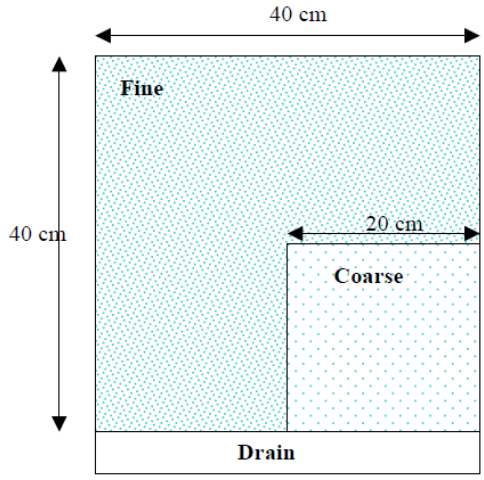

Figure A.5 schematic layered drainage system

For the calculations, mixed form of Richard equations that describe the moisture migration in variably saturated soil was solved using control volume finite element method (CVFE), which is a combination of the finite element and finite volume methods.

$$\frac{\partial \theta}{\partial t} = \nabla \cdot (K(h)\nabla h) + \frac{\partial K}{\partial z} \tag{A.4}$$

where θ = moisture content (a function of pressure head), h = pressure head (negative in the unsaturated region), K = hydraulic conductivity (a function of pressure head). The pressure head, h, is defined as follows:

$$h = \frac{P}{\gamma} \tag{A.5}$$

where P = pressure, γ = specific weight of water. The pressure, P, is equal to the minus of the suction pressure. In terms of the moisture content, the pressure head has three states: 1) $h \geq 0$ when all voids are filled with moisture ($\theta = \theta_{sat}$), 2) $h < 0$ when all voids are filled by capillary action (the moisture content is still $\theta = \theta_{sat}$), and 3) $h < 0$ when $\theta_{res} < \theta(h) < \theta_{sat}$, where θ_{res} = residual moisture content ($h \to -\infty$).

In addition to Richard equation (Equation A.4), there are two auxiliary relationships among the moisture content, hydraulic conductivity, and pressure head: Brooks Corey (1964) and van Genuchten (1980).

Brooks Corey (1964)

$$\theta = \begin{cases} (\theta_{sat} - \theta_{res})(h/h_d)^{-\lambda_1} + \theta_{res}, & h < h_d \\ \theta_{sat}, & h > h_d \end{cases} \quad \text{(A.6)}$$

$$K = K_{sat}\left[\frac{\theta-\theta_{res}}{\theta_{sat}-\theta_{res}}\right]^{\lambda_2} \quad \text{(A.7)}$$

where λ = material constant.

van Genuchten (1980)

$$\theta = \begin{cases} \frac{\theta_{sat}-\theta_{res}}{(1+|\alpha h|^n)^m} + \theta_{res} & h < h_d \\ \theta_{res} & h > h_d \end{cases} \quad \text{(A.8)}$$

$$K = K_{sat}\left[\frac{\theta-\theta_{res}}{\theta_{sat}-\theta_{res}}\right]^{0.5}\left[1-\left(1-\left[\frac{\theta-\theta_{res}}{\theta_{sat}-\theta_{res}}\right]^{1/m}\right)^m\right]^2 \quad \text{(A.9)}$$

where $\alpha, m, and\ n$ = material parameters.

In this study, the Brooks Corey equations were used with an artificial relationship, C_{val}, to form a solution of the non-linear equations resulting from a discretization of the equation:

$$\theta = \begin{cases} (\theta_{sat} - \theta_{res})(h/h_d)^{-\lambda_1} + \theta_{res}, & for\ h < h_d \\ C_{val}(h - h_d) + \theta_{sat}, & for\ h \geq h_d \end{cases} \quad \text{(A.10)}$$

If the constant C_{val} is small enough (10^{-4} was used in this study), this extended definition has a minimal impact on the results, allowing a continuous relationship between θ and h throughout the solution.

According to MnDOT (2003b), a rapid change in the moisture content cannot be treated well using the Richards equation (Equation A.4), possibly involving discontinuous hydraulic conductivity. The equation A.4 was thus incorporated with a Kirchoff transformation (Crank, 1984) and can be rewritten as follows:

$$\frac{\partial\theta}{\partial t} = \nabla^2\varphi + \frac{\partial K}{\partial z} \quad \text{(A.11)}$$

where $\varphi = \int_0^h -K(\alpha)\, d\alpha$. The governing equation (Equation A.11) was solved using CVFE method, and the first step was generating a mesh of triangular elements that covers the two-dimensional domain with node points located at vertices (Figure A.6). An interface between two layers of material in the drain lies along element edges.

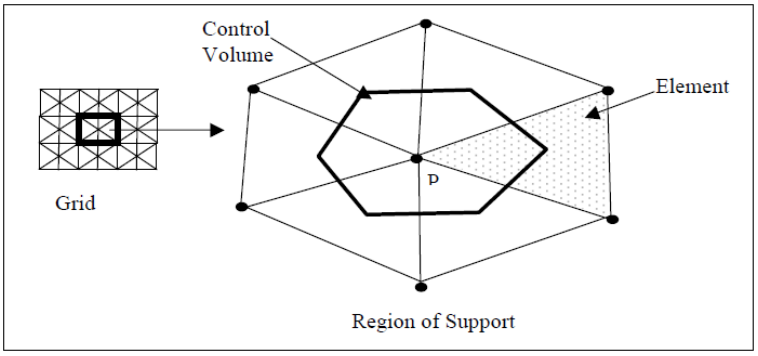

Figure A.6 Basic components in a control volume finite element solution

In each element, an unknown φ is approximated by

$$\varphi(x,z) = N_1\varphi_1 + N_2\varphi_2 + N_3\varphi_3 \tag{A.12}$$

where N = linear function of x and y arranged such that N_P takes the value of unity at node P and vanishes on the line segment opposite node P (Zienkiewicz and Taylor, 1989). Within this arrangement, a control volume is constructed where the mid points of the element sides are connected to the element centers. Balancing the fluxes across the faces of the control volumes arrives at an algebraic (discrete) Equation A.11 as follows:

$$A_P\bar{\theta}_P - A_P\bar{\theta}_{P,old} = \Delta t \sum_I [a_I(\varphi_I - \varphi_P) + S_I] \tag{A.13}$$

where I = a counter over the nodes in the grid connected to node P, a_I = coefficient, S_I = contribution to the source term that can be associated with node I. The Equation A.13 can be rewritten in terms of total head.

$$A_P\bar{\theta}_P = A_P\bar{\theta}_{P,old} + \Delta t \sum_I K_I^e a_I^e (h_I - h_P) + S_I \tag{A.14}$$

where the sum is over the nodes connected to node P, and each component in the sum includes contributions from both the elements that share the common side between nodes P and I. The discretized equation (Equation A.14) can be solved using the linearization introduced by Celia et al. (1990).

A set of test problems was simulated using MnDrain software and commercial codes, and the results were compared to verify the MnDrain codes (Figure A.7). Figure A.7(a) presents the results for draining a layered column obtained from MnDrain software and Marianelli and Durnford solutions that the accuracy is not lost in regions of rapid change in the solution fields (Marianelli and Durnford, 1998). The result obtained from MnDrain reasonably predicted the sharp discontinuity at the layer interface without leaking. In comparisons of the results for two-dimensional infiltration into a homogeneous domain [Figure A.7(b)], the results were well aligned, clearly indicating that the correct treatment of infiltration is implemented in MnDrain. The last test problem was designed to simulate drainage in a two-dimensional layered system. The moisture contents at interfaces were calculated based on the pressure [Figure A.7(d)], and the results were well aligned [Figure A.7(c)].

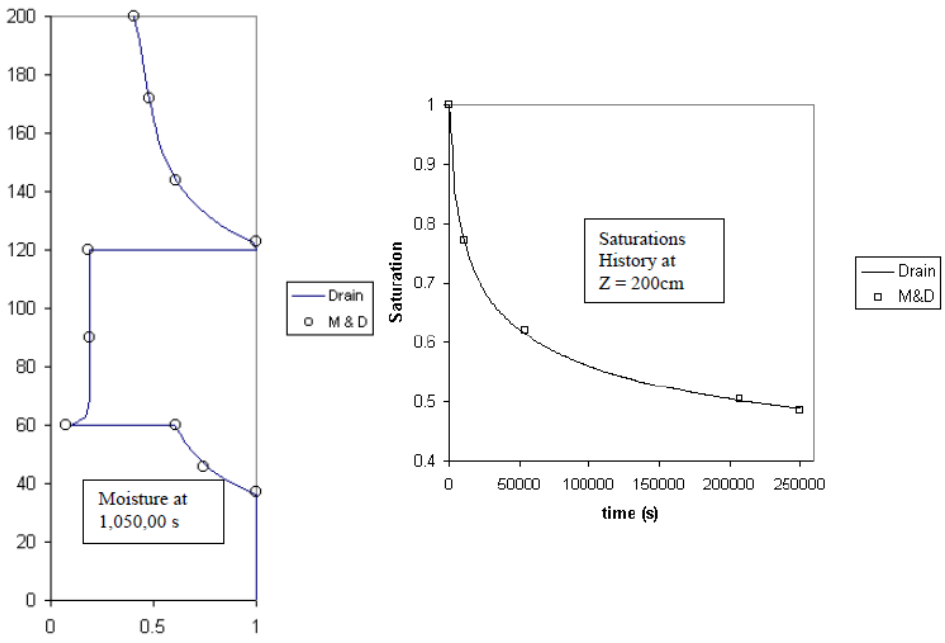

(a)

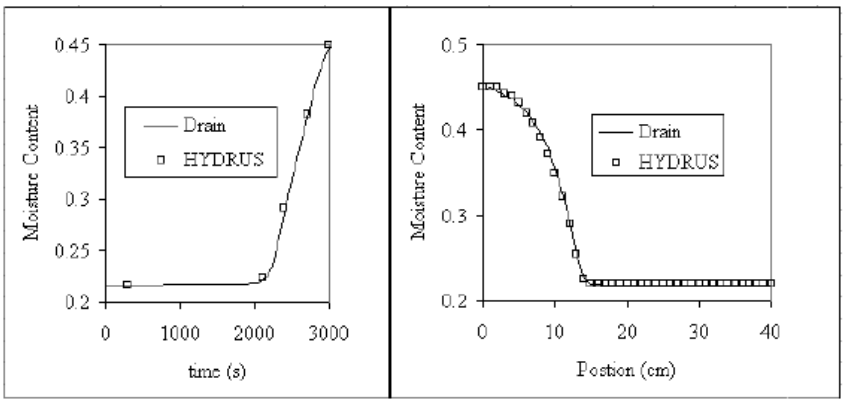

(b)

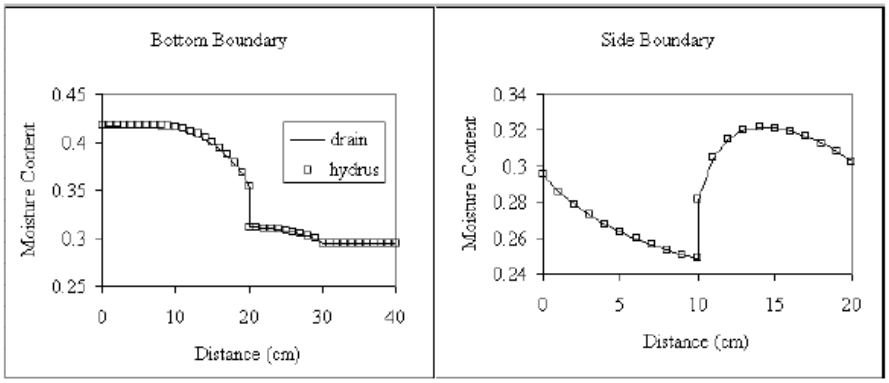

(c)

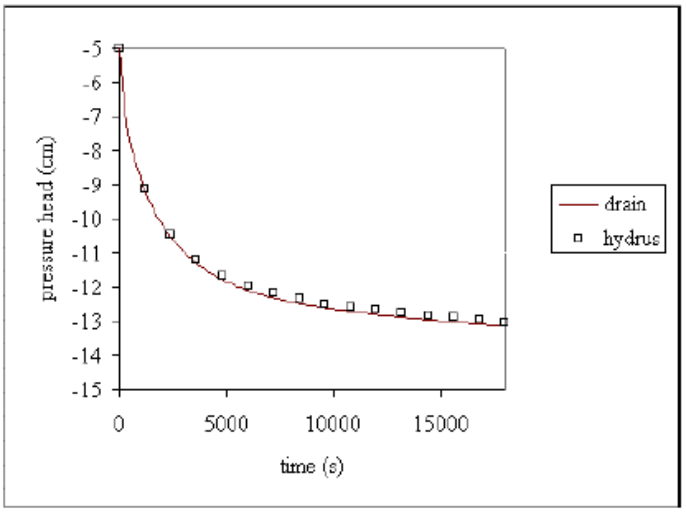

(d)

Figure A.7 Comparisons of simulation results for (a) draining a layered column, (b) infiltration into a two-dimensional homogeneous domain, (c) boundary moisture profiles in two-dimensional layered domain, and (d) pressure head history at layer interface in two-dimensional layered domain

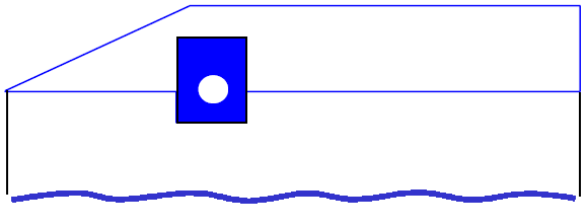

Figure A.8 Schematic of edge drain system

Figure A.8 shows an edge drain system used for MnDrain solution domain. The geometry consists of an initially saturated base, drain trench, and edge drain on a permeable sub-grade with an adjustable water table height. Initial condition of the solution domain was fully saturated with h = 0. Most of the boundary conditions are no flow conditions, except two boundary conditions: 1) The water table, at the bottom of the domain, where a fixed pressure head of h = 0 is applied and 2) the drain pipe surface in the trench where a review boundary condition is applied. In the initial stages of the calculation nodes on the drainpipe, a fixed pressure head of h = 0 needs to be taken. If this condition leads to an influx of moisture into the trench, this fixed head condition is replaced by a no flow condition at that node.

A.4 EFFECTIVE METHODS TO REPAIR FROST DAMAGED ROADWAYS (LRRB, 2003)

Cold weather in Minnesota is the only factor affecting pavement performance that human cannot modify or mitigate. Regarding the cold weather, there are two natural phenomena that damage the pavement system: 1) frost heave that is the expansion and heaving of frost-susceptible subgrade materials as they freeze and 2) frost boil that is the subsequent weakening of those materials as they thaw in spring, which decreases their load-carrying capacity. To provide effective methods to repair the frost damaged roadways, local road research board (LRRB) conducted the literature review and e-mail survey of local governments and developed worksheet and flow chart. To be specific, this research report includes discussions for the mechanics of ground freezing and frost related roadway damage, the environments in which such damage occurs, and measures to evaluate the contributing factors along with recommendations to mitigate them and/or reduce the potential for additional roadway damage.

Subgrade composition, groundwater condition, and drainage quality are key components of the frost related roadway damage, and the areas where the road damage occurs can be defined, in terms of the three components, by three categories: non-uniform subgrades, subgrades near the groundwater, subgrades within low areas. Typically, fine-grained soils, including lean and fat clay, silty clay, non-plastic, fine sands with silt, and elastic silt, are considered as frost-susceptible soils due to the low hydraulic conductivity and the high matric suction. That is, the non-uniform subgrade that locally includes fine-grained soils can cause differential frost heaving and frost boils. Near the groundwater (or local water features, such as lakes and swamps), the frost-susceptible soils also can be expanded due to formations of ice lenses when frozen is largely affected by the capillary action. Lastly, the frost related

road damage can be occurred in subgrades within low areas where water is accumulated (e.g., the accumulation of surface drainage in ditches at low points along a roadway passing through rolling terrain).

There are various repair methods and alternatives to mitigate and repair the frost damage. To appropriately select the treatment option, for the first step, prospective repair alternatives are needed to be evaluated by four steps: 1) construction/maintenance history, 2) visual observation, 3) subgrade evaluation (pavement deflection testing, penetration test borings or auger borings, dynamic cone penetrometer testing), and 4) construction materials. After the assessment of site-specific issues, the following repair methods should be uniquely selected for the site that has unique conditions:

1) Scarification, blending and re-compaction: suited for situations where subgrade uniformity appears to be more critical than groundwater or surface drainage,
2) Removal, surface compaction and re-compaction: suited for frost heave rather than frost boil repair where the loss of support to the paved surface is limited,
3) Removal and replacement: suited for non-uniform areas where both frost heaves and frost boils are present and situations where the extent and/or magnitude of frost damage is strongly influenced by shallow groundwater trapped in layered soils and present in low areas,
4) Northern Minnesota practice: cost-effective practice that uses woven or non-woven geotextile covered with 8 to 12 inches of granular material,
5) Embankment modification: in shallow groundwater situations or in low areas, raising the existing alignment provides sufficient clearance to i) reduce the impact that groundwater and infiltrating subsurface drainage has on subgrade stability and pavement performance, ii) reduce the extent to which excavations need to be advanced into wet, saturated or potentially unstable materials, and iii) support pavement materials on a uniform cushion of higher quality material than may have existed,
6) Transitions: material transitions (e.g., replacing weak or poorly draining subgrade materials with higher strength or more free-draining subgrade materials) can cause unfavorable amounts of differential frost heave. Tapering the edges of corrective excavations (e.g., 4:1 taper for general, 5:1 taper for a low-volume city street, 20:1 taper for highway repair) is thus required to reduce potential differential movements,
7) Constructability – stabilization, separation and reinforcement: general subgrade or excavation bottom stabilization can be achieved with the aid of chemical additives such as lime or fly ash, which absorb excess moisture and facilitates compaction. Geosynthetics (e.g., non-woven and woven geotextiles or geogrids) also can be placed over excavation bottoms to achieve subgrade stability and limit the migration of fine-grained subgrade particles into coarse-grained backfills,
8) Considerations for alternative subgrade materials: other synthetic and structural products, such as Geofoam®, shredded or chipped tires, wood chips, geocells, are available to help solve frost damage problems.

Finally, there are two strategies to reduce and limit subgrade moisture: surface drainage and subsurface drainage. The magnitude of subgrade heaving upon freezing and strength loss upon thawing can be significantly reduced by surface drainage systems. The surface drainages in urban areas include storm

drainage systems and the installation of curb and gutter. In rural areas, pavements are sloped to drain into ditches that ultimately carry water into streams, lakes, swamps or other low areas. Groundwater movement and percolation of surface drainage into pavement subgrades can saturate and weaken the subgrades. For outlets of water in the subgrade, drainpipes are installed below free-draining subbase layers or below the aggregate base layer where a subbase is not provided.

A.5 EVALUATING ROADWAYS SUBSURFACE DRAINAGE PRACTICES (MNDOT, 2009A)

This research project evaluated the efficacy of drainage systems of roadway base materials in a newly constructed eight-mile section of County Sate Aid Highway No. 35 (CSAH 35) in Nobles County, MN, based on experiments. The experiments included three drainage treatments: 1) drains on the roadway edge, 2) drains along the roadway centerline at depth of 2 ft., and 3) drains along the roadway centerline at depth of 4 ft, and each of the configurations was replicated six times, with the outflow for each replication outlet through a tipping-bucket flow monitoring system. The results were examined whether the elevation of the roadway relative to the surrounding landscape or the orientation of the drains at either side of the road had a significant impact on the efficacy of the drain. The CSAH 35 was separated into 87 sections (500-feet long for each section), and the 87 sections were divided into three sample populations: 1) 37 sections for relatively flat highway sections, 2) 23 sections for sloping section (about 1% - 3% slope), and 3) 27 sections for culverts and/or road intersections. Among 37 sections in the first population, 30 sections were randomly chosen for one of the three drainage treatments. From the second population, 10 sections were chosen for edge drains.

Tipping bucket device was buried at or near ground level (for safety precaution) to directly monitor a volume of the water flow. The results indicated edge drains collected much more water than the other two centerline drains combined during the two-year period (2006-2007). Volumes collected during both March and April were considerably higher than those of the other months. In result comparisons for the effect of install elevations, in general, drains at the lower elevation had a higher drain volume during March and April monitoring periods, but those during the rest of the year the drainage volumes did not show the tendency that depends on the elevation.

In addition to the tipping bucket apparatus, EM38, which is an electromagnetic induction instrument, was used to indirectly obtain relative moisture content of the subgrade material. Specifically, EM38 measured electrical conductivity of the subgrade, and then relative moisture content was estimated based on soil texture, temperature, and differences in the electrical conductivity. The measurements using EM38 were taken vertically and horizontally in five locations of each drain site: north of road, north shoulder, center, south shoulder, and south of road. The key findings were as follows: 1) electrical conductivities measured with the vertical orientation of the EM38 were higher than those measured with the horizontal orientation; 2) electrical conductivities for the edge drains were higher than those for the centerline drains (taken in selected days of July and August of 2006 and April of 2007), while electrical conductivities for both 2 ft and 4 ft centerline drains were very close one to another. For the measurements in May 2007, however, electrical conductivities were slightly higher for the 2 ft centerline

drainage, while those for both the edge drains and the 4 ft centerline drains were very similar; 3) the measurements located away from the center of the road were higher than those obtained at the center, except measurements taken for the 2 ft centerline on July 10, 2006, and both the 2 ft and 4 ft centerline drains on July 11, 2006, where the higher measurements were obtained right in the center of the road; 4) as the centerline drain configurations have only one drain at each location, there is an uncertainty about whether there is a difference between edge drains on one side of the road or the other.

Statistical analyses (ANOVA, t-test, F-test) were also conducted to: 1) compare the effectiveness of drainage of base and subgrade materials where the drain configuration is either the conventional edge drain or centerline drain, 2) compare the effectiveness of drainage of base and subgrade materials where drain configuration is either the location of drains along the entire roadway or only in the low points, and 3) assess the capability of EM38 to estimate relative moisture content of base and sub-grade material for both unpaved and paved surfaces. The statistical results were as follows: 1) there were differences between the edge drains and both the 4-ft and the 2-ft centerline drains, while there was no significant difference between the two centerline drains. Consequently, edge drain is the recommended drainage treatment because the edge drains collected much more water than the other two treatments; 2) in comparison of drainage orientation on the north and south side of the road, there was no significant differences between drains located at either side of the road. These results indicate that drains located at either side of the road collected approximately the same amount of water; therefore, both locations must have drains installed; 3) there was no significant differences between drains located at either high or low areas of the road. That is, both elevations must have drains installed as drains placed in both high and low areas of the road collected similar amount of water; 4) there was statistical difference between the means of the electrical conductivity measurements and the EM38 orientation; 5) there was no interaction between the drainage and the EM38 orientation; 6) there was statistical difference between the means of the electrical conductivity measurements and the drainage.

In addition to the statistical analyses, unsaturated water flow through the three drainage configurations was numerically modeled using COMSOL Multiphysics (based on Richards equation) to evaluate the efficiency of alternative drain tile placement configurations with respect to volumes of water removed and degree of reduction of water content beneath the pavement. Figure A.9 presents the model geometries and boundary conditions used in the modeling. The predominant soil types found along CR 35 was found to be composed of Prinsberg Silty Clay Loam and Clarion Loam. Weather data was taken from National Climatic Data Center. An average daily precipitation for the most rain intensive months March-June 2007 was found to be 2.29 mm. For bottom boundary condition, constant head pressure and impermeable condition were used. The initial conditions corresponded to a condition where the soil is very close to saturation, a condition that might exist shortly after snowmelt or frost thawing in the spring.

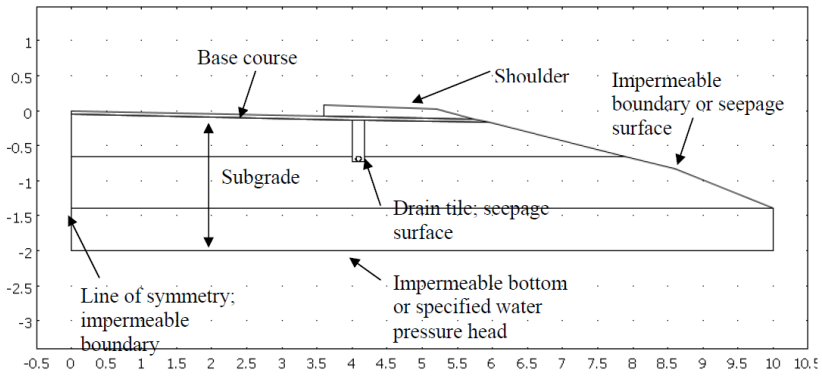

(a)

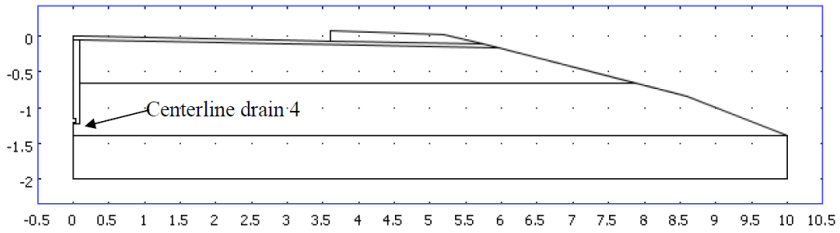

(b)

Figure A.9 Model geometries and boundary conditions for (a) edge drain and (b) centerline drain

The modeling results showed that the 4-ft depth centerline drain removes more of the infiltrated water when the soil beneath the pavement subgrade is essentially impermeable. However, if the initial conditions are drier, it turns out that the edge drain is the most effective for all conditions. For the case where the lower boundary was not impermeable, the results showed that the edge drain is the most effective to remove excess water. In the area where CR 35 was located, this impermeable condition was probably more the rule than the exception.

Potential impact of crushed concrete used in base course materials on drain tile condition was also evaluated because carbonate dissolution leads to deposits of carbonate onto the geofabric of the drain tile, when overused, resulting in plugging the entries to the drain. Drain tile samples were collected using a tracked backhoe, shovel, and hole saw at three locations on each of the roads and then analyzed by visual inspections and measurements of the relative amount of carbonate precipitates on the fabric and in the sand samples (using 1 M HCL solution). The acid test results indicated that, for the samples from CR 35, all the geofabric samples and two of the three trench sand samples showed no fizzing/bubbling action in response to application of the acid. For the trench sand sample that did show some reaction to the application of the acid, the reaction was moderate. In all the samples from CR 32, the results showed strong reaction to application of the acid. This strong reaction is an indication of presence of calcium carbonate in both the geofabric samples as well as in the sand. As there was no crushed concrete in the shoulder or in the base course material in CR 32 samples, no reaction with the

CR 32 was expected; however, the results were contrary. Moreover, more reaction was expected for the samples from CR 35 because a significant amount of crushed concrete was used in the shoulder along that roadway. It might be that there has not been sufficient time for migration of significant amounts of calcium carbonate to the tile geofabric or the trench sand since the conditions for CR 35 have only been in place for about 4 years.

In addition to the evaluation of crushed concrete on edge drain condition, in Chapter 8, open graded base drainage systems were evaluated using EM 38 measurements and statistical analyses. Due to high water table conditions in Worthington, MN, pavements were rapidly degraded (e.g., transverse cracks, alligator cracking), and thus open graded base drainage systems were recently used to control the potentially high-water table conditions. Moisture conditions beneath selected section of four residential streets in the area were measured using EM 38 (five readings separated 7-8 ft apart) to evaluate the performance of the current design in comparison to previous designs, and then the data was statistically analyzed using ANOVA to discover existing differences between the two pavement conditions. The key results were as follows: 1) for both vertical and horizontal orientations of the EM38, values collected on July 20 (mid-summer) were lower than those collected on June 22 probably due to drier conditions following drainage after spring. In terms of the orientation, electrical conductivities corresponding to the vertical orientation were consistently higher than those corresponding to the horizontal orientation because the vertical orientation reads to larger depths (i.e., more metallic utilities are sensed within the vertical readings); 2) in a two-way ANOVA test for the drainage system and the EM 38 orientation, there were differences i) between the means of the electrical conductivity measurements and the drainage conditions and ii) between the means of the electrical conductivity measurements and the EM38 orientation. There was also interaction between the road and the EM38 orientation; 3) in two one-way ANOVA tests for each of the EM 38 orientations using electrical conductivities from averages of the cross sections and the five points in each cross section, the results indicated that the treatments (roads) were different; 4) Turkey test results indicated that there was statistical difference among all the roads compared, except those pairs located close to each other; 5) Scheffé test results showed i) statistical differences among all comparisons for the June 22 readings, except those performed on roads located close to each other, ii) difference for the July 20 readings only when comparing Cecillee Street vs. Eckerson Drive and Pleasant Street vs. Spring Avenue for the vertical orientation, iii) and differences in Eckerson Drive vs. Spring Avenue and Pleasant Street vs. Spring Avenue for the horizontal orientation. In conclusion, Spring Avenue might be the road with a least effective drainage system, followed by Cecillee Street. Both Pleasant Street and Eckerson Drive performed in a pretty similar way.

A.6 SUBSURFACE DRAINAGE MANUAL FOR PAVEMENTS IN MINNESOTA (MNDOT, 2009B)

Problems associated with rapid deterioration and unsatisfactory performance of pavement systems are directly related to the accumulation of excessive moisture in subgrade and granular layers, and the potential problems include 1) softening of the pavement layers and subgrade by becoming saturated and remaining so for prolonged periods, 2) degradation of the pavement and subgrade material qualities due to interaction with moisture, and 3) loss of bonding between pavement layers due to

saturation with moisture (ERES, 1998; ERES, 1999). More importantly, pavement failures can be occurred due to the groundwater and seepage, such as piping, erosion, internal flooding, and excessive uplift and seepage forces (Cedergren, 1973). Accordingly, proper design, construction, and maintenance for drainage systems should take the following considerations: 1) sources of moisture in pavement (e.g., infiltration through edge and discontinuities of the pavement, capillary action and vapor movement, seepage), and how to stop moisture from reaching the pavement subsurface, 2) distresses caused or accelerated by excessive moisture in pavement systems, 3) types and components of drainage systems, and 4) identifying the benefits and risks of providing subsurface pavement drainage. This manual comprehensively presented the methods and procedures to be applied in assessing subsurface drainage needs in pavements, selection of appropriate drainage systems, implementation of recommended designs, as well as providing guidelines to practicing engineers in Minnesota for design, construction, and maintenance of subsurface drainage systems, for both new and existing pavements. The manual also included discussions and procedures on evaluation of cost effectiveness of subsurface drainage systems.

First, the need (e.g., benefits, importance) for subsurface drainage systems was summarized. As moisture infiltration through the pavement base layers is not easy to be prevented (by joint sealing or other methods), incorporating drainable pavement systems (e.g., permeable base, separator layer, edge drains, transverse drains) is important to remove any surface water which cannot be prevented from entering the pavement structure. ERES (1999) described key factors to determine the need for incorporation of a subsurface drainage system in new and/or existing pavement structures: 1) traffic loads including volume and weight (axle), 2) factors that influence the amount of free water entering the pavement system including climatic factors of rainfall and temperature (freezing and thawing), ground water, roadway geometry, and pavement type and condition, 3) factors that increase potential for moisture-related pavement damage, such as i) subgrade type, strength, and condition, ii) type of pavement material used, and iii) design features (e.g., pavement thickness, shoulder design, etc.).

Three effective approaches to control and/or reduce moisture related pavement problems are: 1) to provide adequate cross slopes and longitudinal slopes to quickly drain moisture from pavement surface, thereby minimizing infiltration into the pavement structure, 2) to use material and design features, such as stabilized cement (CTB) or lean concrete bases (LCB) in Portland cement concrete, also known as PCC pavement, that are not sensitive to the effects of moisture, and 3) to remove moisture that enters the pavement system promptly. Table A.2 summarizes pavement distresses caused by poor subsurface drainage and appropriate drainage solutions (ERES, 1999).

Table A.2 Pavement distresses and appropriate drainage solutions

	Distresses Affected by Subsurface	Other Design Features Affecting the Performance	Effective Drainage
AC Pavement on Granular Base	Fatigue cracking	Structural design (thickness of asphalt bound layers)	Edgedrains, permeable base*
	Rutting	Structural design, AC mix design	
	AC stripping	AC mix design	Permeable base*
Full-Depth AC Pavement	Transverse crack deterioration	Structural design	Permeable base*
	Fatigue cracking	Structural design	Edgedrains, permeable base*
	Rutting	Structural design, AC mix design	
	AC stripping	AC mix design	Permeable base*
JPCP	Pumping & faulting	Dowel, base type, widened slab	Edgedrains, permeable base*
	Slab cracking	Slab thickness, joint spacing, PCC strength, tied PCC shoulder, base type	permeable base*, edgedrains
	D-cracking	Aggregate type and gradation, mix design	Daylighting, edgedrains, permeable base*
JRCP/CRCP	Crack deterioration	Steel design, slab thickness, base type	Edgedrains
	D-cracking	Aggregate type and gradation, mix design	Daylighting, edgedrains

*With edgedrain or daylighting

The geometry of a highway plays an important role in the design of a pavement drainage system. The well-designed pavement would provide an effective method to prevent surface water from infiltrating into the pavement system through cracks and joints. This can be accomplished by providing adequate cross slopes and longitudinal slopes to quickly drain moisture from the pavement surface.

There are typically five subsurface drainage types: longitudinal edge drains, transverse and horizontal drains, permeable bases, drainage blankets, and well systems. Groundwater control system (e.g., well system) is designed to remove and/or control the flow of water, and infiltration control system (e.g., longitudinal edge drains) is designed to remove water that seeps into the pavement structural section. Well-designed drainable pavement system should include: full-width permeable base, or non-erodible base under the AC- or PCC-surfaced pavement, a separator layer under the permeable base to prevent contamination from the subgrade materials, and longitudinal edge drains with closely spaced outlets, or edge drains 'daylighting' directly into a side ditch.

The goal of drainage is to remove all drainable water in the pavement subbase layer as quickly as possible. For Interstate highways and freeways, it is suggested that 50 percent of the drainable water be drained within 2 hours. However, for highest class roads carrying very high volumes of traffic, a criterion

of draining 50 percent of drainable water in 1 hour is suggested (ERES, 1999). The time-to-drain design approach considers both the flow capacity and the storage capacity of the permeable base. The time to drain, t, is determined using equation:

$$t = T \times m \times 24 \quad \text{(A.15)}$$

where t = time-to-drain a specified percentage of drainable water (hours), T = time factor, m = 'm' factor (days).

Base materials are important in the subsurface drainage design. In past highway pavement constructions, primary function of the base course was to provide uniform support without adequate drainage, resulting in failure of the pavement due to pumping and erosion. Recently, the impermeable bases have been replaced to permeable bases, which are open graded base materials (OGBM) to rapidly drain infiltrated water from pavement structures, support pavement construction operations, and provide necessary support for the pavement structure. Performance of the permeable base is dependent on physical properties that govern permeability, effective porosity, and frost susceptibility, and the physical properties include particle-size distribution, plasticity characteristics, soil classification, dry density, void ratio, porosity, mineralogical composition, nature of the permeant, and degree of saturation. For measuring the permeability, *in situ* and laboratory (if the field test is not feasible) measurements are recommended. When determining permeability of coarse granular materials, Darcy's law may be invalid as water flow under nature conditions may become non-laminar. To evaluate the permeability in turbulent flow at great hydraulic gradients, correction factors can be applied (Cedergren, 1977). The permeabilities have been often estimated empirically (Table A.3 and A.4).

Table A.3 Typical soil permeability (Carsel and Parrish, 1988; Domenico and Schwartz, 1990; Rawls et al., 1992)

Soil Type	Saturated Hydraulic Conductivity, Ks (ft/day)	Effective Porosity (mean)
Gravel	84 to 8400	0.42
Coarse Sand	0.24 to 1700	0.28
Medium Sand	0.12 to 140	0.3
Fine Sand	0.048 to 58	0.32
Loamy Sand	12	0.4
Sandy Loam	3.6	0.41
Loam	0.72	0.43
Silt, Loess	0.002 to 58	-
Silt Loam	0.36	0.49
Till	0.55 to 2.9	-
Clay	0.0012 to 2.9	0.39
Sandy Clay Loam	0.9	0.33
Silty Clay Loam	0.07	0.43
Clay Loam	0.2	0.39
Sandy Clay	0.1	0.32
Silty Clay	0.02	0.42
Limestone	0.29 to 5,600	-
Limestone, Dolomite	0.00024 to 1.7	0.001 – 0.005
Sandstone	1.7 to 8.4	0.005 – 0.1
Siltstone	0.0036 to 2.9	-
Shale	0.0005 to 2.9	0.005 – 0.05

Table A.4 Typical soil permeabilities, apparent specific gravity, and effective porosity (Hansen et al., 1979; James 1988)

Soil Texture	Representative Saturated Hydraulic Conductivity, Ks (ft/day)	Range Saturated Hydraulic Conductivity, Ks (ft/day)	Effective Porosity (%)
Sandy	4	2 to 20	0.23
Sandy Loam	2	1 to 6	0.22
Loam	1	0.6 to 1.6	0.16
Clay Loam	0.6	0.2 to 1.2	0.13
Silty Clay	0.2	0.02 to 0.4	0.11
Clay	0.4	0.1 to 0.8	0.09

Figure A.10 presents a chart to empirically estimate permeability of granular drainage and filter materials (Moulton, 1980; NYDOT, 1973). The chart was developed by correlating statistically the measured permeability for many samples with those properties known to exert an influence on permeability (Barber and Sawyer, 1952; Chu et al., 1955). According to the test results, the most significant properties are the effective grain size, D_{10} , the porosity, n, and the percent passing the No.

200 sieve, P_{200}, and are known to explain over 91 percent of the variation in the coefficient of permeability (Moulton, 1980). The prediction equation derived from the correlation is given by

$$k = \frac{6.214\times10^{5}(D_{10})^{1.478}(n)^{6.654}}{(P_{200})^{0.597}} \text{ (ft/day)} \qquad \text{(A.16)}$$

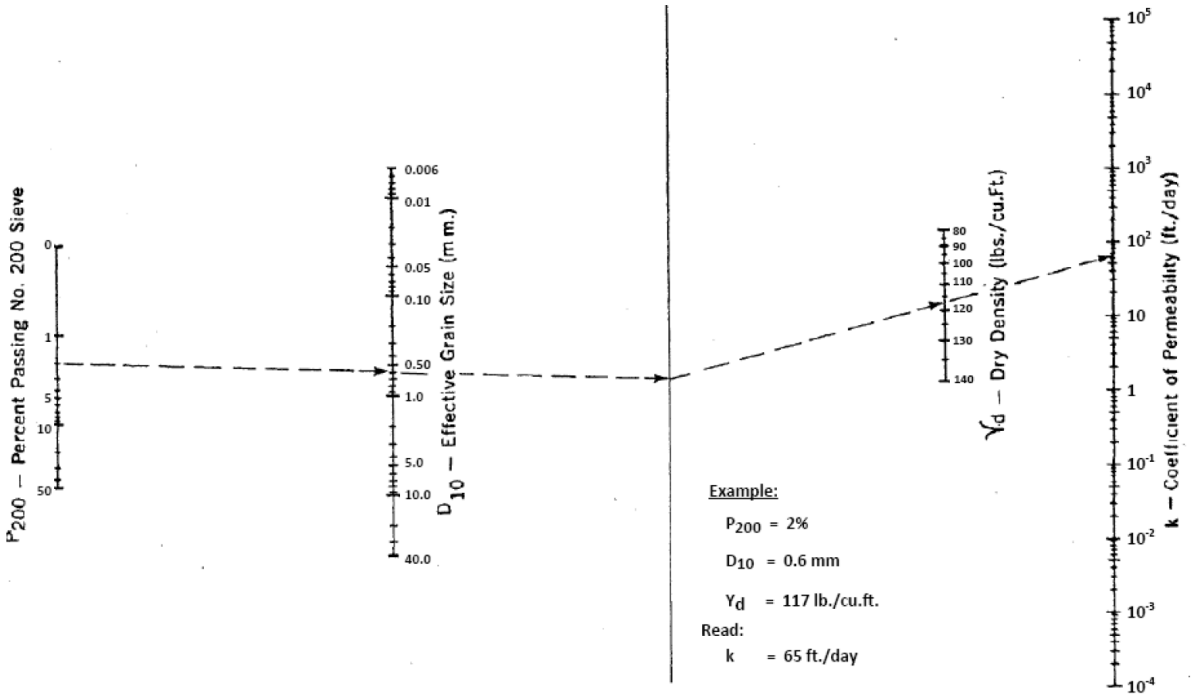

Figure A.10 Chart for estimating permeability of granular drainage and filter materials

In many practices, a new pavement layer is overlaid onto an existing distressed pavement. As the exiting distressed pavement serves as the base course that possibly includes a significant amount of cracking (i.e., high permeability) and/or fracture, in the design of subsurface drainage systems, the effective permeability of the distressed pavement should be taken into account. Retrofitted edge drains placed alongside the existing pavement collect water not only from the original base course (base material underlying the existing pavement) and the subgrade material, but also from the fracture existing pavement.

In addition to the permeability, the hydraulic conductivity of a block of fractured pavement (concrete or asphalt) can be estimated by assuming that the flow in a single fracture is similar to the flow between two parallel plates. Then, if the fractures are all aligned in the same direction at a uniform spacing, the

equivalent hydraulic conductivity of a length of fractured pavement flow is given by (Zimmerman and Bodvarrson, 1996)

$$K_f = 3600 \frac{gb^3}{vS} \quad \text{(A.17)}$$

where K_f = the equivalent saturated hydraulic conductivity facing in the fracture direction (in/hr), b = the mean width of fractures (in), S = the spacing between fractures (in), g = the acceleration of gravity (ft/sec^2), and v = the kinematic viscosity of water (ft^2/sec). The Equation A.17 can be used to estimate the equivalent hydraulic conductivity in each of the fracture directions, transverse and longitudinal. It should be noted that the equivalent hydraulic conductivity of the fractured pavement can be larger than the hydraulic conductivity of typical base course materials.

Frost susceptibility of the subgrade soils and the depth of frost penetration are important in the subsurface drainage design during periods of thawing (Moulton, 1980). This is because melt water from thawing ice masses should be removed as rapidly as possible by suitable drainage layers to prevent a saturation of the pavement structural section. These are essential factors in limiting both the duration and magnitude of the reduction in supporting power of the subgrade, base, and subbase during periods of spring thaw (Cedergren, 1973; Cedergren, 1974).

There are two main permeable base materials: stabilized and unstabilized. Both materials should consist of durable, crushed, angular aggregate, passing number 4 sieve, with few or no fines (FHWA, 1992). These should meet the FHWA requirements for a Class B aggregate in accordance with the AASHTO M 283-83 (FHWA, 1992), Coarse Aggregate of Highway and Airport Construction. The aggregates should meet the AASHTO T 96-87 specifications for durability to abrasion wear due to freeze-thaw in accordance with AASHTO T 104. In Minnesota, the specifications for an unstabilized base is represented by the following gradation for percent passing: 1”, 100 %; ¾”, 65-100 %; 3/8”, 35-70 %; No. 4, 20-45 %; No. 10, 8-25 %; No. 40, 2-10 %; No. 200, 0-3 %. For the stabilized base, a representative gradation for percent passing is given by: 1 ½”, 100 %; 1”, 95-100; ½”, 25-60 %; No. 4, 0-10 %; No. 8, 0-5 %. As can be seen from these two gradations, the gradation for the stabilized material is much coarser. The main difference between the two types of base materials is in the size of the constituent aggregates. Unstabilized materials contain high content of finer size aggregates, which provide stability through increased aggregate interlock. However, this results in lower material permeability. Unstabilized permeable bases generally have a permeability in the range of 1,000 to 3,000 feet per day (Moulton, 1980). The permeability of this material is approximately 1,400 ft/day. Because stabilized base materials achieve stability through treatment with asphalt or concrete additives, the aggregates can have a larger size, leading to higher permeabilities than those of the unstabilized materials. The permeability of this gradation is approximately 6,800 ft/day. During construction, the coefficient of uniformity of greater than 4 is recommended for the unstabilized permeable base courses to provide required stability for the equipment and activities (Moulton, 1980).

Hard surfaced pavements typically divided into two categories: 1) flexible pavement that includes conventional asphalt concrete (AC), full-depth AC, and AC rehabilitation and 2) rigid pavement that includes jointed plain concrete pavement (JPCP), jointed reinforced concrete pavement (JRCP), continuously reinforced concrete pavement (CRCP), and PCC rehabilitation. Drainage requirements are unique for each of these types of pavement. Concrete, or rigid, pavements generally have lower permeability than asphalt pavements, and will more effectively impede water infiltration into the subgrade layer.

Usefulness and effectiveness of the subsurface drainage system depends on their performance. However, performances of the many systems are lower than expectations due to poor design, construction, and/or maintenance (ERES, 1999). Criteria for excellent drainage require that the permeable aggregate base (PAB) layer be able to remove at least 50 percent of the drainable water from the pavement structural section in less than two to three hours after cessation of the precipitation event (MnDOT, 1994). To optimally perform the subsurface drainage systems, drainage materials are placed well, stable, dry, free from loose material, and completed to true line and grade (Moulton, 1980). On completion of construction of these drainage systems, inspection should be conducted to verify that these conditions have been met. Necessary measures should be taken to prevent the intrusion of foreign material into any portion of the drainage system due to construction operations and natural rainfall events during and immediately following construction.

Lastly, a number of studies have reported on the cost-effectiveness of subsurface drainage systems in addressing accelerated moisture related pavement deterioration problems. Smith et al. (1990) compared cost and performance data and the results indicated that addition of a permeable base to be cost-effective. This is because a minimum increase in AC pavement life of 4 years through use of a permeable base, and a 50 percent increase in life of PCC pavement. Accurate comparison of costs of different materials would require one to consider the real cost of the material in the pavement on a yield basis. A general recommendation in the incorporation of subsurface drainage systems is that their total costs should never exceed 2% of the total costs of installation of the pavement structure.

A.7 CULVERT PIPE SERVICE LIFE IN MINNESOTA (MNDOT, 2012)

Culvert is a structure that allows water flow under roads or other structures (e.g., railroad). Although the culvert traditionally consists of concrete or metal pipes, alternative materials, such as coated metal, have been introduced. As the current MnDOT Drainage Manual includes limited information on the pipe selection, in this research project, literature, design/construction practices, available databases, and manufacturer opinions were extensively reviewed to improve the guidance (Chapter 2 in the MnDOT Drainage Manual) for practitioners in the selection of appropriate culvert pipe materials and life spans.

According to MnDOT (2012), there was huge disagreement in terms of compaction (i.e., whether compaction requirements are being achieved). Poor compaction, as well as uneven bedding and unexpected settling, causes joint separation, which is a structural pipe failure where the joints between

individual sections of pipe widen (AASHTO, 2007). AASHTO (2017) Chapter 14 described that placing pipe in multiple stages should be avoided as getting consistent compaction at the transition is difficult. MnDOT (2012) also indicated that there are several solutions to alleviate the concerns over inadequate bedding and compaction practices: 1) more formal education for installers on pipe bedding, 2) using rigid pipes that have less risk for compaction related issues, 3) recording installation, and 4) increase in the penalty for a failed pipe. In addition, the construction inspectors have found that replacing organic soils with select backfill helps reduce differential settlement, despite the soil replacement is not a common practice.

APPENDIX B
RELATIONSHIPS BETWEEN MINIMUM SATURATION AND INDEX PROPERTIES

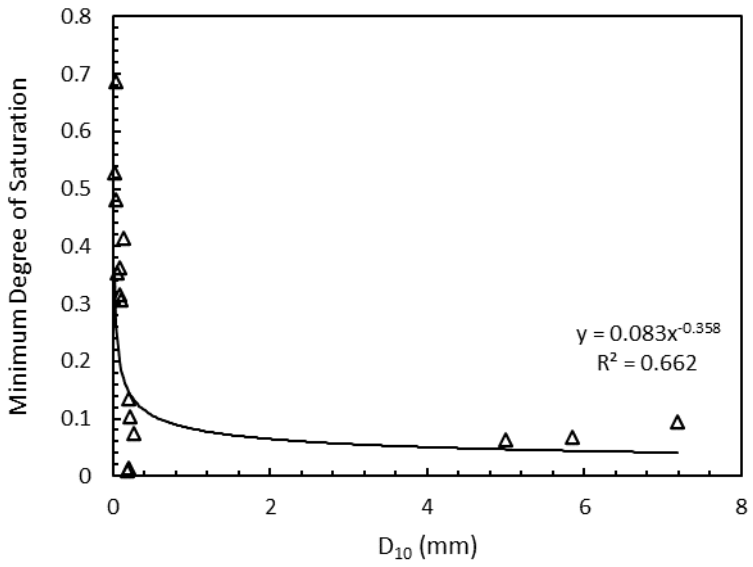

Figure B.1 Relationship between minimum degree of saturation and D_{10}

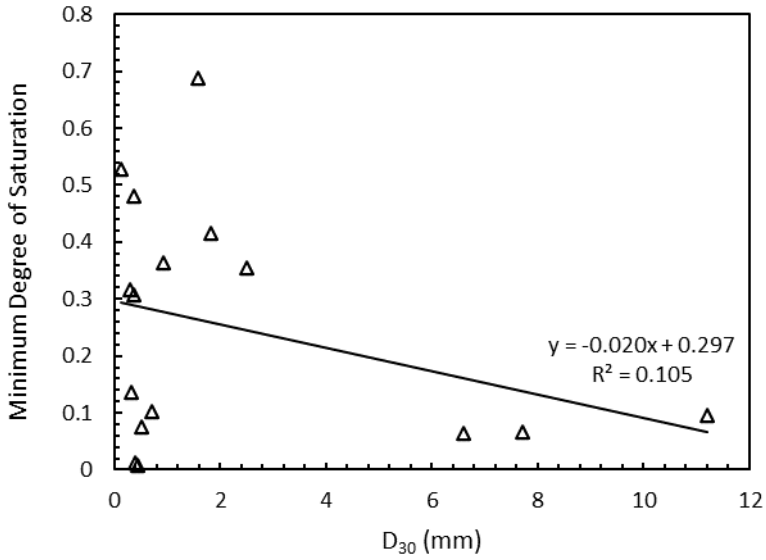

Figure B.2 Relationship between minimum degree of saturation and D_{30}

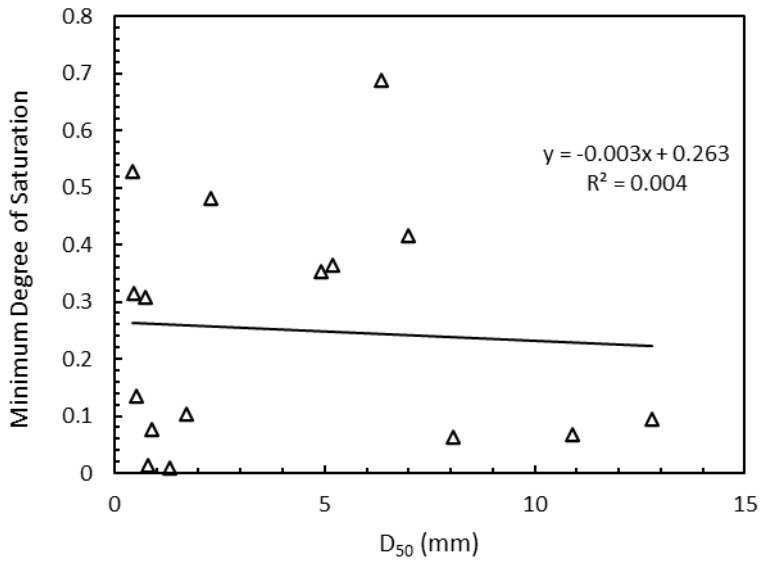

Figure B.3 Relationship between minimum degree of saturation and D_{50}

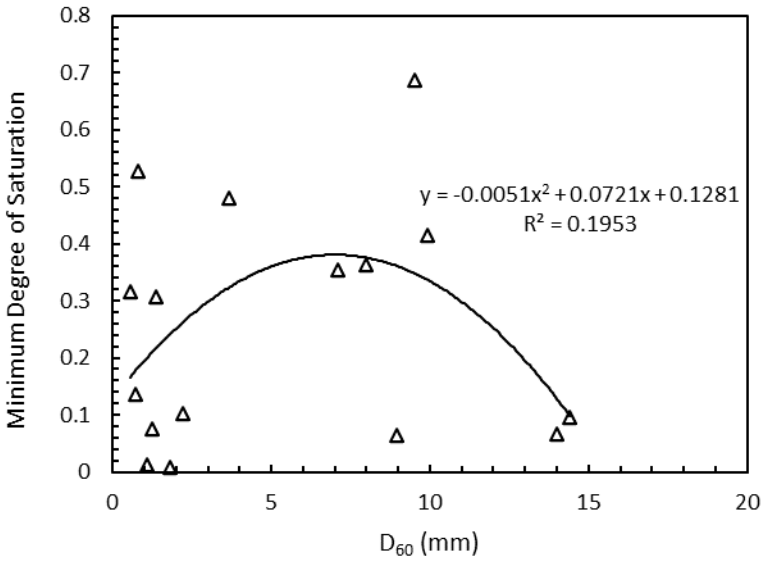

Figure B.4 Relationship between minimum degree of saturation and D_{60}

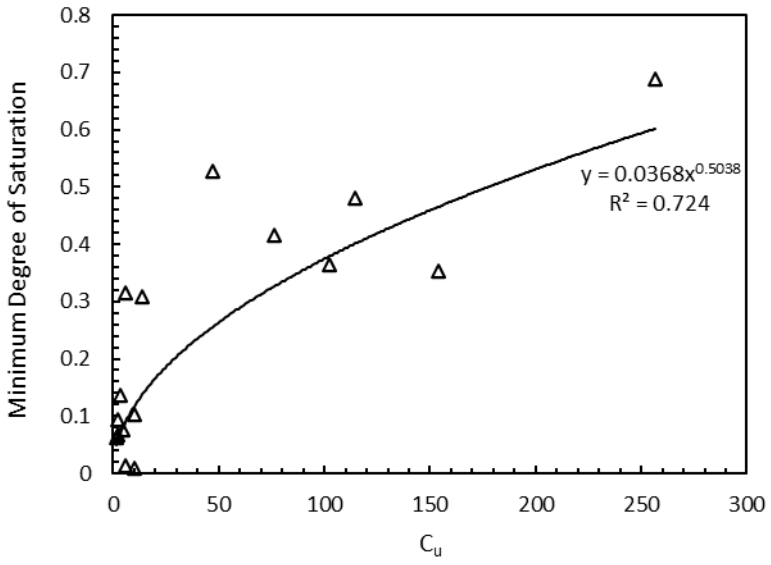

Figure B.5 Relationship between minimum degree of saturation and C_u

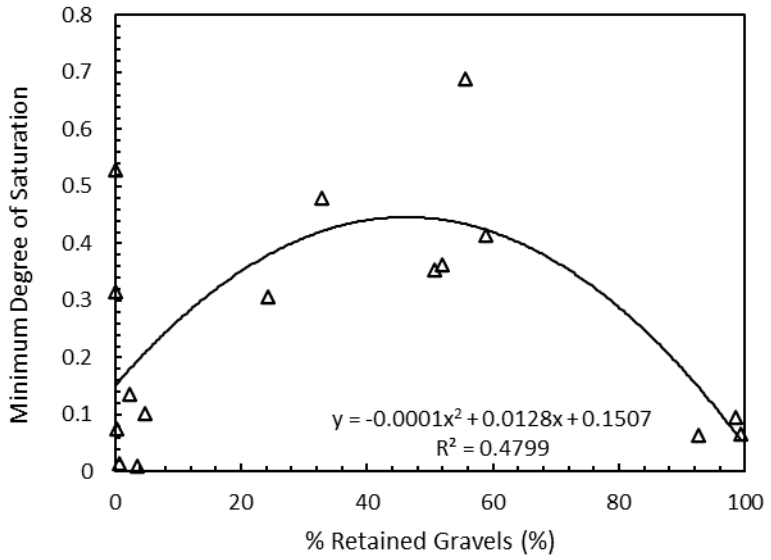

Figure B.6 Relationship between minimum degree of saturation and % retained gravels

APPENDIX C
EMPIRICAL AND THEORETICAL RELATIONS FOR ESTIMATING HYDRAULIC CONDUCTIVITY AND SOIL-WATER CHARACTERISTIC CURVES

C.1 EMPIRICAL AND THEORETICAL RELATIONS FOR ESTIMATING HYDRAULIC CONDUCTIVITY OF COARSE AGGREGATES AND SANDS

In this section, empirical equations to estimate K_{sat} are reviewed and summarized. Methods are differentiated into those based on grain size (C.1.1), void ratio (C.1.2), fines content (C.1.4), and material type (C.1.5). The formulations summarized here are neither comprehensive nor complete, but rather are selected to represent a range of applicable approaches with primary applicability to coarse aggregates and sands.

C.1.1 Methods based on Particle Size Distribution

Because the pore structure that governs moisture migration in soil and the particle-size distribution (PSD) that bounds the pore structure are related, PSD has been extensively used in formulations to estimate K_{sat} of coarse-grained soil.

Hazen (1892)

The classical Hazen formula (1892) provides an estimate of K_{sat} applicable to uniformly graded soils (0.1mm < D_{10} < 3mm, uniformity coefficient < 5) via proportionality to d_{10} (grain size at 10% finer). Equations C.1a and C.1b present the original Hazen and modified equations, respectively.

$$K[m/s] = \beta \frac{g}{v}[1 + 10(n - 0.26)]d_{10}^2 \quad \text{(C.1a)}$$

$$K[m/s] = \beta C d_{10}^2 \quad \text{(C.1b)}$$

where $\beta = 6.54 \times 10^{-4}$, g = gravitational constant of the fluid, v = kinetic viscosity of the fluid, n = porosity, d_{10} = effective particle diameter, C = Hazen coefficient in 1/[cm·s].

Seelheim (1880)

Prior to Hazen (1892), Seelheim (1880) noted that K_{sat} (herein K) should be related to the squared value of some of pore diameter and proposed an equation to estimate hydraulic conductivity based on median particle diameter.

$$K[m/s] = 3570 d_{50}^2 \quad \text{(C.2)}$$

where d_{50} = median particle diameter.

Slichter (1899)

Slichter (1899) performed experiments involving steady motion of groundwater and derived an equation for soil permeability based on porosity and effective particle diameter.

$$K[m/s] = \beta \frac{g}{v} n^{3.287} d_{10}^2 \quad \text{(C.3)}$$

where $\beta = 0.01$, g = gravitational constant of the fluid, v = kinetic viscosity of the fluid, n = porosity, d_{10} = effective particle diameter (0.01 mm < d_{10} < 5 mm).

Kruger (1918)

Kruger (1918) proposed an empirical equation for medium-grain sands (C_u > 5) based on particle gradation and porosity. Vukovic and Soro (1992) present the equation in different forms, including:

$$K[m/s] = \beta \frac{g}{v} \frac{n}{(1-n)^2} d_e^2 \quad \text{(C.4)}$$

where $\beta = 4.3 \times 10^{-5}$, g = gravitational constant of the fluid, v = kinetic viscosity of the fluid, n = porosity, d_e = effective grain, $\frac{1}{d_e} = \sum_{i=1}^{n} \frac{\Delta g_i}{d_i}$, g_i = the fractional percent weight retained on individual sieves, d_i = the mean grain diameter in mm of the corresponding fraction.

Terzaghi (1925)

Terzaghi (1925) proposed an equation based on porosity and effective particle size for large-grained sands:

$$K[m/s] = \beta \frac{g}{v} \left(\frac{n-0.13}{\sqrt[3]{1-n}} \right)^2 d_{10}^2 \quad \text{(C.5)}$$

where $\beta = 10.7 \times 10^{-3}$ for smooth grains and 6.1×10^{-3} for coarse grains, g = gravitational constant of the fluid, v = kinetic viscosity of the fluid, n = porosity, d_{10} = effective particle diameter.

Zunker (1932; from Lu *et al*. 2012)

Similar to Kruger (1918), Zunker (1932) proposed an equation based on porosity and effective particle size.

$$K[m/s] = \beta_z \frac{g}{v} \frac{n}{(1-n)^2} d_e^2 \quad \text{(C.6)}$$

where $\beta = 2.4 \times 10^{-3}$ for uniform sand with smooth, rounded grains and 1.4×10^{-3} for uniform composition with coarse grains, 1.2×10^{-3} for nonuniform composition, 0.7×10^{-3} for nonuniform compositions, clayey, with grains, or irregular shape, $\frac{1}{d_e} = \frac{3}{2}\frac{\Delta_{g_1}}{d_1} + \sum_{i=2}^{i=n} \Delta_{g_i} \left(\frac{d_i^g - d_i^d}{d_i^g d_i^d ln \frac{d_i^g}{d_i^d}} \right)$, d_1 = the largest diameter of the finest fraction, $\Delta_{g_1} =$ the weight of the material of the finest fraction in parts of the total weight, d_i^g and d_i^d = maximum and minimum grain diameters of the fraction, respectively, $\Delta_{g_i} =$ the fraction weight in parts of the total weight. Equation C.6 is applicable for fine and medium-grain sands.

Fair and Hatch (1933)

Fair and Hatch (1933) incorporated particle shape and packing factor as follows:

$$K[m/s] = \beta \frac{\rho g}{\mu} \frac{n^3}{(1-n)^2} \frac{1}{m\left(\frac{\theta}{100}\sum_i \frac{P_i}{d_{mi}}\right)} \quad \text{(C.7)}$$

where $\beta = 1$, g = gravitational constant of the fluid, $v =$ kinetic viscosity of the fluid, $n =$ porosity, $m =$ packing factor, 5, θ = sand shape factor, 6 < θ < 7.7 (spherical to angular, respectively), $P_i =$ percentage of sand held between adjacent sieves, $100 \cdot wf_i$, $d_{mi} =$ geometric mean, $\sqrt{d_{s_i} \cdot d_{s_{i+1}}}$, d_{s_i} = the size of the i sieve.

Krumbein and Monk (1943)

Krumbein and Monk (1943) performed statistical analysis for unconsolidated sands using a transformation of the grain-size distribution to a logarithmic frequency distribution.

$$K[\text{darcy}] = \beta \text{GM}_{\xi}{}^{2} e^{-1.31\sigma_{\phi}} \quad \text{(C.8)}$$

where $\beta = 760$, GM_{ξ} = geometric mean diameter in mm, σ_{ϕ} = phi standard deviation, *K* = the constant of proportionality in Darcy's original expression.

Kozeny (1953)

Kozeny (1953) proposed an equation for coarse-grained sands based on porosity and effective particle diameter.

$$K[m/s] = \beta \frac{g}{v} \frac{n^3}{(1-n)^2} d_{10}^2 \quad \text{(C.9)}$$

where $\beta = 8.3 \times 10^{-4}$, g = gravitational constant of the fluid, v = kinetic viscosity of the fluid, n = porosity, d_{10} = effective particle diameter.

Kozeny-Carman (Carman1937, 1956; Kozeny 1927, 1953)

Kozeny (1927) proposed an empirical equation modified by Carman (1937), which became the Kozeny-Carman equation (Equation C.10) based on porosity and effective particle diameter applicable for silts, sands, and gravelly sands (d_{10} < 3mm).

$$K[m/s] = \beta \frac{\rho_w g}{\mu} \frac{n^3}{(1-n)^2} d_{10}^2 \quad \text{(C.10)}$$

where $\beta = 1/180$, g = gravitational constant of the fluid, v = kinetic viscosity of the fluid, n = porosity, d_{10} = effective particle diameter.

Harleman *et al*. (1963)

Harleman *et al*. (1963) performed experiments for single-phase flow dispersion and proposed an equation:

$$K[m/s] = \beta \frac{\rho g}{\mu} d_{10}^2 \quad \text{(C.11)}$$

where $\beta = 6.54 \times 10^{-4}$, g = gravitational constant of the fluid, $v =$ kinetic viscosity of the fluid, $d_{10} =$ effective particle diameter.

Beyer (1964)

Beyer (1964) proposed an empirical equation based on uniformity coefficient ($1 < C_u < 20$), as well as effective particle diameter ($0.06\ mm < d_{10} < 0.6\ mm$).

$$K[m/s] = \beta \frac{g}{v} \log \frac{500}{C_u} d_{10}^2 \quad \text{(C.12)}$$

where $\beta = 6 \times 10^{-4}$, g = the gravitational constant of the fluid, v = kinematic viscosity of the fluid, C_u = uniformity coefficient, $d_{10} =$ effective particle diameter.

Pavchich (Pravedny 1966)

The Pavchich equation estimates K_{sat} of uniform sandy soils based on d_{17} ($0.06mm < d_{17} < 1.5mm$).

$$K[m/s] = \beta \frac{g}{v} d_{17}^2 \quad \text{(C.13)}$$

where $\beta = 0.35$, g = gravitational constant of the fluid, $v =$ kinetic viscosity of the fluid, $d_{17} =$ particle diameter corresponding to 17% finer on the cumulative grain-size distribution curve.

Pavchich (Pravedny 1966; from Oh et al., 2013)

Slightly different forms of The Pavchich equation have been described in the literature, and Oh et al. (2013) describe the Pavchich equation regarding porosity, as well as d_{17}.

$$K[m/s] = C_u^{\frac{1}{3}} * \frac{g}{v} * \frac{n^3}{(1-n)^2} d_{17}^2 \quad \text{(C.14)}$$

where g = gravitational constant of the fluid, v = kinetic viscosity of the fluid, d_{17} = particle diameter corresponding to 17% finer on the cumulative grain-size distribution curve.

NAVFAC DM7 (1974; from Rosas et al., 2015)

Naval Facilities Engineering Command (NAVFAC) suggested a chart to estimate K_{sat} of clean sand and gravel based on the effective particle diameter and void ratio. The chart demonstrates a linear relationship between log(k_{sat}) and log(d_{10}) when: i) 0.1 mm < d_{10} < 2 mm, ii) 0.3 < e < 0.7, iii) 2 < C_u < 12, and iv) d_{10}/d_5 >.

$$K[m/s] = \beta 10^{1.291e-0.6435} d_{10}^{10^{0.5504-0.2937e}} \quad \text{(C.15)}$$

where $\beta = 1$, e = void ratio, d_{10} = effective particle diameter in mm.

Campbell (1985)

Campbell (1985) adopted the unsaturated hydraulic function to estimate unsaturated hydraulic conductivity. The K_{sat} estimation is a function of moisture content as follows:

$$K_{sat} = C(1.3/\rho_b)^{1.3b} \exp(-0.025 - 3.63m_s - 6.88m_c) \quad \text{(C.16)}$$

where C = constant, ρ_b = standard bulk density, 1.3 Mg/m3, $b = -20\psi_{es} + 0.2\sigma_g$, $\psi_{es} = -0.05d_g^{-1/2}$, $d_g = \exp(-0.025 - 3.63m_s - 6.88m_c)$, $\sigma_g = \exp(13.32m_s + 47.7m_c - ln^2 d_g)^{1/2}$, $K_{unsat} = K_{sat}(\psi_e/\psi)^{2+3/b}$, ψ_{es} = air-entry potential at standard bulk density, m_s, m_c = silt and clay fractions, respectively, d_g = geometric mean diameter, σ_g = geometric standard deviation

Campbell and Shiozawa (1992)

As the Campbell (1985) model was criticized by Buchan (1989) and Shiozawa and Campbell (1991), Campbell and Shiozawa (1992) re-derived d_g and ψ_e with six soil data, and results showed higher correlation. Values estimated from Campbell and Shiozawa (1992) gave substantially lower hydraulic conductivity for fine textured soils than K_{sat} of Campbell (1985), but somewhat higher values for coarse-textured soils.

$$K_{sat}[m/s] = 1.5 \times 10^{-5} \exp(-7m_s - 16.7m_c) \quad \text{(C.17)}$$

where $\ln d_g = -0.8 - 3.17m_s - 7.61m_c$, $\psi_e = -0.0003 d_g^{-3/2}$.

Kozeny-Carman (Koenders and Williams, 1992)

Since Kozeny-Carman (1937) proposed the empirical equation, the Kozeny-Carman equation was developed for densely packed bed that includes silts, sands, and gravelly sands as follows:

$$K = \frac{1}{v} \chi n \left(\frac{n}{1-n}\right)^2 d_{50}^2 \quad \text{(C.18)}$$

where v = fluid kinetic viscosity, χ = proportionality coefficient, 0.0035 ± 0.0005, d_{50} = median particle diameter.

Sauerbrei (from Vukovic and Soro 1992)

Sauerbrei cited in Vukovic and Soro (1992) proposed an equation to estimate K_{sat} of sand and sandy clay (d_{17} < 0.5 mm) based on porosity and d_{17}.

$$K[m/s] = \beta \frac{g}{v} \frac{n^3}{(1-n)^2} d_{17}^2 \quad \text{(C.19)}$$

where $\beta = 3.75 \times 10^{-3}$, g = gravitational constant of the fluid, $v =$ kinetic viscosity of the fluid, $n =$ porosity, $d_{17} =$ particle diameter corresponding to 17% finer on the cumulative grain-size distribution curve.

U.S. Bureau of Reclamation (from Vukovic and Soro 1992)

U.S. Bureau of Reclamation (USBR) cited in Vukovic and Soro (1992) described an empirical equation to estimate K_{sat} of medium-grain sands ($C_u < 5$) based on d_{20}.

$$K[m/s] = \beta \frac{g}{v} d_{20}^{2.3} \quad \text{(C.20)}$$

where $\beta = 4.8 \times 10^{-4}$, g = gravitational constant of the fluid, v = kinetic viscosity of the fluid, d_{20} = particle diameter corresponding to 20% finer on the cumulative grain-size distribution curve in mm.

Alyamani and Sen (1993)

Alyamani and Sen (1993) conducted constant head permeability tests for 22 samples and proposed an empirical equation using the intercept and slope of grain-size distribution:

$$K[m/d] = \beta[I_0 + 0.025(d_{50-}d_{10})]^2 \quad \text{(C.21)}$$

where β =1300, I_0 = the intercept in mm of the line formed by d_{50} [mm] and d_{10} [mm] with the grain-size axis, d_{50} = median particle diameter, d_{10} = effective particle diameter.

Barr (2001)

Barr (2001) proposed a relation derived based on measurable parameters, such as fluid density and viscosity, porosity, and average hydraulic pore radius. The pore radius was calculated using the particle-size distribution assuming spherical particle shape, and the equation is as follows:

$$K[m/s] = \beta \frac{\rho g}{\mu} \alpha m^2 \quad \text{(C.22)}$$

where $\beta = 0.2$, g = gravitational constant of the fluid, v = kinetic viscosity of the fluid, m = the hydraulic radius, which is expressed as a ratio of effective porosity, α, to the surface area, S, $S = C_s S_0(1 - \alpha)$, C_s = a surface area adjusting parameter ($1 < C_s < 1.35$), the surface area per unit mass of solid material = $S_0 = \sum_i S_{oi}$, $S_{oi} = \frac{3}{r_i} w f_i$, r = the radius of the sphere representing the grain (sieve size)

in meters, wf_i = the weight fraction retained in sieve i, ρ = the density of the fluid, g = the gravitational constant of the fluid, μ = the dynamic viscosity of the fluid.

Kozeny-Carman (Carrier, 2003)

Carrier (2003) who intensively compared the Hazen equation and the Kozeny-Carman equation modified the Kozeny-Carman equation as follows:

$$K = \frac{g}{v} C_{KC} \frac{6}{d_e} d_e^2 \frac{n^3}{(1-n)^2} \tag{C.23}$$

where g = gravitational constant of the fluid, $v =$ kinetic viscosity of the fluid, C_{KC} = empirical constant, 480 ± 30, d_e = uniform grain diameter, n = porosity. Equation C.23 is not appropriate for clayey soils, but applicable for silts, sands and gravel sands.

Zamarin (1928; from Lu *et al*., 2012)

Zamarin cited in Lu et al. (2012) calculated effective diameter, d_e, similar to the Kruger equation, and proposed an equation to estimate K_{sat} as follows:

$$K[m/s] = \beta_z \frac{g}{v} \frac{n^3}{(1-n)^2} d_e^2 \tag{C.24}$$

where $\beta = 8.2 \times 10^{-3}$, g = gravitational constant of the fluid, $v =$ kinetic viscosity of the fluid, $n =$ porosity, $\frac{1}{d_e} = \frac{3}{2}\frac{\Delta_{g_1}}{d_1} + \sum_{i=2}^{i=n} \Delta_{g_i} \left(\frac{ln\frac{d_i^g}{d_i^d}}{d_i^g - d_i^d} \right)$, $d_1 =$ the largest diameter of the finest fraction, $\Delta_{g_1} =$ the weight of the material of the finest fraction in parts of the total weight, d_i^g and d_i^d = maximum and minimum grain diameters of the fraction, respectively, $\Delta_{g_i} =$ the fraction weight in parts of the total weight. Equation C.24 is applicable for large-grain sands.

Salarashayeri and Siosemarde (2012)

Salarashayeri and Siosemarde (2012) performed constant head tests to measure K_{sat} of 25 samples and presented statistical analysis for the results. Equation C.25 obtained from multiple regressions on the results describes the relationship between K_{sat} and the gradation.

$$K_{sat} = 10.06 + 118.54(d_{10}) - 12.5(d_{50}) - 7.32(d_{60}) \quad \text{(C.25)}$$

where d_{10} = effective particle diameter, d_{50} = median particle diameter, d_{60} = particle diameter corresponding to 60% finer on the cumulative grain-size distribution curve.

Wang et al. (2017)

Wang et al. (2017) applied the dimensional analysis (Buckingham's Π theorem) to analyze a relationship between K_{sat} and particle-size distribution. In the analyses, effects of mean grain size, grain size uniformity, and porosity were integrated. Then, regression analysis was conducted with 431 samples collected from different depositional environments, and new equation for K_{sat} estimation was proposed as follows:

$$K = C_W \frac{g}{v} d_{10}^2 (\log 10 \frac{g d_{60}^3}{v^2})^{-1} \quad \text{(C.26)}$$

where C_W = fitting parameters, 2.9 x 10-3, g = gravitational constant of the fluid, v = kinetic viscosity of the fluid, 0.89 x 10-6 m2/s at 25 ºC for water, d_{10} = effective particle diameter, d_{60} = particle diameter corresponding to 60% finer on the cumulative grain-size distribution curve.

C.1.2 Methods based on Void Ratio

Carrier (2003)

In Carrier (2003), the Kozeny-Carman equation was compared to the Hazen equation and described for a relationship between K_{sat} and the void ratio.

$$K[cm/sec] = 1.99 * 10^4 (100\%/\{\sum[f_i/(D_{li}^{0.404} * D_{si}^{0.595})]\})^2 * \left(\frac{1}{SF^2}\right) * [e^3/(1+e)] \quad \text{(C.27)}$$

where fi = fraction of soil particles between two sieve sizes, larger (l)and smaller (s), $D_{ave\ i}$ = average particle size retained between sieves, $D_{li}^{0.404} * D_{si}^{0.595}$, assuming the particle size distribution is log-linear between each pair of sieve sizes, e = void ratio, SF = shape factor.

Carrier (2003) noted that Equation C.27 is not appropriate for clayey soils, although it is applicable for nonplastic silts. These conditions apply in silts, sands, and gravelly sands. However, turbulent flow and

the inertia term must be taken into account as the pore size and the velocity increase. The formula is not appropriate if the particle size distribution has a long, flat tail in the fine fraction. The formula does not explicitly account for anisotropy.

Chapuis (2004)

Chapuis (2004) compared two predictive methods—Hazen (Equation C.1) and NAVFAC (Equation C.15). The Hazen equation was extended to any value of porosity that the soil can take when its maximum value of porosity is known (i.e., combined with Kozeny-Carman equation), and the two equations were then evaluated using published laboratory data for sand and gravels (0.13 mm < d_{10} < 1.98 mm, 0.4 < e < 1.5). Then, Equation C.28 was proposed based on a best fit equation in a graph of the logarithm of measured K_{sat} versus the logarithm of $d_{10}^2 e^3/(1+e)$.

$$K[cm/sec] = 2.4622[D_{10}^2 * e^3/(1+e)]^{0.7825} \quad \text{(C.28)}$$

where d_{10} = in mm, e = void ratio. The predictions of Equation C.28 were poor for crushed soils and rocks (0.03 mm < d_{10} < 3 mm, 0.3 < e < 0.7).

Fu *et al.* (2009)

Fu et al. (2009) performed experiments to measure K_{sat} of sandy soils and clay under compressive loading and unloading. According to Fu et al. (2009), permeability is a function of an interaction between loading and pore ratio, and permeability of the soils that have low pressure compactness is much smaller than that of the soils that have high pressure compactness although the permeability of clay that has a high-pressure compaction is always smaller than that of the clay that has a low pressure compaction. Equation C.29 describes the relationship between the pressure and the permeability.

$$k[cm/sec] = \frac{(A_1 - A_2)}{1 + e^{\frac{p - x_0}{\Delta x}}} + A_2 \quad \text{(C.29)}$$

where e = void ratio, p = pressure, A_1 = permeability coefficient at zero load, A_2 = corresponding permeability coefficient for ultimate load, x_0 = corresponding pressure value when the curve has an inflection point, Δx = slope change at each point of the relationship curve.

Wan *et al.* (2010)

Wan et al. (2010) described K_{sat} of aquifers decreases with depth, and the negative exponential model for the relationship between K_{sat} and the depth is as follows:

$$K[m/sec] = k_0 e^{-Az} \quad \text{(C.30)}$$

where $k_0 =$ surface permeability coefficient, $\mathrm{A} =$ attenuation coefficient, $z =$ depth in m.

Zhang and Wang (2014)

Zhang and Wang (2014) conducted static triaxial permeability tests to measure K_{sat} of coarse and fine sands from a deep underground mine where high confining pressure is applied. The results indicated the K_{sat} gradually decreases with increasing the confining pressure, while K_{sat} increases gradually with increasing the hydraulic gradient under the same confining pressure. Equation C.31 describes an exponential function for the relationship between K_{sat} and the confining stress.

$$K[cm/sec] = k_0 e^{-\alpha \sigma_n} \quad \text{(C.31)}$$

where $k_0 =$ initial permeability coefficient, $\alpha =$ coefficient, $\sigma_n =$ effective confining pressure.

Ren *et al*. (2016)

According to Ren et al. (2016), the classical Kozeny-Carman equation is not applicable for clayey soils, and accordingly Ren et al. (2016) applied the effective void ratio concept to derive a new K_{sat}-void ratio relationship based on the Poiseuille's law. The proposed equation (Equation C.32) showed a better capability than other models to estimate measured K_{sat} of a wide range of soils from coarse-grained to fine-grained.

$$K = C \frac{{e_t}^{3m+3}}{1+{e_t}^{\frac{5}{3}m+1}[(1+e_t)^{m+1}-{e_t}^{m+1}]^{\frac{4}{3}}} \quad \text{(C.32)}$$

where e_t = total void ratio, m = a positive constant for a given soil, $C = \frac{1}{C_F}\frac{\gamma_w}{\mu\rho_m^2}\frac{1}{S_s{}^2}$, C_F = a dimensionless shape constant, with a value about $C_F \approx 0.2$, S_s [m^2/g]= the specific surface area of particles, γ_w = unit weight of fluid [N/m^3]; ρ_m [kg/m^3] = particle density of soil, μ [$N{\cdot}s/m^2$] = fluid dynamic viscosity.

Dungca *et al*. (2018)

Dungca et al. (2018) performed experiments to evaluate K_{sat} of road base materials blended with fly ash and bottom ash and a multiple regression to predict K_{sat} at different percentage of bottom ash content and void ratio (Equation C.33). Equation C.33 is applicable to estimate the vertical K_{sat} given the percentage of bottom ash content and void ratio.

$$\mathrm{K}[cm/sec] = exp^{-14.2634+0.88735\mathrm{B}+13.361\mathrm{e}} \quad \text{(C.33)}$$

where B = percent bottom ash content, e = desired void ratio.

C.1.3 Methods based on Level of Compaction Effort

State of compaction is one of the key parameters affecting the permeability, primarily in terms of changes in pore structures (e.g., size, shape, tortuosity). Mokwa and Trimble (2008) performed permeability testing for measuring permeability of coarse-graded materials (crushed aggregates) and proposed empirical equations for estimating the permeability based on gradation and relative compaction (RC). Specifically, an equation based on pore parameters and the relative compaction (RC) was developed by the data evaluation and logarithmic regression to estimate k for crushed base course materials (Equation C.34).

$$\ln k\,[cm/sec] = \frac{1}{0.17F}\left[\frac{G_S\gamma_w}{RC\gamma_{dmax}} - 1\right] - 10.77 \quad \text{(C.34)}$$

where k = permeability in cm/s, F = the percent material finer than the No.10 sieve, G_s = the specific gravity, γ_w = the unit weight of water in pcf, γ_{dmax} = the maximum unit weight in pcf, RC = the relative compaction

C.1.4 Methods based on Fines Content

Bouchedid and Humphrey (2005) investigated permeabilities and gradations of subbase materials used for Maine roads in eight field projects. Fines content of 70% was averagely increased after an average of 12 years, most likely due to a combination of degradations from compaction during construction and passing vehicle, weathering from frost action, and infiltration of fines from the subgrade. Due to the increase in fines content, the average permeability of the standard subbase (5.9×10^{-4} cm/s) was significantly lower than FHWA recommendation (0.35 cm/s). For the empirical relationship between fines content and the permeability, Bouchedid and Humphrey (2005) conducted multivariable regression analysis and proposed an equation to estimate permeability of subbase material (Equation C.35).

$$\log(k)\,[cm/sec] = -2.74487 - 0.0939125F - 0.00743402C_u \quad \text{(C.35)}$$

where $F =$ the percent fines in percent, $C_u =$ coefficient of uniformity. Equation C.35 is applicable for compacted aggregates that have rounded particle shape (not angular crushed aggregates), fines content between 3% and 14%, and the coefficient of uniformity between 10 and 80.

C.1.5 Methods based on Material Type

Cone penetration test (CPT) is an *in situ* test for investigating soil properties and mapping soil profiles (i.e., soil type), and the soil behavior chart obtained from the CPT has been used to estimate *in situ* permeability (Robertson, 2010; Elhakim, 2016).

$$For\ 1.0 < I_c \leq 3.27\ ,\ k[m/sec] = 10^{(0.952-3.04I_c)} \quad \text{(C.36a)}$$

$$For\ 3.27 < I_c \leq 4.0\ ,\ k[m/sec] = 10^{(-4.52-1.37I_c)} \quad \text{(C.36b)}$$

$$I_c = [(3.47 - \log Q_{tn})^2 + (\log F_r + 1.22)^2]^{0.5} \quad \text{(C.36c)}$$

where $I_c =$ the soil behavior type index, $Q_{tn} = [(q_t - \sigma_{vo})/P_a](P_a/\sigma'_{vo})^n$, $F_r = [f_s/(q_t - \sigma_{vo})]100\%$, $q_t =$ CPT corrected cone resistance, $f_s =$ CPT sleeve friction, $\sigma_{vo} =$ in situ total vertical stress, $\sigma'_{vo} =$ in situ effective vertical stress, $n = 0.381(I_c) + 0.05(\sigma'_{vo}/P_a) - 0.15$, where n ≤ 1.0, $P_a =$ atmospheric pressure in same units as q_t, σ_{vo}, and σ'_{vo}. According to Elhakim (2016), I_c is determined iteratively by assuming a value of n to compute Q_{tn}. When the soil becomes finer, I_c increases resulting in a decrease in the soil permeability. Equation C.36 is useful in providing a detailed permeability profile with depth

based on CPT results. The permeability values estimated from the CPT readings are approximately half to one order of magnitude higher than the measured permeability using the falling head field test.

APPENDIX D
COMPARISONS OF SATURATED HYDRAULIC CONDUCTIVITIES FOR 16 SAMPLES OBTAINED FROM EXPERIMENTS AND ESTIMATIONS

Table D.1 Saturated hydraulic conductivity obtained from experiment and Alyamani and Sen (1993)

Sample	K_{sat} (cm/sec)		% Difference
	Experiment	Alyamani and Sen (1993)	
#1 (SP-SM)	0.0021	0.0083	119.06%
#2 (SW-SM)	0.0027	0.0086	104.13%
#3 (SM)	0.0073	0.0070	4.79%
#4 (GM)	0.1693	0.0280	143.28%
#5 (SP)	0.0489	0.0625	24.48%
#6 (GP)	0.6957	39.5393	193.08%
#7 (SW)	0.0236	0.0461	64.57%
#8 (SP)	0.005	0.0330	147.31%
#9 (GP)	0.6196	31.2352	192.22%
#10 (SP)	0.0104	0.0467	127.20%
#15 (GM)	0.0159	0.0421	90.39%
#16 (SM)	0.0004	0.0004	10.45%
A1 (GW-GM)	0.0298	0.0707	81.38%
A2 (GP)	0.5618	60.1033	196.30%
A3 (SP)	0.0224	0.0381	51.98%
A4 (GW-GM)	0.1759	0.0367	130.97%

Table D.2 Saturated hydraulic conductivity obtained from experiment and Beyer (1964)

Sample	K_{sat} (cm/sec)		% Difference
	Experiment	Beyer (1964)	
#1 (SP-SM)	0.0021	0.0098	129.18%
#2 (SW-SM)	0.0027	0.0096	111.85%
#3 (SM)	0.0073	0.0004	180.28%
#4 (GM)	0.1693	0.0006	198.51%
#5 (SP)	0.0489	0.0832	51.88%
#6 (GP)	0.6957	46.4989	194.10%
#7 (SW)	0.0236	0.0472	66.62%
#8 (SP)	0.005	0.0321	146.16%
#9 (GP)	0.6196	35.8147	193.20%
#10 (SP)	0.0104	0.0502	131.35%
#15 (GM)	0.0159	0.0002	194.25%
#16 (SM)	0.0004	0.0002	80.76%
A1 (GW-GM)	0.0298	0.0081	114.67%
A2 (GP)	0.5618	72.5822	196.93%
A3 (SP)	0.0224	0.0419	60.66%
A4 (GW-GM)	0.1759	0.0025	194.50%

Table D.3 Saturated hydraulic conductivity obtained from experiment and Chapuis (2004)

Sample	K_{sat} (cm/sec)		% Difference
	Experiment	Chapuis (2004)	
#1 (SP-SM)	0.0021	0.0057	91.71%
#2 (SW-SM)	0.0027	0.0042	43.66%
#3 (SM)	0.0073	0.0014	134.39%
#4 (GM)	0.1693	0.0025	194.13%
#5 (SP)	0.0489	0.0748	41.90%
#6 (GP)	0.6957	8.5648	169.95%
#7 (SW)	0.0236	0.0208	12.63%
#8 (SP)	0.005	0.0083	49.38%
#9 (GP)	0.6196	5.9724	162.40%
#10 (SP)	0.0104	0.0211	67.99%
#15 (GM)	0.0159	0.0013	170.00%
#16 (SM)	0.0004	0.0005	29.95%
A1 (GW-GM)	0.0298	0.0093	104.65%
A2 (GP)	0.5618	12.9845	183.41%
A3 (SP)	0.0224	0.0285	23.98%
A4 (GW-GM)	0.1759	0.0034	192.51%

Table D.4 Saturated hydraulic conductivity obtained from experiment and Harleman et al. (1963)

Sample	K_{sat} (cm/sec)		% Difference
	Experiment	Harleman et al. (1963)	
#1 (SP-SM)	0.0021	0.0055	89.73%
#2 (SW-SM)	0.0027	0.0066	84.34%
#3 (SM)	0.0073	0.0006	167.52%
#4 (GM)	0.1693	0.0013	196.84%
#5 (SP)	0.0489	0.0448	8.75%
#6 (GP)	0.6957	21.8332	187.65%
#7 (SW)	0.0236	0.0303	24.92%
#8 (SP)	0.005	0.0207	122.09%
#9 (GP)	0.6196	15.9494	185.04%
#10 (SP)	0.0104	0.0255	84.18%
#15 (GM)	0.0159	0.0009	179.17%
#16 (SM)	0.0004	0.0002	75.83%
A1 (GW-GM)	0.0298	0.0108	93.73%
A2 (GP)	0.5618	32.9809	193.30%
A3 (SP)	0.0224	0.0235	4.87%
A4 (GW-GM)	0.1759	0.0039	191.36%

Table D.5 Saturated hydraulic conductivity obtained from experiment and Original Hazen (1892)

Sample	K_{sat} (cm/sec)		% Difference
	Experiment	Original Hazen (1892)	
#1 (SP-SM)	0.0021	0.0066	103.89%
#2 (SW-SM)	0.0027	0.0055	68.45%
#3 (SM)	0.0073	0.0010	153.56%
#4 (GM)	0.1693	0.0020	195.35%
#5 (SP)	0.0489	0.0010	192.33%
#6 (GP)	0.6957	0.4422	44.56%
#7 (SW)	0.0236	0.0004	194.05%
#8 (SP)	0.005	0.0001	189.30%
#9 (GP)	0.6196	0.3039	68.38%
#10 (SP)	0.0104	0.0003	187.54%
#15 (GM)	0.0159	0.0000	199.74%
#16 (SM)	0.0004	0.0000	197.30%
A1 (GW-GM)	0.0298	0.0001	198.30%
A2 (GP)	0.5618	0.7007	22.00%
A3 (SP)	0.0224	0.0004	193.15%
A4 (GW-GM)	0.1759	0.0000	199.91%

Table D.6 Saturated hydraulic conductivity obtained from experiment and Modified Hazen (1892)

Sample	K_{sat} (cm/sec)		% Difference
	Experiment	Modified Hazen (1892)	
#1 (SP-SM)	0.0021	0.0086	121.85%
#2 (SW-SM)	0.0027	0.0104	117.58%
#3 (SM)	0.0073	0.0010	151.33%
#4 (GM)	0.1693	0.0021	195.06%
#5 (SP)	0.0489	0.0702	35.80%
#6 (GP)	0.6957	34.2225	192.03%
#7 (SW)	0.0236	0.0475	67.27%
#8 (SP)	0.005	0.0324	146.52%
#9 (GP)	0.6196	25.0000	190.33%
#10 (SP)	0.0104	0.0400	117.46%
#15 (GM)	0.0159	0.0014	168.29%
#16 (SM)	0.0004	0.0003	34.52%
A1 (GW-GM)	0.0298	0.0169	55.25%
A2 (GP)	0.5618	51.6961	195.70%
A3 (SP)	0.0224	0.0369	48.81%
A4 (GW-GM)	0.1759	0.0061	186.63%

Table D.7 Saturated hydraulic conductivity obtained from experiment and Kozeny (1953)

Sample	K_{sat} (cm/sec)		% Difference
	Experiment	Kozeny (1953)	
#1 (SP-SM)	0.0021	0.0003	143.72%
#2 (SW-SM)	0.0027	0.0002	167.90%
#3 (SM)	0.0073	0.0001	196.77%
#4 (GM)	0.1693	0.0001	199.71%
#5 (SP)	0.0489	0.0093	135.95%
#6 (GP)	0.6957	3.9852	140.55%
#7 (SW)	0.0236	0.0018	171.43%
#8 (SP)	0.005	0.0006	159.75%
#9 (GP)	0.6196	2.5140	120.91%
#10 (SP)	0.0104	0.0019	139.57%
#15 (GM)	0.0159	0.0001	198.70%
#16 (SM)	0.0004	0.0000	183.58%
A1 (GW-GM)	0.0298	0.0007	191.44%
A2 (GP)	0.5618	6.7824	169.40%
A3 (SP)	0.0224	0.0027	156.75%
A4 (GW-GM)	0.1759	0.0002	199.60%

Table D.8 Saturated hydraulic conductivity obtained from experiment and Kozeny-Carman

Sample	K_{sat} (cm/sec)		% Difference
	Experiment	Kozeny-Carman	
#1 (SP-SM)	0.0021	0.0023	9.10%
#2 (SW-SM)	0.0027	0.0016	52.58%
#3 (SM)	0.0073	0.0004	179.34%
#4 (GM)	0.1693	0.0008	198.08%
#5 (SP)	0.0489	0.0624	24.20%
#6 (GP)	0.6957	26.6582	189.83%
#7 (SW)	0.0236	0.0121	64.10%
#8 (SP)	0.005	0.0037	28.78%
#9 (GP)	0.6196	16.8170	185.79%
#10 (SP)	0.0104	0.0124	17.38%
#15 (GM)	0.0159	0.0003	191.44%
#16 (SM)	0.0004	0.0001	110.96%
A1 (GW-GM)	0.0298	0.0044	148.97%
A2 (GP)	0.5618	45.3701	195.11%
A3 (SP)	0.0224	0.0182	20.87%
A4 (GW-GM)	0.1759	0.0012	197.33%

Table D.9 Saturated hydraulic conductivity obtained from experiment and Salarashayeri and Siosemarde (2012)

Sample	K_{sat} (cm/sec)		% Difference
	Experiment	Salarashayeri and Siosemarde (2012)	
#1 (SP-SM)	0.0021	0.0131	144.69%
#2 (SW-SM)	0.0027	0.0035	26.63%
#3 (SM)	0.0073	-	-
#4 (GM)	0.1693	-	-
#5 (SP)	0.0489	0.0243	67.19%
#6 (GP)	0.6957	0.5380	25.57%
#7 (SW)	0.0236	-	-
#8 (SP)	0.005	0.0021	81.21%
#9 (GP)	0.6196	0.5053	20.31%
#10 (SP)	0.0104	0.0253	83.52%
#15 (GM)	0.0159	-	-
#16 (SM)	0.0004	0.0009	77.55%
A1 (GW-GM)	0.0298	-	-
A2 (GP)	0.5618	0.6909	20.61%
A3 (SP)	0.0224	0.0171	26.88%
A4 (GW-GM)	0.1759	-	-

Table D.10 Saturated hydraulic conductivity obtained from experiment and Sauerbrei (1932)

Sample	K_{sat} (cm/sec)		% Difference
	Experiment	Sauerbrei (1932)	
#1 (SP-SM)	0.0021	0.0078	114.91%
#2 (SW-SM)	0.0027	0.0047	54.63%
#3 (SM)	0.0073	0.0006	168.11%
#4 (GM)	0.1693	0.0298	140.05%
#5 (SP)	0.0489	0.0685	33.42%
#6 (GP)	0.6957	22.0922	187.79%
#7 (SW)	0.0236	0.0197	17.93%
#8 (SP)	0.005	0.0051	2.22%
#9 (GP)	0.6196	14.7614	183.89%
#10 (SP)	0.0104	0.0152	37.75%
#15 (GM)	0.0159	0.0029	138.34%
#16 (SM)	0.0004	0.0004	7.69%
A1 (GW-GM)	0.0298	0.0075	119.27%
A2 (GP)	0.5618	47.3758	195.31%
A3 (SP)	0.0224	0.0239	6.51%
A4 (GW-GM)	0.1759	0.0034	192.52%

Table D.11 Saturated hydraulic conductivity obtained from experiment and Slichter (1899)

Sample	K_{sat} (cm/sec)		% Difference
	Experiment	Slichter (1899)	
#1 (SP-SM)	0.0021	0.0015	35.88%
#2 (SW-SM)	0.0027	0.0011	86.33%
#3 (SM)	0.0073	0.0002	187.38%
#4 (GM)	0.1693	0.0005	198.84%
#5 (SP)	0.0489	0.0317	42.70%
#6 (GP)	0.6957	13.9599	181.01%
#7 (SW)	0.0236	0.0078	101.06%
#8 (SP)	0.005	0.0026	62.73%
#9 (GP)	0.6196	9.0906	174.48%
#10 (SP)	0.0104	0.0077	29.93%
#15 (GM)	0.0159	0.0002	194.49%
#16 (SM)	0.0004	0.0001	141.77%
A1 (GW-GM)	0.0298	0.0028	165.87%
A2 (GP)	0.5618	23.1215	190.51%
A3 (SP)	0.0224	0.0104	72.81%
A4 (GW-GM)	0.1759	0.0008	198.23%

Table D.12 Saturated hydraulic conductivity obtained from experiment and Terzaghi (1925)

Sample	K_{sat} (cm/sec)		% Difference
	Experiment	Terzaghi (1925)	
#1 (SP-SM)	0.0021	0.0017	22.18%
#2 (SW-SM)	0.0027	0.0011	85.06%
#3 (SM)	0.0073	0.0003	184.85%
#4 (GM)	0.1693	0.0006	198.61%
#5 (SP)	0.0489	0.0402	19.60%
#6 (GP)	0.6957	17.6143	184.80%
#7 (SW)	0.0236	0.0089	90.78%
#8 (SP)	0.005	0.0024	69.75%
#9 (GP)	0.6196	11.3995	179.38%
#10 (SP)	0.0104	0.0090	13.95%
#15 (GM)	0.0159	0.0003	193.72%
#16 (SM)	0.0004	0.0001	131.56%
A1 (GW-GM)	0.0298	0.0032	161.41%
A2 (GP)	0.5618	29.2952	192.47%
A3 (SP)	0.0224	0.0129	54.13%
A4 (GW-GM)	0.1759	0.0008	198.09%

Table D.13 Saturated hydraulic conductivity obtained from experiment and U.S. Bureau of Reclamation

Sample	K_{sat} (cm/sec)		% Difference
	Experiment	U.S. Bureau of Reclamation	
#1 (SP-SM)	0.0021	0.0021	0.45%
#2 (SW-SM)	0.0027	0.0026	3.20%
#3 (SM)	0.0073	0.0001	192.53%
#4 (GM)	0.1693	0.0455	115.32%
#5 (SP)	0.0489	0.0066	152.65%
#6 (GP)	0.6957	4.9297	150.53%
#7 (SW)	0.0236	0.0079	99.37%
#8 (SP)	0.005	0.0033	42.10%
#9 (GP)	0.6196	3.5243	140.19%
#10 (SP)	0.0104	0.0032	106.87%
#15 (GM)	0.0159	0.0015	166.45%
#16 (SM)	0.0004	0.0001	148.84%
A1 (GW-GM)	0.0298	0.0024	169.82%
A2 (GP)	0.5618	10.4592	179.61%
A3 (SP)	0.0224	0.0033	148.81%
A4 (GW-GM)	0.1759	0.0013	197.15%